Spin-up of UK Earth System Model 1 (UKESM1) for CMIP6

A. Yool[1], J. Palmiéri[1], C.G. Jones[2], A.A. Sellar[3], L. de Mora[4], T. Kuhlbrodt[5], E.E. Popova[1], J.P. Mulcahy[3], A. Wiltshire[3], S.T. Rumbold[5], M. Stringer[5], R.S.R. Hill[3], Y. Tang[3], J. Walton[3], A. Blaker[1], A.J.G. Nurser[1], A.C. Coward[1], J. Hirschi[1], S. Woodward[3], D.I. Kelley[6], R. Ellis[6], S. Rumbold-Jones[3,5]

[1]National Oceanography Centre, European Way, Southampton SO14 3ZH, UK
[2]National Centre for Atmospheric Science, University of Leeds, Leeds LS2 9JT, UK
[3]Met Office, FitzRoy Road, Exeter, Devon EX1 3PB, UK
[4]Plymouth Marine Laboratory, Prospect Place, Plymouth PL1 3DH, UK
[5]National Centre for Atmospheric Science, University of Reading, Earley Gate, Reading RG6 6BB, UK
[6]Centre for Ecology and Hydrology, Wallingford OX10 8BB, UK

Key Points:

- Earth system components and spin-up protocol of UKESM1 for CMIP6 outlined
- Ocean-only (5000y) and Land-only (1000y) phases used prior to fully-coupled finalising of spin-up (500y)
- Evaluation of spin-up protocol presented, including cross-component validation of piControl state and drift

---

Corresponding author: Andrew Yool, axy@noc.ac.uk

This article has been accepted for publication and undergone full peer review but has not been through the copyediting, typesetting, pagination and proofreading process, which may lead to differences between this version and the Version of Record. Please cite this article as doi: 10.1029/2019MS001933

Abstract

For simulations intended to study the influence of anthropogenic forcing on climate, temporal stability of the Earth's natural heat, freshwater and biogeochemical budgets is critical. Achieving such coupled model equilibration is scientifically and computationally challenging. We describe the protocol used to spin-up the UK Earth system model (UKESM1) with respect to pre-industrial forcing for use in the 6th Coupled Model Intercomparison Project (CMIP6). Due to the high computational cost of UKESM1's atmospheric model, especially when running with interactive full chemistry and aerosols, spin-up primarily used parallel configurations using only ocean/land components. For the ocean, the resulting spin-up permitted the carbon and heat contents of the ocean's full volume to approach equilibrium over ˜5000 years. On land, a spin-up of ˜1000 years brought UKESM1's dynamic vegetation and soil carbon reservoirs towards near-equilibrium. The end-states of these parallel ocean- and land-only phases then initialised a multi-centennial period of spin-up with the full Earth system model, prior to this simulation continuing as the UKESM1 CMIP6 pre-industrial control (piControl). The realism of the fully-coupled spin-up was assessed for a range of ocean and land properties, as was the degree of equilibration for key variables. Lessons drawn include the importance of consistent interface physics across ocean- and land-only models and the coupled (parent) model, the extreme simulation duration required to approach equilibration targets, and the occurrence of significant regional land carbon drifts despite global-scale equilibration. Overall, the UKESM1 spin-up underscores the expense involved and argues in favour of future development of more efficient spin-up techniques.

Plain Language Summary

Earth system models (ESMs) are an important tool for understanding the Earth and for projecting how climate change may affect natural and human systems. For simulations of ESMs to separate anthropogenic influences on climate from the background state, the stability of the unperturbed system is critical. However, achieving this equilibrium is both scientifically and computationally challenging. Here, we describe how this was achieved for one such model, UKESM1, for the 6th Coupled Model Intercomparison Project (CMIP6). Due to the cost of the full model, especially when running with atmospheric chemistry and aerosols, much of UKESM1's spin-up to equilibrium made use of ocean- and land-only configurations. Millennial-scale spin-up phases of these component-only models were used to initialise a final centennial-scale phase of the full model to reach pre-industrial equilibrium targets. The stability and realism of UKESM1's spun-up state was then evaluated across a broad range of properties. A number of lessons were drawn from this spin-up including the extreme simulation duration required to reach equilibrium. A key conclusion is the importance of developing efficient techniques to spin-up ESMs.

1 Introduction

To a first approximation, the behaviour of the Earth system (ES) is governed by the dynamics and interactions of the two geophysical fluids – the atmosphere and the ocean – that comprise the majority of the planet's surface substrate. Despite a number of similarities, these two fluids diverge in many other respects, including a critical difference in the timescales of their internal dynamics. Features in the atmosphere form and dissipate over periods typically of the order of hours, days or weeks in duration, with a residence time for one of its most dynamic components – water – of only 8.9 days [van der Ent and Tuinenburg, 2017]. In contrast, while the ocean's surface readily exchanges and interacts with the atmosphere over short timescales, its interior is structured by a vast thermohaline circulation that sluggishly transports water around its basins and into the abyssal deep. Depending upon its location, such water leaving contact with the atmosphere can take decades, centuries or even millennia to overturn completely and come back into contact with the atmosphere. For example, estimated from radiocarbon and from inverse models, the waters of the deep North Pacific have a ventilation age of 1200–1500 years (Gebbie and Huybers [2012]; Khatiwala et al. [2012]), with some model studies suggesting much longer timescales [Wunsch and Heimbach, 2008].

Consequently, with a ventilation timescale of more than a millennium, the ocean component of the Earth system has a long memory – one that can "remember" environmental perturbations far longer than other components such as the atmosphere and land surface [Ciais et al., 2013]. In addition, the ocean is the largest active reservoir of carbon in the Earth system, approximately 40000 petagrams carbon (Pg C) [Ciais et al., 2013]. Relative to the atmosphere – where the concentration of carbon dioxide (CO_2) has been of long-standing interest – this represents a store more than 50 times greater [Ciais et al., 2013]. A consequence of this is that even small imbalances in the air-sea exchange of CO_2 can lead to large changes in atmospheric CO_2 [Kwon et al., 2009]. Furthermore, biogeochemical processes within the ocean, such as those of the biological pump [Raven and Falkowski, 1999], can significantly alter seawater chemical composition, with implications for the wider carbon system when deep water parcels finally re-establish contact with the atmosphere.

The land system represents another significant store of carbon in the Earth system. On land, carbon is stored both in living biomass and in soil as decaying organic carbon.

Relative to the ocean, the total land reservoir is comparatively small (approximately 2200 Pg C vs. 40000 Pg C; Ciais et al. [2013]). Nonetheless, the more rapid timescale of interaction between the land and atmosphere leads to the terrestrial carbon content being strongly influenced by climate variability. Turnover timescales in the living and decaying pools of carbon mean that, like the ocean, equilibration of the land system requires extended periods of model spin-up.

These significant reservoirs of carbon, and their relatively slow turnover times, whether through sluggish ventilation or gradual decay processes, have important implications for simulations of Earth system models (ESMs) aimed at studying the influence of human perturbations on the system. Principally, in fully–coupled ESMs, where both the climate and CO_2 are free to evolve, to robustly detect human perturbations requires the ocean and land carbon stores be in temporal equilibrium before any human forcing is imparted. If this temporal stability is not achieved then the slow equilibration trend of either carbon reservoir could be confused with, and even influence, any human-induced trend, confounding the detection of human forcing of the system. For instance, in a model with natural land or ocean carbon pools outgassing, such drift will mask ingassing fluxes driven by the steady accumulation of anthropogenic CO_2 in that atmosphere.

Separate to its carbon reservoir, ocean spin-up also serves to bring its physical state, particularly ocean heat content, as well as the biogeochemical cycles of other elements, into equilibrium. On land, spin-up serves to bring the various vegetation types into balance with their local climate (temperature, water and nutrient availability, etc.) and, through ecological competition, with each other.

The desirability of a well-equilibrated ESM is typically offset by the computational cost of achieving this. While most experimental simulations may only be years, decades or centuries in duration, full spin-up typically requires of order one to tens of millennia of simulation. In the case of the ocean, on top of the estimated ventilation timescales of the ocean's "oldest" watermasses [Khatiwala et al., 2012], spin-up must further account for biogeochemical "shuffling" of nutrients, such as the downstream effects of a model's biological pump on the nutrient concentrations of its deep, and then upwelling, watermasses. Ocean physical properties are similarly affected, with the distinction that, in gradually changing the seawater bulk properties, spin-up also alters the ocean density and potential energy field, with consequences for the very circulation that is spinning everything up.

Consequently, techniques for model spin-up are diverse, reflecting spin-up aspirations (i.e. physics or biogeochemistry or both), model cost (i.e. computational or wallclock or both) and the availability of suitable engineering solutions (i.e. does model code permit particular accelerated modes of spin-up).

The most conventional, and arguably "best" approach, is simply to run the model for a long period of time (simulated and wallclock). This ensures that spin-up is consistent with the normal model operation, and avoids introducing any artifacts caused by spin-up "shortcuts". With continual advances in the power and availability of computational resources, this approach should become less burdensome with time, with past models becoming easier to spin-up to equilibrium. However, our parallel increase in knowledge and understanding favours increasingly well-resolved and more complex models, whose aspirations foster a "Red Queen" effect within the modelling community (with some notable exceptions; Cui et al. [2011]). That is, while computational gains should permit faster spin-up, they actually favour increased realism, with the result that spin-up remains computationally expensive despite these gains. Consequently, this "brute force" approach to spin-up remains tantalisingly out of reach for state-of-the-art ESMs.

While ocean ventilation in the Earth system is relatively sluggish, ocean models are usually computationally faster than their atmosphere counterparts, to which they are coupled. Resolution may be comparable (as in UKESM1), but the absence of detailed radiation schemes, typically fewer advected tracers, and automatically fewer grid cells because of the occurrence of land, means ocean-only models typically exhibit greater wallclock efficiency. Consequently, one spin-up approach called "online ocean-only" is to run a decoupled ocean component with appropriate surface boundary conditions, and simulate the majority of ocean equilibration without the more expensive atmosphere. This approach is facilitated by the atmosphere's relatively rapid equilibration, such that it can readily both provide surface forcing, and be "re-attached" to the ocean for a comparatively brief period at the end of spin-up.

The online ocean-only approach also extends to land spin-up which, like the ocean, can include elements (e.g. soil carbon) that require extended simulation periods. Much like the ocean, the land can be driven by atmospheric forcing at its boundary, sparing the cost of full atmospheric simulation. It differs in that the modelled system typically has reduced vertical resolution, and its prognostic variables (carbon reservoirs, vegetation types) are not advected. As such, while the three-dimensional nature of the ocean means that it remains moderately expensive to run even on its own, the reduced number of levels and lack of advection means the land spin-up is computationally less of a burden.

A further approach, "offline ocean-only", separates the spin-up of ocean physics from that of biogeochemistry, by treating ocean circulation itself as just another part of the forcing. Once circulation has stabilised, either in full Earth system or ocean-only mode, it is used as a three-dimensional climatology to transport tracers of marine biogeochemistry. In this way, the subsequent cost of calculating ocean physics is avoided, permitting a more computationally-efficient spin-up. A superficially similar approach to "offline ocean-only" is that of the transport matrix method (TMM; Khatiwala et al. [2005]; Khatiwala [2007]). Rather than explicitly using a stored model circulation to drive biogeochemical tracers, this method describes the spatial connectivity driven by ocean circulation as a sparse matrix that can efficiently be used as a transport operator. While both of these approaches serve to spin-up passive tracers at a somewhat reduced computational cost, both still require an equilibrium physical circulation in the first place, which in turn requires its own spin-up. As we need to spin-up both the physical circulation and ocean biogeochemistry of UKESM1, our ocean spin-up here makes use instead of the "online ocean-only" to do both in tandem.

Note that the discussion above effectively assumes equilibration is always for the good, essentially because of the resulting reduction in model drift. However, as imperfect tools, models do not necessarily converge towards a state similar to that of the real Earth system, and extended spin-up is liable to produce a divergent state relative to the true observed state (while revealing model biases). Paradoxically, by reducing model drift while increasing model bias, equilibration can seemingly reduce a model's skill when evaluated against observations [Séférian et al., 2016]. Conversely, by limiting spin-up, a model will diverge less from its (typically) observationally-derived initial state, and its state will show smaller biases (if greater drift). Nonetheless, the need for a stable control simulation from which to initialise historical runs (and then future projections) is more important than such considerations. Not least because the drift from an observation-based initial condition is likely larger, over the first few hundred years of a simulation, than the anthropogenic signal we wish to detect.

Within the Coupled Model Intercomparison Project Phase 6 (CMIP6), the Diagnostic, Evaluation and Characterization of Klima (DECK) protocol [Eyring et al., 2016] describes the baseline simulations that all participating models must undertake to "benchmark" their performance. An underpinning part of the DECK is the production of a pre-industrial control (piControl) simulation from which model states can be drawn to initialise simulations for both the DECK and other Model Intercomparison Projects (MIPs). While the DECK outlines certain boundary conditions for this piControl (e.g. atmospheric CO_2 concentrations, orbital parameters, a mean solar cycle, etc.), it does not specify a particular methodology or duration for the production of this model state. This stems partly from the variety of models participating in CMIP, and the resulting difficulty in defining universal criteria for models that range widely in complexity, resolution and degree of internal coupling. Additionally, the potential computational cost of spin-up is a factor, with participating groups varying in their access to compute resources. Some MIP protocols, such as C4MIP [Jones et al., 2016], suggest equilibrium criteria for participating models, but the DECK requirement of a multi-century piControl to shadow MIP simulations is intended as a means to quantify (and control for) drift in CMIP6 simulations. This situation largely repeats that of CMIP5, where total spin-up durations varied widely from only 200 years up to almost 12,000 years [Séférian et al., 2016]. As well as this wide span of spin-up durations, the CMIP5 models summarised by Séférian et al. [2016] also varied widely in the spin-up methodology used. Models adopted various offline, accelerated offline and component-only online approaches, often in unique combinations, prior to final periods of fully-coupled simulation. However, in the absence of formalised guidance or commonly-accepted spin-up procedures, the documentation of spin-up typically remains a lower-priority activity. Nonetheless, a number of studies have examined aspects of spin-up, such as how specifically to equilibrate ("spin-down") from modern initial conditions to the preindustrial state [Stouffer et al., 2004], quantifying the sources of drift or variability in spun-up models Doney et al. [2006], and how drifts can be corrected without introducing bias [Hobbs et al., 2016]. Furthermore, an increasing number of studies document the approaches used to spin-up ESMs (more comprehensive examples include: Watanabe et al. [2011]; Séférian et al. [2013]; Lindsay et al. [2014]).

Here we document the spin-up procedure followed in preparing a pre-industrial control state of the new ESM, UKESM1, for the CMIP6 DECK and MIP experiments. The manuscript begins with a brief description of UKESM1 and its main components, followed by an extensive description of the procedure employed to equilibrate UKESM1 to CMIP6 pre-industrial forcing. We then show the evolution of the model's state during spin-up, from both the parallel ocean- and land-only spin-up activities, followed by the final, fully–coupled model. The model's degree of equilibration and biases in its final state are discussed, together with potential future avenues for addressing these. In addition to the results presented in the main body of this manuscript, supplementary material includes additional tables and figures to document the spin-up and performance of UKESM1.

2 Methods

2.1 UKESM1 description

UKESM1 is a new state-of-the-art ESM comprised of components that represent both physical and biogeochemical aspects of the Earth's atmosphere, ocean, cryosphere and land systems. It is built on the recent Hadley Centre Global Environment Model version 3 Global Coupled (GC) climate configuration, HadGEM3 GC3.1 (Williams et al. [2017]; Kuhlbrodt et al. [2018]). This physical core model is extended through the addition of ocean and land biogeochemistry, and interactive stratospheric–tropospheric trace gas chemistry, which predicts atmospheric oxidant fields as input to the aerosol model as well as a range of radiatively active gases (e.g. O_3, CH_4, N_2O). As well as including dynamics internal to their components, these Earth system additions couple where it is believed that they potentially feedback upon one another (either negative and damping, or positive and amplifying), or where they impact the time-evolution of the physical climate system. For example, atmospheric aerosols play a key role in mediating the transfer or absorption of radiation within the atmosphere, and their occurrence and behaviour is an outcome of interactions between chemical and physical processes in the atmosphere, ocean and ice (Halloran et al. [2010]; Carslaw et al. [2010]; Quinn and Bates [2011]; Myhre et al. [2013]; Kok et al. [2018]). Representing and understanding the nature of such linkages between components is of critical importance if models are to accurately represent the true Earth system sensitivity to anthropogenic forcing.

Figure 1 presents a schematic diagram of the components included within UKESM1, together with an indication of the nature of the coupling between them. In outline, atmosphere and land components are closely coupled together as a single, integrated executable, use a common grid and time-step, and communicate their states directly at each time-step without the need for a coupler. The same is true for the three ocean components – dynamics, sea-ice and biogeochemistry – which are also coupled together as a single executable. The two executables – atmosphere-land and ocean-ice-biogeochemistry – communicate once every 3 hours through interface layers, labelled OASIS3-MCT_3.0 (Valcke [2013]; Craig et al. [2017]) in Figure 1.

The atmosphere of UKESM1 as represented by GA7.1 represents the physical dynamics of the atmosphere, including processes such as mass transport, radiative transfer, thermodynamics and the water cycle. Coupled to the GA7.1 is the UK Chemistry and

Aerosols model (UKCA; Morgenstern et al. [2009]; O'Connor et al. [2014]), which represents stratospheric and tropospheric chemistry, as well as aerosols via the GLOMAP-mode scheme [Mann et al., 2010], with dust represented by a binned scheme [Woodward, 2011]. UKESM1 differs from GA7.1 in its treatment of the natural emissions of monoterpenes, dimethyl sulphide (DMS) and primary marine organic aerosols (PMOAs), which are interactively calculated from elements of the land and ocean components, permitting feedbacks between the biosphere and aerosol / cloud-radiative behaviour in UKESM1. A further coupling that uniquely links the land to the ocean in UKESM1 is the production of wind-borne mineral dust as a function of simulated climate and bare soil on land, and which can fuel ocean productivity (and uptake of CO_2) by supplying bioavailable iron. See Mulcahy et al. [2018], Sellar et al. [2019] and Archibald et al. [2020] for further details concerning atmospheric chemistry in UKESM1.

The physical ocean component of UKESM1 is represented by the Nucleus for European Modelling of the Ocean model (NEMO; Madec et al. [2016]) for its dynamical circulation, and by the Los Alamos sea-ice model (CICE; Rae et al. [2015]) for its marine cryosphere. More complete descriptions of the NEMO and CICE configuration used in UKESM1, including details of its sensitivity and resulting tuning, can be found in Storkey et al. [2018], Ridley et al. [2018] and Kuhlbrodt et al. [2018]. Marine biogeochemistry is represented by the Model of Ecosystem Dynamics, nutrient Utilisation, Sequestration and Acidification (MEDUSA-2.1), which includes the cycles of nitrogen, silicon, iron, carbon and oxygen. The version used in UKESM1 is identified as MEDUSA-2.1, to distinguish it from its earlier parent model, MEDUSA-2, described in Yool et al. [2013]. Developments made for UKESM1 include: 1. replacement of its carbonate chemistry with the MOCSY-2.0 scheme of Orr and Epitalon [2015]; 2. the addition of an empirical submodel of surface seawater DMS concentration [Anderson et al., 2001]; 3. various code improvements including adaptations for variable volume (VVL) and upgrading to utilise the XML Input-Output Server (XIOS) adopted by NEMO [Meurdesoif, 2013].

The land component of UKESM1 is represented by the Joint UK Land Environment Simulator (JULES; Best et al. [2011]; Clark et al. [2011]), which handles physics and integrated biogeochemistry. This is closely coupled with the Top-down Representation of Interactive Foliage and Flora Including Dynamics model (TRIFFID; Cox [2001]; Jones et al. [2011]), a dynamic global vegetation model that represents plant and soil dynamics on land. Developments since CMIP5 include: 1. updating of plant growth and turnover parameters to reflect the plant trait database, TRY [Kattge et al., 2011]; 2. an increase in the number of plant functional types (PFTs) from five to thirteen, further permitting the distinction of evergreen / deciduous plants and tropical / temperate evergreen trees [Harper et al., 2016]; 3. the emission of volatile organic compounds (VOCs; e.g. Pacifico et al. [2015]); 4. limitation on terrestrial primary production (and therefore CO_2 uptake) through the availability of soil and plant nitrogen. Land-use by agriculture is represented in TRIFFID by reserving fractions of each grid cell for crops and pasture, with these fractions prescribed as external forcing that can vary with time. The Greenland and Antarctic land icesheets are represented via a sub-gridscale scheme described in Shannon et al. [2019]. For further details of UKESM1's land component, please refer to Sellar et al. [2019].

By default, UKESM1 has a relatively coarse horizontal resolution of N96 (approximately 135 km) in the atmosphere and 1° (approximately 73 km) in the ocean. Vertical resolution is 85 levels in the atmosphere (with a model top at 85 km), and 75 levels in the ocean (with a maximum depth of 6 km), with, in both cases, high vertical resolution focused at the interface between the two fluids. This resolution corresponds to the HadGEM3 N96ORCA1 configuration, a full description of which can be found in Kuhlbrodt et al. [2018].

In the work described here, the fully coupled version of UKESM1 was only utilised for a restricted (latter) portion of the full spin-up process. This was in part because of its high computational cost, but also because this cost is largely associated with atmospheric components that spin-up to equilibrium much more quickly than the ocean or the land. The majority of the spin-up was therefore performed using parallel ocean-only and land-only versions of UKESM1, forced at their surface boundary conditions by atmospheric output from a shorter coupled model simulation. More complete details of the fully-coupled UKESM1, including an analysis of its pre-industrial and historical climate, can be found in Sellar et al. [2019].

2.2 UKESM1 spin-up

Spin-up of UKESM1 utilised a combination of phases using coupled climate, ocean-only, land-only and full Earth system coupled versions of the model (with and without interactive atmospheric chemistry). The development cycle of the full model occurred in parallel with spin-up activities, with the result that spin-up did not use a single version of the model throughout. Periodically, model improvements and bugfixes were applied between model phases. The last segment of spin-up did employ the final coupled version of UKESM1.

Figure 2 presents an overview diagram of the spin-up procedure. Several primary branches of parallel spin-up are shown, each focused on the equilibration of separate ES components: ocean, land and atmospheric chemistry. Model states (i.e. restart files of prognostic variables) were shared between these main branches during the full spin-up, with the main points of restart state sharing specifically identified. To illustrate underlying operational details, Supplementary Tables S1 to S3 present the chains of simulations performed as part of the "ocean", "land" and "atmosphere" branches of spin-up (respectively the top, middle and bottom paths of Figure 2). Significant changes along these branches are switches from component-only to coupled branches, the switch from prescribed, non-interactive atmospheric chemistry (designated UKESM1-CN) to fully interactive chemistry (UKESM1), and the adoption of component model states as initial conditions from other branches. Since it is the longest branch in terms of total simulated years, attention focuses here on the ocean branch summarised in Supplementary Table S1.

As noted previously, the largest active carbon and heat reservoir in the Earth system is the ocean, and imbalances in this reservoir can have a large impact on simulation drift. Consequently, the ocean spin-up branch was prioritised and operationally began first, principally in ocean-only mode before switching to a fully-coupled mode with prescribed, non-interactive atmospheric chemistry (designated UKESM1-CN). This was followed by land spin-up, which also started in land-only mode and also subsequently transitioned to UKESM1-CN mode. Finally, the fully-coupled model, complete with interactive atmospheric chemistry (designated UKESM1), was spun-up. The ocean, land and atmosphere states from these parallel branches were then finally combined into a UKESM1 simulation (identifier u-av472; Supplementary Table S1 that led into the pre-industrial control simulation (identifier u-aw310; Supplementary Table S1.) This piControl was then simulated for a duration of more than 1000 years both to act as a control for numerous other simulations in CMIP6, and to serve as a source of initial states for the CMIP6 Historical ensemble of UKESM1. This latter ensemble forms the subject of the analyses of Sellar et al. [2019] and Archibald et al. [2020].

UKESM1 is the successor ESM to CMIP5's HadGEM2-ES, and, as noted already, this latter model is the source of some components in UKESM1. The spin-up procedure adopted for HadGEM2-ES also parallels that used here for UKESM1, with periods of ocean- and land-only spin-up followed by a final phase of fully-coupled simulation, although with some significant differences [Collins et al., 2011]. Unlike UKESM1's ocean, where observationally-derived initial conditions were used, spin-up of HadGEM2-ES was initialised using an existing ocean state from the preceding HadGEM1 model used in CMIP3 [Johns et al., 2006]. This included both physical and biogeochemical state variables, with the new biogeochemical variables introduced in HadGEM2-ES initialised with climatogical (silicic acid) or uniform (total iron) values. Similarly to UKESM1, this ocean state was then spun-up in ocean-only mode under model atmospheric forcing for 400 y, but with the advantage of starting from the previous spun-up state of HadGEM1. In the case of the land component, HadGEM2-ES used an acceleration technique in which, after 3 y periods of coupled simulation, the model's land state was implicitly extrapolated forwards by 100 y before returning to a further period of conventional coupled simulation. This procedure was repeated 4 times, advancing the land state of HadGEM2-ES by 400 y. This approach did not fully equilibrate refractive soil organic material because of the timescales its equilibration (e-folding of 50 y), and its sensitivity to sub-annual litter input. Spin-up of the model's soil carbon was instead achieved using 2000 y of offline simulation of this reservoir, forced using monthly fields of litter inputs. The ocean and land states obtained using these procedures were then used in a final period of fully-coupled simulation under pre-industrial conditions for 280 y, to produce a piControl state.

2.2.1 Detailed spin-up approach

The key motivating factor in our spin-up was minimising drift in the Earth system's carbon cycle, and attention was strongly focused on the net air-sea CO_2 flux. Analysis by Séférian et al. [2016] found the diverse array of spin-up protocols followed during preparation for CMIP5 resulted in models that exhibited large differences in simulated fields, and potentially biased performance evaluations. Recognising this, Jones et al. [2016] suggest a drift criterion of $\leq$ 10 Pg C century^{-1} (i.e. a long-term average of $\leq$ 0.1 Pg C y^{-1}) for net fluxes between the atmosphere, land and ocean reservoirs as part of the C4MIP protocol [Jones et al., 2016]. Note that both the land and ocean components of UKESM1 only exchange carbon with the atmosphere component and not directly with each other (e.g. via rivers).

To evaluate this particular target, as well as track a range of critical physical and biogeochemical properties (e.g. ocean heat content, surface temperature, top-of-atmosphere heat balance, Atlantic meridional overturning circulation, sea-ice cover, etc.), the spin-up was monitored throughout using the Met Office Climate Model Monitoring tool (CMM) and BGC-val tools [de Mora et al., 2018]. Running routinely in parallel with the spin-up simulations, these tools greatly facilitated rapid decision-making during model development, as well as identifying undesireable drifts or model errors.

The spin-up path began with a short physical climate simulation (run ID u-ai567; the full list of run IDs is given in Supplementary Tables S1 to S3) using a prototype of HadGEM3 GC3.1 (Williams et al. [2017]; Kuhlbrodt et al. [2018]) using CMIP6 pre-industrial control forcing. This constitutes the physical core of UKESM1. This simulation was initialised from rest (i.e. with zero u and v velocity fields), with observationally-derived initial conditions for the ocean (EN4; Good et al. [2013]), and initial states for the atmosphere and sea-ice drawn from a GC3.0 simulation Kuhlbrodt et al. [2018]. After 30 years, the atmospheric state of this simulation was judged to be sufficiently spun-up to serve as a source of forcing data for ocean-only configurations, and the simulation was continued to provide a further 30 year period of forcing data.

The forcing data collected from this GC3.1 simulation (and for subsequent forcing) consisted of 1.5 m air temperature, air humidity, 10 m wind velocities (U and V directions), surface downwelling short- and long-wave radiation, precipitation (rain and snow) and aeolian dust flux at 3 hour frequency, and river runoff at monthly frequency. These data fields are the same as those available in observationally-derived reanalysis forcing datasets, such as CORE [Large and Yeager, 2009] and DFS [DRAKKAR Group, 2007], although at higher temporal resolution for heat and freshwater fluxes. In addition to these properties, fields of ocean surface temperature and salinity were collected from the same GC3.1 simulation at monthly frequency for relaxation purposes.

Based on the variability found in the atmospheric component of GC3.1, a forcing period of 30 years was selected as broadly representative of interannual patterns (but see later). Test simulations using repeated cycles of this forcing did not find any significant issues associated with the forcing "kick" imparted between cycles (i.e. upon reaching the end of year 30, year 1 is simply recycled). This approach of recycling forcing has previously been used successfully with NEMO-MEDUSA [Couldrey et al., 2016].

After this initial spin-up phase with HadGEM3-GC3.1, a successor phase was prepared using an ocean-only configuration of a UKESM1 prototype (run ID u-aj588). The ocean physical state of this (i.e. ocean, sea-ice, icebergs) was initialised using the model state at end of year 30 of the preceding GC3.1 simulation. The ocean biogeochemical state was initialised using observationally-derived fields from the World Ocean Atlas 2009 (WOA09; Garcia et al. [2010a]; Garcia et al. [2010b]) and Global Ocean Data Analysis Project v1.1 (GLODAPv1.1; Key et al. [2004]) climatologies. Fields of dissolved inorganic nitrogen (DIN), silicic acid and dissolved oxygen were drawn from WOA09, while pre-industrial DIC and alkalinity were drawn from GLODAPv1.1. Following Yool et al. [2013], the fields of DIC and alkalinity from GLODAPv1.1 were modified to interpolate over large regional lacunae in the original climatology (the revised GLODAPv2 climatology was not fully available at this time; Lauvset et al. [2016]). Note that although older climatologies were used to initialise run u-aj588, subsequent evaluation primarily uses their revised and updated equivalents, World Ocean Atlas 2013 and GLODAPv2.

Once initialised, this ocean-only configuration was run under repeated cycles of the initial atmospheric forcing data for a total of 1890 years (i.e. 63 cycles of 30 years; run IDs u-aj588 and u-ak900). During this initial, extended period of spin-up, a difference in the bulk formulae for atmosphere to ocean momentum flux between the coupled UKESM1 and the ocean-only configuration was found. Changing this calculation so the ocean-only model mimicked the coupled model calculation led to the updated ocean-only run u-an869. However, because of the long duration of the initial ocean-only phase, and a consistent "direction of travel" in the carbon cycle, this subsequent phase (u-an869) used the end state of the initial phase (u-aj588) for its initial condition. This new ocean-only phase also allowed an update to the atmospheric forcing that was taken from a longer duration spin-up of the UKESM1 prototype, again using a 30-year period.

This subsequent phase was run for a further 2905 years (96.5 cycles; including run ID u-ar538). During this ocean-only phase, trial simulations of the full coupled ESM, initialised using ocean states drawn from the ocean-only spin-up, found that the two modes were comparable – though not identical – in terms of their evolving ocean properties and in net air-sea CO_2 flux, with these test coupled runs typically reaching an equilibrated state within 150 years. During this ocean-only phase net air-sea CO_2 declined to less than 0.1 Pg C y^{-1}, as desired. Upon reaching this CO_2 target, spin-up was switched from ocean-only mode to coupled Earth system mode.

Having determined the ocean-only configuration had reached a near-equilibrium state, these ocean conditions were used to initialise the coupled ESM, which ran for a further 500 years of spin-up before the start of the CMIP6 piControl. The first 300 years of this coupled spin-up used the faster UKESM1-CN configuration of the model to maximise the equilibration of the ocean and terrestrial biosphere in the available time. This UKESM1-CN configuration differs from the full UKESM1 model by using prescribed chemical oxidants taken from a parallel UKESM1 pre-industrial run, but is otherwise identical; see Appendix A of Sellar et al. [2019] for details.

The fully-coupled model required some science changes during this final coupled spin-up to address important biases, many of which emerged as a result of coupling components which had previously been spun up separately. These changes are extensively described in Section 3 of Sellar et al. [2019]. The magnitude and impact of these changes decreased as the spin-up progressed, and the last 200 years were performed with the final UKESM1 science settings, and with the full-complexity model configuration (e.g. interactive atmospheric chemistry now included).

In parallel to the ocean spin-up, there were separate spin-up phases for terrestrial biogeochemistry and atmospheric chemistry, prior to their introduction into the main spin-up simulation (Figure 2). The land state, and in particular forest cover and the soil carbon and nitrogen pools, takes many hundreds of years to equilibrate with the surface climate and carbon fluxes. Some aspects of land cover, such as grass cover, equilibrate relatively quickly, so initial priority was therefore given to improving simulation of slower equilibrating aspects, such as forest cover and soil carbon, with subsequent tunings applied to the grass plant functional types and snow-vegetation interactions. However, as the whole system is interactive, changes in grass colonisation affects soil carbon and nutrients which, in turn, feeds back on vegetation productivity. The land was initially spun up in a 1000-year offline simulation of the JULES land surface model, driven by surface forcing from a GC3.0 simulation, a prototype of fully-coupled UKESM1. This land-only phase was, itself, initialised using the land state from a land-only simulation run in excess of 10,000 years using CRU-NCEP reanalysis forcing as derived for the Global Carbon Project [Le

Quéré et al., 2018]. Prior to this, the land model was run in excess of 10,000 years using CRU-NCEP observation-based meteorology from the Global Carbon Project. Similar to the ocean-only spin-up, this approach considerably reduces simulation cost. The land system underwent a further 665 years of coupled UKESM1-CN spin-up, including the implementation of final tunings, before being used to re-initialise the land state for the final, 200 year UKESM1 spin-up phase. Thus, the terrestrial BGC fields experienced 865 years of coupled spin-up in total, following the initial 1000 year offline spin-up.

Atmospheric timescales (ranging from minutes to tens of years) are much shorter than those of the land and ocean. Nevertheless, a coupled spin-up of 230 years was performed prior to the resulting atmospheric state being combined with the evolving ocean and land states to initialise a final 200 y period of coupled UKESM1 spin-up. This extended duration was required because of solar radiation and surface temperature differences between UKESM1-CN and UKESM1 that impacted the land carbon and nitrogen pools. It also served to avoid any impacts on the model's climate which might arise if the chemical tracers were far from equilibrium with the other components at initialisation. The atmospheric chemical tracers therefore experienced 410 years of pre-industrial coupled simulation during the spin-up (as did the rest of the atmosphere component).

In summary (with reference to Figure 2), the separate ocean and land spin-up states were combined into a single model initial condition after, respectively (4800 + 230) years of ocean spin-up and (1000 + 710) years of land spin-up. After a further 80 years of coupled integration, atmospheric chemistry fields were also combined with the evolving land and marine 3D fields, providing a final initial state for a further 200 years of coupled UKESM1 spin-up. We deemed the spin-up to be complete when this adjustment amounted to a multi-decadal land carbon flux of less than 0.1 Pg C y^{-1} (averaged over a century), as recommended in the C4MIP experimental protocol noted already Jones et al. [2016].

This simulation then initialised all components of the UKESM1's piControl simulation, from which pre-industrial initial states were drawn for the CMIP6 historical ensemble (see the CMIP6 implementation paper of Sellar et al. [2019]).

2.3 Analysing the UKESM1 spin-up

The complexity of UKESM1 means a complete evaluation needs to be spread over several dedicated studies. Such studies to date include atmospheric chemistry in Archibald et al. [2020] and aerosols in Mulcahy et al. [2018]. The physical climate model that underpins UKESM1, HadGEM3, is assessed at the same atmosphere-ocean resolution in Kuhlbrodt et al. [2018]. Meanwhile, an overview of the entire model, analysed for the near-present using the CMIP6 historical ensemble, is provided by Sellar et al. [2019].

Evaluation here is focused primarily on the spin-up period itself to analyse the equilibration pathway of key climate-relevant properties. The model state of the piControl simulation – the end point of spin-up – is then briefly analysed to evaluate the scientific performance of UKESM1. This is done across the point from which the piControl is first used to initialise CMIP6 Historical simulations. Evaluation of the piControl focuses on the slow timescale variables that need to be spun-up. The piControl continues beyond this point as a reference simulation for all other CMIP6 experiments.

The selection of the piControl somewhat complicates model evaluation since most target fields only have near-present day observations available. Such data contains signals of ongoing anthropogenic climate change that are absent in the pre-industrial period that the piControl aims to represent. In the case of the deep ocean, one focus of the spin-up described here, these signals are relatively minimal or absent, but they are manifest in the surface ocean, the atmosphere and the land, although natural or background processes are arguably still dominant for numerous variables. As such, intercomparison with observations is still informative, so long as differences are appropriately interpreted. Sellar et al. [2019] provides comparisons of UKESM1 at Historical period time-points aligned with modern observations.

The specific observational datasets used for evaluation include:

- World Ocean Atlas 2013, for ocean physics (interior; Locarnini et al. [2013]; Zweng et al. [2013]) and biogeochemistry (interior, surface; Garcia et al. [2014]; Garcia et al. [2014]) fields
- Hadley Centre Sea Ice and Sea Surface Temperature [Rayner et al., 2003], for ocean SST and sea-ice fields
- Sea-Viewing Wide Field-of-View Sensor (SeaWiFS; O'Reilly et al. [1998], for surface ocean chlorophyll concentration

- Oregon State University Ocean Productivity group, for VGPM [Behrenfeld and Falkowski, 1997], Eppley-VGPM [Carr et al., 2006] and CbPM [Westberry et al., 2008] vertically-integrated primary production
- Global Ocean Data Analysis Project v1.1 [Key et al., 2004] and v2 [Lauvset et al., 2016], for interior and surface carbonate biogeochemistry
- Estimating the Circulation and Climate of the Ocean (ECCO) V4r4 (Forget et al. [2015]; Fukumori et al. [2019]), for ocean circulation
- Smeed et al. [2017] for RAPID time-series measurements of the Atlantic meridional overturning circulation at 26°N
- Poulter et al. [2015] for plant functional type classification
- Loveland et al. [2000] for global land cover characteristics

In addition to the above, model-observation intercomparison makes use of multi-annual periods throughout, rather than focusing on a single year. This aims to account for both interannual variability in the case of synoptic observations for which we have good observational data (e.g. satellite-derived surface fields), and the representative timeframes associated with composite observational datasets that are assembled over time (e.g. point samples of the ocean interior). Observational products differ in their availability and reference periods, but in general are available from the late 20th century, and typically used here for the period 1995 to 2010.

3 Results

3.1 Time evolution of the spin-up simulations

In the following, time-series analysis focuses initially on the ocean spin-up branch because of its extended duration. Time-series analysis of the land- and atmosphere branches (per Figure 2) focuses on periods closer to the start of the piControl when these shorter branches have merged with the ocean branch.

The panels of Figure 3 (and Supplementary Figure S1) track key physical properties over the full duration of the ocean branch of the spin-up. The panels break the spin-up into sections coloured according to different run modes: two ocean-only phases, a coupled UKESM1-CN phase, a fully-coupled UKESM1 phase, and a final section that corresponds to the formal CMIP6 DECK piControl. Supplementary Table S1 presents the full list of run IDs associated with the spin-up period depicted, with some continuous phases actually split between several run IDs. In each case the panels in Figure 3 present the 30-year rolling averages of the properties, together with the corresponding 30-year interannual range.

In terms of volume-averaged ocean bulk properties, while – unsurprisingly – neither exhibit large interannual variability when averaged globally, both temperature and salinity experience long-term drifts across ocean-only and fully coupled phases, and it is noticeable that the trends in the ocean-only phase are reversed (at least somewhat) during the coupled phase.

In the case of volume-averaged temperature (Figure 3, row 1), an upward drift of approximately +0.06°C ky^{-1} during the ocean-only phase flips to a downward drift of approximately -0.25°C ky^{-1} when UKESM1 transitions to fully coupled simulation. For salinity (Supplementary Figure S1), a slight upward drift of +0.0015 PSU ky^{-1} is approximately reversed in the transition between ocean-only and fully coupled phases.

In the ocean-only phase, the small salinity trends are related to strong surface salinity relaxation and water flux balancing, while in the fully coupled phase they reflect the conservation of water across the modelled Earth system. Meanwhile, modest drift in the heat content of the ocean-only phase is explained by the use of repeating surface forcing derived from a period of GC3.1 coupled spin-up simulation that exhibited a +0.2 W m^{-2} global mean, top-of-atmosphere (TOA) radiation imbalance (downward directed) under which the ocean warms. Disequilibrium creates a situation in which the upper boundary of the ocean is consistently driven in one direction. The switch to fully coupled UKESM1 (in which the global mean net TOA radiation balance is effectively 0 W m^{-2}) permits a correction of this, as the slightly-too-warm ocean can then properly exchange heat with the dynamic overlying atmosphere. In short, the excess heat gained by the ocean during the ocean-only spin-up is lost again during the coupled phase of spin-up.

The panels of Figures 3 and **??** showing the corresponding surface quantities indicate more distinct behaviour for temperature and salinity. The former finds comparable ocean-only and coupled phases once the bulk formulae are harmonised across the two model configurations. The latter shows surface salinity returning to its observationally-derived initial value after a prolonged period of lower salinity during ocean-only spin-up.

Unlike the full-ocean averages of temperature and salinity, northern and southern sea-ice areas (Figure 3, row 2) are highly dynamic, with large interannual variabilities across both ocean-only and fully coupled phases. In the coupled model, this variability in sea-ice area shows marked multidecadal patterns. In the ocean-only phase, sea-ice trends in both hemispheres quickly equilibrate ($<$ 100 y) under the repeating atmospheric forcing, albeit to slightly different averages between the forcings used. In the fully coupled phase, interannual variability is comparable in magnitude in the north, but noticeably larger in the south, and does not appreciably settle down in either hemisphere during the (short) duration of the fully coupled phase. Sea-ice area and its seasonality is discussed further later.

Finally, row 3 of Figure 3 shows two important metrics of ocean circulation, the Atlantic Meridional Overturning Circulation (AMOC) at 26°N and the Antarctic Circumpolar Current (ACC) transport through Drake Passage. The AMOC characterises the poleward flow of warm water in the North Atlantic, playing both an important role in heat transport and the conditioning of water masses leading to deep water formation in the subpolar Atlantic [Smethie et al., 2000]. Since 2004, the AMOC has been well-observed by the RAPID array at 26.5°N, with an annual average ranging between 14.6–19.3 Sv [Smeed et al., 2017]. Drake Passage is a "pinchpoint" for the circular ACC that rings Antarctica, with a role in framing the continent's isolated and cold climate, and in climate variability modes such as the Southern Annular Mode (SAM) [Majewski et al., 2009]. The ACC is balanced by the meridional density gradient throughout the depth of the ocean, which, in turn, is set up by the wind and buoyancy forcing at the surface [Meredith et al., 2011]. While not permanently instrumented like the AMOC, Drake Passage is intermittently sampled, with its transport estimated at 173 ± 11 Sv [Donohoe et al., 2016].

UKESM1's pre-industrial AMOC is typically lower than that found by RAPID, but it necessarily omits the present-day greenhouse gas (GHG) and aerosol forcing. By contrast, all UKESM1 runs over the historical period simulate an AMOC that strengthens by approximately 2 Sv to a maximum of around 17 Sv in the 1990s Sellar et al. [2019]. This is almost certainly linked to northern hemisphere aerosols changing the simulated inter-hemispheric energy gradient, cooling the north relative to the south, with AMOC strength responding to this.

During the first portion of the ocean-only phase ("Ocean 1" in Figure 3), both the AMOC and Drake Passage transport are at the bottom end of their observed ranges, and at significantly lower values than those found in the corresponding coupled UKESM1 precursor that provided the atmospheric forcing. As noted earlier, investigation of this uncovered a discrepancy in the bulk formulae used in the transfer of momentum between the atmosphere and ocean, with the ocean-only model following that of CORE [Large and Yeager, 2009] and the coupled model following COARE 3.5 [Edson et al., 2013]. This was rectified in the subsequent, longer portion of ocean-only spin-up where the coupled model formulation was used ("Ocean 2" in Figure 3). Nonetheless, we retained the first portion of spin-up because we judged that it achieved an ocean carbon state that was closer to equilibrium than the initial state in spite of this discrepancy.

A potential issue in using distinct ocean-only and fully coupled spin-up phases is a mismatch in the behaviour of the model between these phases. In ocean-only mode, the ocean model experiences the atmosphere as unchanging forcing, in fully coupled mode, the ocean model dynamically interacts with the overlying atmosphere, potentially modifying the evolving atmospheric forcing. Broadly mirroring Figure 3, Figure 4 compares the behaviour of both phases for physical properties across a 200 y period from the time point at which the coupled phase branches from the ocean-only phase with the coupled ocean initialised using the ocean-only state. Although the ocean-only phase is generally equilibrated at this point, to more clearly evaluate the significance of this transition, it was continued past this branch point.

In the case of temperature (Figure 4, row 1) and salinity (Supplementary Figure S2), the volume-integrated panels show the differences between the equilibrium values to which the two phases have converged, or are converging. At the surface, SST in the coupled phase remains close to that of its ocean-only parent (with larger interannual variability), while SSS quickly (< 100 years) equilibrates at a slightly higher value (though with similar interannual variability; see Supplementary Figure S2).

In the case of sea-ice (Figure 4, row 2), the coupled phase very quickly shows larger interannual to interdecadal variability, but the longer-term behaviour takes a more extended period to manifest (visible in Figure 3). The difference between the two spin-up phases is more obvious in the case of southern hemisphere ice, where the cyclic 30-year forcing period used in the ocean-only phase precludes the large multidecadal variability exhibited by the coupled model.

The pattern of increased variability in southern sea-ice closely corresponds to that of variability of coupled mode Drake Passage transport in row 3 of Figure 4. Here, high transport is associated with reduced sea-ice area, and vice versa, with the two properties connected via periodic deep ocean mixing off Antarctica influencing the latitudinal gradient of the ocean density field across the Southern Ocean and the Antarctic sea-ice extent in a coherent manner (as discussed by Latif et al. [2013]; de Lavergne et al. [2014]). In the ocean-only phase, ACC interannual variability is low (< 10 Sv), but grows quickly as the coupled phase begins, reaching almost 40 Sv within the time period shown. As Figure 3 shows, this magnitude largely persists during the piControl simulation, with strong centennial-scale variation in Drake Passage transport.

The change between spin-up phases is more slight for the AMOC, and after an initial shock (< 100 years), the AMOC between the two phases remains similar (Figure 3). And, unlike the relationship between Drake Passage transport and southern sea-ice, the AMOC's relationship with northern sea-ice is less clear. As noted, AMOC strength is related to the inter-hemispheric energy gradient Marshall et al. [2014]. Poleward heat transport driven by a strong AMOC might be expected to correlate with increased melt of northern sea-ice. However, AMOC strength at 26°N does not show such a clear correlation because the underlying relationship is more complex. For example, northern hemisphere cooling, relative to that in the south, can act to both directly increase Arctic sea-ice, and intensify the meridional energy gradient, leading to a strengthening of the AMOC, which can negate the direct cooling influence on sea-ice decrease. Furthermore, AMOC strength is also influenced by buoyancy and freshwater fluxes out of the Arctic, which impact the occurrence of deep water formation Liu et al. [2019].

Across the ocean's physical parameters, the ocean-only and coupled phases do show similar patterns and magnitudes of variability. There is limited evidence of strong shocks as the model's state branches, and most properties quickly adjust, although the ocean's different equilibrium heat content between the phases manifests in the change of inflection of long-term drifts. Nonetheless, the prescribed 30 y atmospheric forcing in the ocean-only phase clearly prevents the model from reproducing the longer-term modes visible in the fully coupled phase, most noticeably in the circulation of the Southern Ocean.

Remaining with the ocean, Figure 5 shows corresponding spin-up time-series for several key marine biogeochemistry metrics, over both the full period of the ocean branch spin-up, and for the same 200 y overlapping period for the ocean-only to fully coupled transition.

As already noted, the most significant features of this spin-up branch lie with how the two periods of ocean-only spin-up differ in response to a change to the formulation of surface momentum exchange. In the intergrated primary production panel, addressing this discrepancy results in a global increase of 15%. The mechanism for this large increase lies in the increased momentum transfer, which can be seen in row 2 of Figure 5 to deepen average mixed layer depth (47 m to 50 m), leading to elevated surface DIN concentrations that fuel productivity. This change between the ocean-only phases is markedly larger than the 4% decrease in primary production driven mainly by an 8% decrease in aeolian deposition of iron as the 30 year cycle of dust forcing becomes dynamic in the fully coupled simulation. It is also noticeable that the model's productivity response to such transitions requires a longer period to equilibrate than seen for the earlier physical properties. Here, periods of at least several hundred years, and approaching 1000 y, are necessary for the model to reach a new quasi-steady state. Nonetheless, despite only a 30 y cycle in forcing during the ocean-only stages, the interannual variability of productivity is similar, though slightly greater, to that in fully coupled UKESM1. This can also be seen in intercomparison of the 100 y sections of ocean-only and fully coupled simulation.

Bar a short initial period of ingassing, net air-sea exchange of CO_2 is, on average, outgassing across the entire spin-up and into the piControl. Interannually, both ingassing and outgassing occur, but the long-term trend is to steadily outgas as equilibrium is approached. As already mentioned, an initial target for average net air-sea flux was 0.1 Pg C y^{-1}, and this was reached after around 3500 y, during the ocean-only stage of spin-up. By the start of Historical ensemble simulations, an annual average outgassing flux of around -0.04 Pg C y^{-1} had been reached, with a multi-centennial range of approximately -0.35 to 0.25 Pg C y^{-1}. Due to the repeating 30 y cycle of surface forcing (e.g. wind-driven piston velocity), progress towards this equilibrium is steadier during the ocean-only phase (with the exception of the jump between ocean-only stages), although the range of interannual variability is very similar between ocean-only and fully coupled phases. The continuous outgassing of CO_2 from the ocean is indicative of a model bias in ocean carbon content and is discussed in more detail later.

The bottom two panels of Figure 5 show how productivity and air-sea exchange vary interannually across the transition between the ocean-only and fully-coupled phases. While there is a slight offset in primary production between these phases, the modelled variability is otherwise largely consistent. The same is true for air-sea CO_2 flux, for which both phases oscillate interannually around near-zero net flux. Overall, and much as with the model's physics, the differences between the two spin-up modes are relatively minor.

Together with the physical responses shown in Figure 4, these results indicate that the coupled model largely adjusts to a new equilibrium after around 150 y, even when its ocean is initialised from the end of an ocean-only simulation.

Finally, switching to the terrestrial system, Figure 6 illustrates the spin-up pathway of the carbon reservoirs in living biomass and soil, and the global fractional cover of three major aggregate land surface types: forests, grasslands and bare soil. Unfortunately, due to archiving issues not all of the model data are available. Any data gaps, however, occur earlier than 500 years before the piControl, so do not affect our evaluation of the model's final equilibrium state. The land spin-up branch began with the land surface model being run offline under 30-year cycles of meteorological data drawn from a prototype of UKESM1. The land-model was run for approximately 1000 years offline until the globally-averaged vegetation cover and carbon and nitrogen pools (results not shown) reached a quasi-equilibrium state. These were then used to initialise the coupled model at timepoint #1 of Figure 6. As is evident from the immediate drift the land-model run offline has a different stable state to the coupled model, reflecting the importance of land-atmosphere coupling and differences in meteorology to the forcing used offline. Subsequently, after further 30 years at timepoint #1 (Figure 6), the turnover rate parameters were scaled to lower values to increase the size of the soil carbon and nitrogen pools. At the same time, the soil carbon and nitrogen pools were rescaled to be consistent with these turnover rate changes. The spin-up of the vegetation fractions continued with an additional tuning applied to the rate at which grass can expand and colonise bare ground, which was reversed at timepoint #2 (Figure 6). The result was a rapid decrease in grass cover and concurrent increase in bare soil over a 10-year period. Over the course of the next 600 years the spin-up continued with some changes made to parameters controlling snow-vegetation interaction and the rate of grass colonisation resulting in a close to stable global mean state at the start of the final spin-up at timepoint #3 (Figure 6). The drifts in soil and vegetation carbon over the course of the piControl were -0.07 and 0.0025 Pg C y^{-1} respectively over the first 1000 years of the piControl, well within the C4MIP acceptable range. The drift in tree cover is also small at less than 0.5% over 1000 years.

Although the global drift may be small, it can be more significant at the regional level, particularly if some regions are compensating for changes in carbon or vegetation cover in other regions. Figure 7 shows the drift in soil carbon across seven major biomes for the final part of spin-up and the piControl. The drift in most biomes is less than 0.001 Pg C y^{-1} with the exception of the tundra, boreal and desert regions. Tundra and boreal regions lose soil Carbon at -0.012 and -0.017 Pg C y^{-1} of carbon per year respectively. This reflects the particularly long residence of soil carbon in these regions and therefore the greater time required for the pools to equilibrate. The desert regions continue to accumulate carbon at 0.002 Pg C y^{-1} responding to changes made during the spin-up phase to grass colonisation rates and therefore the flux of litter to the soil carbon. The pools also demonstrate some long-term variability. For instance across the 250 years corresponding to the first Historical ensemble member, the Savanna biome accumulates 3 Pg C despite having lost carbon during the preceding spin-up period. Consequently, we recommend that any analysis accounts for both the ongoing drift in terrestrial carbon pools and the multi-annual variability. Further, our regional drifts imply that benchmarking global drift pools is a necessary but possibly insufficient condition for evaluating the equilibration of land carbon models. Future spin-up efforts may wish to execute longer spin-ups in order to equilibrate all regions and ecosystems.

The atmosphere adjusts rapidly (over days or weeks) to a changed external forcing, such as associated with different sea surface temperatures or incoming top of the atmosphere (TOA) solar radiation. We therefore, are generally not overly concerned with the spin up of atmospheric variables when bringing ESMs into balance with a pre-industrial forcing. Nevertheless, one of the primary constraints used to evaluate ESM simulations of the pre-industrial period is that, averaged over sufficiently long timescales, the global mean net TOA radiation balance should be zero (0 W m^{-2}). This was a leading constraint used in developing UKESM1. A consequence of a zero TOA net radiation balance is that, also averaged over sufficiently long timescales, the global mean energy content of the climate system should be temporally stable. As ocean heat content constitutes the overwhelming majority of energy in the climate system Trenberth et al. [2014], this constraint equates to a temporally stable global mean ocean heat content. Observational constraints of the absolute value of the pre-industrial ocean heat content are not available, neither are constraints on the component, solar (shortwave) and Earth-emitted (longwave), TOA radiation fluxes. Observational estimates of global mean TOA radiation components and ocean content do exist for present-day conditions, albeit with non-negligible uncertainties (Loeb et al. [2009]; Stephens et al. [2012]; Cheng et al. [2017]). However, both estimates include an anthropogenic component. Observational estimates of pre-industrial (more correctly the very early industrial period, e.g. 1850 to 1900) global mean surface air temperature (GSAT) do exist (e.g. HadCRUT4, Morice et al. [2012]; GISSTMP, Lenssen et al. [2019]), although observation coverage is limited during this early period. With this in mind, our primary targets for the UKESM1 pre-industrial atmosphere are: a near-zero global mean net TOA radiation balance and a temporally stable GSAT, close to observational estimates for the 1850-1900 period. As a consequence of these two constraints, temporally stable Arctic and Antarctic mean sea ice amount and volume is also a useful constraint.

Figure 8 summarizes these quantities over the final 500 years of the coupled spin up. The first 300 years of this run uses UKESM1 with offline atmospheric chemistry (referred to as UKESM1-CN), with ozone and chemical oxidants prescribed from an earlier pre-industrial simulation of UKESM1 with interactive chemistry. The latter 200 years are with interactive atmospheric chemistry enabled. The simulation is initialized at year minus 500, in the ocean by fields derived from the ocean-only spin up (u-ar538) and on land and in the atmosphere using fields from the parallel land-spin up run of UKESM1-CN (shown in Figure 8). At year minus 200, interactive atmospheric chemistry is activated and the required chemistry fields initialised based on output from the parallel "UKESM1 spin-up for atmospheric chemistry" run shown in Figure 8. All other prognostic fields are propagated from the UKESM1-CN spin up run (u-ar783 → u-au835, years -500 to -200) into the final UKESM1 spin-up (years -200 to 0).

The primary spin-up characteristic in Figure 8 is an increase (of 1 Wm-2) in both global mean TOA net downward solar (SW) and outgoing longwave (LW) radiation, leading to a near-zero, global mean net TOA radiation budget at year 0 (the start of the piControl simulation). This shift clearly occurs at the point when UKESM1-CN switches to include interactive chemistry (UKESM1) and results from two differences between these model configurations: (i) in the manner marine-emitted DMS is processed through to cloud condensation nuclei (CCN) in the model atmosphere, and (ii) in the simulation of stratospheric ozone. Both differences influence the absorption and reflection of solar radiation and therefore net TOA solar radiation. As a result of these differences, and to retain a near-zero global mean net TOA radiation balance as we transitioned form offline to interactive chemistry, it was necessary to introduce a small tuning to the parameterization of seawater DMS in UKESM1 (see Sellar et al. [2019] for more details). This tuning acted to reduce seawater DMS in biologically inactive regions of the global oceans, reducing the average cloud droplet number in marine clouds and thereby reducing the simulated atmospheric solar reflectivity and retaining the desired near-zero net TOA radiation balance (-0.09 W m^{-2} downward; Sellar et al. [2019]).

From the start of the UKESM1 piControl (year 0 on Figure 8), slower timescale variability in GSAT appears to largely disappear, in concert with a reduction in the variability of Antarctic sea ice. In the early part of Figure 8 these variables exhibit an inverse correlation, driven by variability in ocean overturning in the far Southern Ocean (as discussed earlier). While it is tempting to conclude the final coupled tuning reduced this internal variability, we note that similar timescale variability does intermittently reappear in later periods of the full UKESM1 piControl. Finally, long-term mean GSAT during the first 200 years of the piControl is around 287.5K (13.35°C), suggesting a cold bias of 0.3-0.4°C in UKESM1 compared to available observational estimates for the period 1850-1900 (Morice et al. [2012]; Lenssen et al. [2019]).

3.2 Equilibrium state

We now analyse the equilibrium state that results from the confluence of all three spin-up branches, focusing on the UKESM1 piControl simulation from the point at which CMIP6 Historical ensemble members begin to be drawn. This time-point occurs early in the piControl simulation but at a point where UKESM1 was judged to be sufficiently equilibrated. The strategy for using the piControl as the source for the Historical ensemble, and additionally its role in controlling for model drift, is described in detail by Sellar et al. [2019]. We use a decadal climatology of the piControl from this point throughout.

3.2.1 Ocean

Figure 9 compares simulated sea surface temperature (SST) with the HadISST observation-derived product, HadISST, for the period 1870-1879 [Rayner et al., 2003]. This period is chosen as it is closest to that which the piControl simulation aims to represent (1850), but note that HadISST is a data-assimilated reanalysis product with relatively limited observational constraint for this time period (but see Supplementary Figure S3).

Northern and southern summer periods are shown, together with the differences between the model and observations. In general terms, the model shows very similar patterns to those observed, both geographically and seasonally. Nonetheless, the difference plots show persistent biases in the model, including a warm Southern Ocean, warm upwelling regions and strong cold bias in the western North Atlantic. The latter feature is the most pronounced of a series of zonal, dipole-like biases in the North Atlantic, which include warm biases off the eastern seaboard of North America and in the Irminger / Iceland basins, and a cold bias in the Greenland-Iceland-Norwegian (GIN) Sea.

In the case of the Southern Ocean, this warm SST bias is primarily driven by a corresponding positive bias in downward shortwave radiation that originates in cloud biases (i.e. in cloud amount and albedo). The warm SST biases in upwelling regions are principally a result of the relatively coarse resolutions of UKESM1's ocean and atmosphere components. In the ocean, the model cannot represent the necessary small-scale features of coastal upwelling, while in the atmosphere, coastal wind forcing cannot be resolved. The root of the North Atlantic dipole bias has a similar cause, with resolution causing the separation of the Gulf Stream from the eastern seaboard of North America to occur too far south, resulting in a path that is too zonal Kuhlbrodt et al. [2018].

Figure 10 illustrates the seasonal extents of northern and southern sea-ice, again compared to the same period of HadISST (but see Supplementary Figure S4). In the Arctic, modelled sea-ice extent is always greater than that observed, with the excess ranging between 1–4 10^6 km^2 seasonally, but greatest around the annual sea-ice minimum. By contrast, in the Antarctic, it is the simulated minimum sea-ice extent that most closely matches that observed, but modelled sea-ice growth is conspicuously weaker, leading to a maximum extent only around two-thirds of that observed. These patterns of sea-ice biases generally align with the SST biases in the GIN Sea (cooler) and Southern Ocean (warmer).

Switching to focus on the ocean interior, Figure 11 illustrates the biases of temperature and salinity within the ocean, again compared to the WOA. In each case, the plots present so-called "thermohaline circulation" sections that centre the zonal averages of both major basins around the interconnecting Southern Ocean (see Figure 11 for more details).

In the case of potential temperature, UKESM1 shows a general warm bias in the upper 3 km, a smaller cold bias below this. This pattern differs between basins, with the Atlantic showing a much stronger bias, particularly in the upper 1 km of the subtropics (30°S–30°N), where it can exceed 4°C. The corresponding region of the Pacific generally shows a cool bias, although with a more complicated structure. Despite the marked warm bias in its surface waters noted earlier, the Southern Ocean shows generally weaker biases, particularly in its main Pacific sector. Similarly, the salinity biases in UKESM1 broadly track those of temperature, with a similar strong positive bias in the subtropical Atlantic, and a negative bias in the subtropical Pacific.

Moving to ocean circulation, Figure 12 shows the global streamfunctions of meridional overturning circulation (MOC) for the model and the observationally-derived Estimating the Circulation and Climate of the Ocean (ECCO; Forget et al. [2015]; Fukumori et al. [2019]) product. Qualitatively, the simulated MOC broadly follows that observed, with a strong positive cell focused in the upper water column, driven by the AMOC, and a weaker negative cell at depth, driven by Antarctic Bottom Water formation. Compared to that in ECCO, the model exhibits a slightly weaker Deacon Cell centred around 50°S [Döös and Webb, 1994], indicative of weaker surface wind stress over the model's Southern Ocean. The maximum strength of the model's deep AABW cell is also weaker than estimated in ECCO. Supplementary Figure S5 shows the corresponding simulated MOC patterns for the Atlantic and Indo-Pacific sections. In the Atlantic strong northward flow in the surface of the Atlantic is balanced by the production at high latitudes of NADW that flows southward at depth, and overlies an Antarctic Bottom Water (AABW) cell driven from the Southern Ocean. However, while the strength of this northward flow is similar to that observed as noted earlier (cf. Figure 3), circulation of the large AABW cell underlying the NADW in the Atlantic is very weak (especially when compared to the corresponding cell in the Pacific). As noted in Figure 11, this cell is characterised by cool and fresh biases that are indicative of a Southern Ocean origin. While this pool is fed in part by Antarctic Bottom Water (AABW), it shows biogeochemical properties that are suggestive of a more sluggish transport than typical for this watermass (see later).

Switching to marine biogeochemistry, Figure 13 shows model-observation intercomparison of three fields of key properties: surface nitrogen nutrient, surface chlorophyll and vertically-integrated primary production. In each case, these fields are annual averages, with the nutrient field drawn from the present-day climatology of the World Ocean Atlas 2013 [Garcia et al., 2014], and the lower two fields from the period 2000-2009.

Row 1 shows DIN, the main limiting nutrient for biological productivity across the World Ocean. The general pattern of higher values in upwelling regions and at higher latitudes, particularly the Southern Ocean, and low values in ocean gyre regions is simulated. However, the model does display a number of marked biases: concentrations are markedly elevated in and around equatorial Pacific upwelling, particularly in the adjacent South Pacific. These discrepancies stem from upwelling of excessively DIN-rich deep water, as is clearer from ocean interior concentrations (see later). These patterns of mismatch in MEDUSA-2.1 are very similar to those found previously by Yool et al. [2013] with MEDUSA-2 (despite a considerably longer period of spin-up).

Row 2 shows the observed and modelled surface chlorophyll concentrations [O'Reilly et al., 1998]. While, again, MEDUSA-2.1 captures the broad patterns of the observed field, agreement is much weaker, and the model displays a number of strong biases. Most clearly, simulated Southern Ocean concentrations are noticeably higher, with elevated concentrations also seen in Equatorial and subtropical Pacific concentrations, in keeping with the corresponding DIN excess availability. Away from the Pacific, oligotrophic gyre concentrations are much more biased downwards, with relatively large regions of very low chlorophyll in the subtropical Atlantic. Spatial patterns in this basin are also somewhat aberrant with a pronounced patchiness that is absent in the observations.

As noted by Yool et al. [2013] (and Kwiatkowski et al. [2014]), chlorophyll is generally poorly represented in marine biogeochemistry models, with models frequently performing much better for fields of other bulk properties (nutrients, carbon) and productivity. As well as its observed high dynamic range (note the plot log scale), Yool et al. [2013] suggest that this may stem from the strong plasticity (in reality and in models) of chlorophyll:carbon ratios relative to other quantities, and the resulting high dynamic range.

Finally, row 3 shows vertically-integrated net primary production, with observations represented by the simple average of three observationally-estimated products, VGPM [Behrenfeld and Falkowski, 1997], Eppley-VGPM [Carr et al., 2006] and CbPM [Westberry et al., 2008]. Although this is empirically derived from satellite chlorophyll (as well as other fields), MEDUSA-2.1's agreement with it is greater than for surface chlorophyll. The observed patterns of low and high values are generally reproduced, again with biases. These include excessive productivity in the Southern Ocean throughout the year, more latitudinally-focused productivity in the equatorial Pacific, and noticeably low productivity in the North Atlantic.

As discussed, one of the drivers for UKESM1's spin-up is equilibration of the marine carbon reservoir. Figure 14 compares the observed and simulated surface concentrations of DIC and total alkalinity [Lauvset et al., 2016]. DIC here is an observation-based estimate of pre-industrial DIC as this biogeochemical property has changed significantly since the beginning of the industrial revolution (especially so in the surface; Lauvset et al. [2016]). Modelled DIC concentrations generally show good agreement with the observed estimates, although model DIC is somewhat elevated in the Southern Ocean, while biased low in the Indonesian Archipelago and parts of the Arctic (although data availability remains somewhat limited in this region). While the patterns of model surface alkalinity are similar to those observed, alkalinity is generally lower in the model, and there are noticeable biases, particularly in the North Pacific and, again, the Indonesian Archipelago.

Since alkalinity acts in part as a buffering capacity for DIC, generally lower sea surface alkalinity will reduce the amount of DIC in surface waters, and, in turn, the ocean interior. The interior impacts can be seen in Figure 15 and Supplementary Figure S6, which respectively show DIC and alkalinity along thermohaline transect sections (see earlier). These show both lower alkalinity in the upper 1 km of the water column, and the correspondingly lower DIC throughout the ocean interior. This is most obvious in the southward-moving NADW and in the deep waters (> 1 km) of the North Pacific, where model bias can exceed 100 mmol C m^{-3}.

3.2.2 Land

Figure 16 presents a biome-based evaluation of land cover at the end of UKESM1 spin-up against two observationally-derived estimates, the IGBP and CCI products. The upper panel provides a geographical perspective of where different biomes are located, while the lower panel shows the fraction of each land cover type that occurs in each biome for the model and from the data products, keeping in mind that vegetation type, amount and geographical distribution are dynamically predicted in UKESM1. Overall, the model performs well, with simulated biomes largely capturing their observed compositions, although there are some biases. With the exception of the high latitude biomes, such as boreal forest and (especially) tundra, UKESM1 underestimates the observed fractional cover of C3 grasses. In tropical forest, it is largely replaced by broadleaf trees, while in extratropical forests and deserts its low bias is countered by a high bias towards C4 grasses. In the grassland and savanna biomes, where grasses are found to dominate, C3 grasses are displaced by forest, mostly by broadleaf trees in savanna and needleleaf trees in grasslands. C4 grasses, meanwhile, are typically biased positive, while modelled shrubs show mixed biases with observations across the biomes. In terms of bare ground (i.e. no vegetation cover), UKESM1 only shows a bias in the tundra biome where C3 grasses are overly abundant. As the IGBP and CCI products are assembled from present-day observational datasets, they include vegetation cover changes driven by human influences. At least in part, the land "biases" identified in UKESM1 are consistent with these changes in land cover, and therefore indicate the problem of evaluating a pre-industrial climate state using present-day observations.

Figure 17 complements Figure 16 by illustrating the geographical patterns of fractional cover of each land cover type. As noted, UKESM1 simulates excessive broadleaf forest cover and extent in the tropics, particularly in South America, but also in Africa and southeast Asia. However, UKESM1 does not include fire feedbacks, which may explain some of this overestimate. Inclusion of an interactive treatment of fire in other models [Hantson et al., 2016], as well as in our land surface scheme when driven by observed climate improves this type of vegetation bias [Burton et al. , 2019]. The geographical range of needleleaf forest is generally modelled well, though fractional cover is elevated in northern boreal forests, and there is an anomalous Asian forest in the vicinity of Tibet. As well as being biased low, the extent of UKESM1's C3 grasses is noticeably circumscribed, with almost no grasslands in southeast Asia, and reduced extents in Europe and the Americas. However, as already mentioned, UKESM1 does erroneously simulate solid C3 grass cover across northern Siberia. The geographical cover of C4 grasses is better than for C3 grasses, but there is a marked positive bias in Australia, as well as westerly displacements of their abundance in both the northern and southern Americas. Shrub cover is generally underestimated across the world, with exceptions only in Asia, again around northern Siberia and Tibet. Finally, UKESM1's patterns of bare soil generally map well to those observed. The exceptions lie in high northern latitudes, where tundra areas have excessive C3 and shrub cover in UKESM1.

4 Discussion

The new UKESM1 model has been jointly developed by NERC and the UK Met Office to represent the fully-coupled Earth system with a state-of-the-art level of realism. UKESM1 succeeds its CMIP5 predecessor, HadGEM2-ES, and while incorporating evolved forms of components from this earlier model, is almost a wholly new model. A particular effort was made to ensure that coupling between ES components and physical climate components was fully prognostic, enhancing the utility of UKESM1 for investigating future coupled ES feedbacks. As part of its preparations towards use in CMIP6, UKESM1 requires the production of a pre-industrial control state that can be used to initialise the DECK and other MIP experiments. Critically, this piControl should exhibit a near-steady state climate so that forced trends introduced to the model Earth system in various experiments are clearly distinct, and not confounded by model drift.

The primary components of the Earth system are its major reservoirs of heat and carbon – the atmosphere, the ocean and the land. The physical sizes of these components, and the timescales of the major processes that govern them, both physical and biogeochemical, mean that equilibration to achieve a steady state is necessarily prolonged relative to the perturbation experiments typically performed in CMIP6. Furthermore, the full ESM is computationally expensive to run, with a turnaround time of only a few simulated years per wallclock day. However, the most expensive component of UKESM1, the atmosphere and its attendant chemistry, is also the fastest to equilibrate. Consequently, the strategy adopted here was to spin-up the slow equilibrating components, the ocean and the land, decoupled from the atmosphere, and to only bring the full model together once much of their time evolution was complete.

In the case of the ocean, a period of 4800 years of ocean-only simulation was required to achieve a net air-sea CO_2 flux within the threshold suggested by the C4MIP community. In the case of the land, a corresponding period of 1000 years was used to bring the modelled reservoirs of carbon into the same net balance with the atmosphere. During both of these phases, the individual component models were run in forced mode, under an atmospheric dataset (bulk properties, heat and freshwater fluxes, winds) derived from simulations of precursor versions of UKESM1 run with preindustrial forcing. Subsequently, the model states from both component-only spin-up branches were combined with the atmosphere, and UKESM1's spin-up was finalised in fully-coupled mode, first with prescribed atmospheric chemistry (UKESM1-CN), and subsequently with interactive chemistry also activated.

The branch of ocean spin-up found relatively rapid stabilisation (<< 1000 y) of near-surface physical variables and major circulation metrics. Interior temperature and salinity, however, exhibit prolonged drift, which changes sign from ocean-only to coupled phases, although in the case of temperature, of very low magnitude compared to simulated trends over the Historical period [Sellar et al., 2019]. Biogeochemical processes, such as productivity and surface nutrients, typically had somewhat slower stabilisation (≈ 1000 y). Net ocean surface carbon flux, like interior temperature, essentially exhibited steady decrease over the spin-up, slowly reaching a net flux below the target threshold. Examination of interior carbon concentrations shows that this slow decline is a function of the marine biogeochemistry model "favouring" a slightly lower total carbon inventory, driven, at least in part, by a bias towards lower sea surface alkalinity (cf. Halloran et al. [2015]). A notable, if unwelcome, feature of the ocean-only phase of spin-up was a bulk formulae discrepancy that initially resulted in lower momentum transfer between the atmosphere and ocean in the ocean-only configuration compared to the coupled model. While this clearly affected the absolute magnitudes of properties across the model (Figures 3 and 5), this was amended without any significant lasting impact on the broad state of the ocean, with the subsequent revised period of ocean-only spin-up ultimately coming to more closely resemble that of the final, fully-coupled model. The transition between the ocean-only and fully-coupled phases was found to introduce a "kick" across the model, although the immediate effects of this were typically found to quickly (≈ 100 simulated years) settle, followed by slower evolution to a slightly different final coupled state, for some predicted variables.

Overall, the ocean-only spin-up compares well with that in fully-coupled mode. Inevitably, the modes and scale of variability exhibited in the ocean-only configuration are reduced compared to that of the fully coupled model (e.g. Drake Passage transport), partly because of the limited variability in the short period of atmospheric forcing used, but mostly because the absence of coupled responses between the ocean and atmosphere. In terms of model biases, several were noted in the ocean's physical and biogeochemical spun-up pre-industrial state, most significantly the carbon deficit already noted.

The inclusion of an interactive nitrogen cycle in UKESM1 has made for very a slow spin-up because of the interaction between soil and vegetation. The mineralisation of soil inorganic Nitrogen fertilises vegetation and encourages growth and the turnover and quality of vegetation litter affects the soil state. The spin-up of the model has through necessity gone hand in hand with the application of tunings and fixes as the model advances to being frozen and ready without the possibility of a long (in excess of 500 years) spin-up post-freeze. The computationally-efficient offline JULES model, forced using surface level atmospheric fields, was used initially for approximately 1000 years of spin-up. However, when subsequently coupled directly to the atmosphere the model's behaviour was found to differ, primarily because in the coupled model the change in vegetation state is able to feedback on the climate. The result is that an extended period of online spin-up is still required. Furthermore, the model shows some long periods of variability making it hard to assess the degree of drift whilst model integrations are proceeding.

One of the further challenges is deciding on an appropriate pre-industrial state given the general lack of observational data for the 1850s. We generally rely on present day data such as the landcover (Figure 16) and make informed assessments around the expected level of change over the past due to land-use change and the role of climate.

In UKESM1, we have achieved a near spun-up state for the ocean and land carbon pools well within the requirements of C4MIP for making assessments of carbon budgets for climate targets. However, as is shown in Figure 7 there can be significant regional drifts, which in some cases may oppose each other and give the impression of a better steady state. In UKESM1, the land is generally losing carbon driven by soil carbon losses in the Boreal and Tundra biomes. These are the regions with the slowest carbon residence times and therefore the most difficult to equilibrate. The high latitude losses are slightly offset by the small positive drift we see in the Savana biome. While both the land and ocean components are losing carbon to the atmosphere, its fixed pre-industrial CO_2 concentration masks this. However, in the fully-coupled emission-driven model, these net fluxes to the atmosphere would result in a positive drift in atmospheric CO_2. The spin-up of the emission-driven model is a separate activity that takes advantage of the more completely spun-up state from a later time point of the piControl.

In terms of the major Earth system quantities pertinent to anthropogenic change, the duration of spin-up in UKESM1 allowed these to reach quasi-equilibrium. After tuning (see Sellar et al. [2019]), net top-of-atmosphere radiation balance reached -0.09 W m^{-2} by the conclusion of UKESM1 spin-up, compared to the perturbed present-day net flux of approximately 0.61–0.81 W m^{-2} [Johnson et al., 2016]. Surface ocean temperature drift for the same spin-up period was 0.016 °C $decade^{-1}$, as compared with observation-based estimated ranges during the historical period of 0.042 to 0.054 °C $decade^{-1}$ (1880–2012) and 0.072 to 0.124 °C $decade^{-1}$ (1979–2012) [Hartmann et al., 2013]. Exchange of CO_2 between the atmosphere, land and ocean, reached net fluxes of 0.020 and -0.039 Pg C y^{-1} with the land and ocean respectively over the final century of spin-up, well below the C4MIP target of 0.1 Pg C y^{-1} sought [Jones et al., 2016].

In the preceding analysis of equilibration, the focus has largely concerned the exchanges of carbon between the land, ocean and atmosphere components of the model. Table 1 presents the linear trends in ocean properties at different depth horizons for the final 500 y periods of both the ocean-only and fully-coupled spin-up phases. While carbon fluxes fall below C4MIP's drift criterion (see Figures 5 and 6), it is clear that the ocean's state is still drifting, and that these drifts have generally increased with the transition from the long duration ocean-only phase to the much shorter duration fully-coupled phase.

As already noted, drifts in ocean temperature between these phases are a response, respectively, to a heat flux imbalance in ocean-only forcing, and the subsequent equilibrating response when fully-coupled. Trends in nitrogen and iron nutrients have levelled off during the long ocean-only phase, but have grown into the fully-coupled phase as dust-forcing both changes and becomes more dynamic. Opposite sense trends result in these two nutrients, and are much larger in the upper ocean where the change in iron is affected. Meanwhile, although the air-sea flux continues to equilibrates, drift in the ocean's surface carbon cycle is affected by a more dynamic hydrological cycle that increases surface alkalinity (tracking salinity; Jiang et al. [2014]), buffering higher DIC concentrations.

In general, model drift is greater at the surface than at depth, although this varies between properties, most obviously dissolved oxygen. Here, surface concentrations are essentially controlled by the temperature-dependent solubility of this gas, while interior concentrations are affected by remineralisation of sinking organic material. As noted previously, the fully-coupled phase has slightly lower production of organic material because of reduced dust deposition and greater iron limitation. In turn, this translates to elevating interior oxygen as less oxygen is consumed.

Overall, Table 1 underscores the difficulty in equilibrating ESMs, especially where spin-up modes such as ocean-only incompletely capture the behaviour of the fully-coupled model.

A number of lessons can be drawn from the experience of the spin-up of UKESM1.

Inevitably, biases occur across the model components, but a particularly marked bias is that of the ocean's dissolved inorganic carbon pool. As illustrated in Figure 15, UKESM1 shows a general deficit in ocean DIC concentration, together with patterns of bias that align with those in nutrients and oxygen. Some of these biases stem from deficiencies in modelled circulation, but MEDUSA-2.1's biogeochemistry plays a key role in others. While some minor tuning of model parameters took place during the development of UKESM1, no tuning to improve these interior ocean biases was undertaken, principally because of the timescales necessary (simulated and wallclock) to equilibrate changes to identify improvement [Yool et al., 2013]. As noted earlier, there are offline and accelerated simulation modes that can assist with this, although none were mature enough within the infrastructure of UKESM1 to be used during CMIP6 preparations. As such, a key lesson, and future aspiration for UKESM1, is the adoption of techniques for more rapid model equilibration, to facilitate both the identification and tuning-out of such biases.

Focusing on the component-only phases of spin-up, an obvious lesson lies in ensuring the interface exchanges between model components and the atmosphere are calculated in a manner consistent with that of the fully-coupled model. As the ocean results show, and drawing also from land-only preparations, inconsistency favours alternative steady states, with the potential to favour different evolutions of heat and carbon between the component-only and coupled configurations. Given the ultimate aim is a spun-up model state consistent with the coupled model, a requirement is that the component models behave as close to the coupled model as possible. It is also worth remarking that, since we expected our ocean-only phase to differ from that of the coupled model because of the absence of ocean-atmosphere interactions, the source of the differences noted in the first ocean-only spin-up phase took time to be discovered. Ideally, the relationship between the fully-coupled and component-only versions of an ESM should be formally examined, both in terms of code and coupling (e.g. the same parameterisations being used with the same input properties in the same ordering, etc.), and in the resulting simulation dynamics.

Another factor that our spin-up experience identified is the selection of the atmospheric forcing itself. Here, our ocean-only phases were driven using atmospheric forcing from periods of GC3.1 piControl simulation in which there was a top-of-atmosphere imbalance. This imbalance (+0.15-0.2 W m^{-2}) is in the GC3.1 run throughout its piControl. This led to our ocean-only model consistently warming during spin-up, admittedly only a small absolute amount, but large enough that the final, fully-coupled spin-up phase could be seen reversing this in response. Since stable ocean heat content is one of the key targets of spin-up, this points to the need for careful selection of atmospheric forcing, again, with the aim to be as consistent as possible with the atmosphere in the target coupled model. On a similar note, another feature of the atmospheric forcing used is its duration and character. Initial experience with limited-duration GC3.1 simulations found only modest variability in the ocean and atmosphere, both in terms of the absolute magnitude of variability and its temporal profile. Consequently, a relatively short, multi-decadal period was selected for use in ocean-only spin-up. However, as results shown here illustrate, the model clearly exhibits variability of much larger magnitude, and with much longer periods, most clearly in UKESM1's Southern Ocean, where Drake Passage transport exhibits strong centennial-scale cycles. While a forced ocean-only model is unable to respond in the same way as the ocean in a fully coupled simulation because of the absence of ocean-atmosphere interactions, the short periods of forcing used here are not necessarily representative of what the full model can produce. Overall, an assessment of the flux biases of downward atmospheric forcing, and the role of slow timescale variability in atmospheric forcing on both, ocean- and land-only spin-up, requires further analysis.

An item that is not apparent in the earlier description of UKESM1's spin-up was its interaction with the model's development cycle. Since UKESM1 includes numerous new model components and developments relative to its CMIP5 predecessor, HadGEM2-ES, it required a lengthy period of development. The timescales associated with CMIP6 and with the throughput of the fully-coupled model (approximately 4 simulated years per 1 wallclock day) meant that development and spin-up necessarily occurred in parallel. While this meant that the spin-up was not "clean" (i.e. was not made using a single identical model throughout), and that it was not without inconsistency as problems were ironed out (e.g. the ocean-only bulk formulae issue), this mode of operation maximised the time available for spin-up. It avoided the need to wait for code freezing of a final version, and permitted the addition of features that would otherwise not have been included. A number of coupling interactions in UKESM1, in particular, became possible because of this flexible approach to the development of UKESM1 from new components and its spin-up. The alternative approach of finalising first would necessarily have either delayed UKESM1's participation in CMIP6 or required the use of a less complete ESM.

Of particular value in the development, tuning and spin-up of UKESM1 was the availability of the BGC-val evaluation suite [de Mora et al., 2018]. Focused on the ocean component, this tool automated the analysis of simulations, providing a range of plots covering geographical, depth and globally-integrated properties, as well as comparisons with observational fields where available. Initially used on a run-by-run basis, BGC-val became invaluable in the intercomparison of multiple runs, and in monitoring the spin-up to identify and avoid runtime or model bias problems. While most ESM groups will already have access to such tools because of the role they can play, we would encourage new entrants to the field to acquire (by adoption or development) such a tool.

5 Conclusions

- The UKESM1 model was spun-up using a combination of component-only phases for land and ocean, followed by a period of fully-coupled simulation
- Component-only phases were spun-up under atmospheric forcing derived from simulations of coupled climate precursors of UKESM1
- Model states from parallel ocean (≈5000 year) and land (≈1600 year) spin-up branches were united with the atmosphere and, later, the full atmosphere chemistry and aerosol component (≈240 year)
- The resulting pre-industrial control has a top-of-atmosphere heat balance of less than -0.09 W m^{-2} and net atmosphere-ocean and atmosphere-land CO_2 fluxes of less than 0.1 Pg C y^{-1}
- Although equilibrated at global scale, analysis of land carbon fluxes indicated that regional shifts were significant, implying that longer spin-up periods are required to ensure regional as well as global equilibration
- Issues encountered during spin-up included consistency of the interfaces of component-only models, the duration and variability of the atmospheric forcing, including its overall consistency with atmospheric forcing in the target coupled model, and the important role played by rapid-turnaround evaluation tools
- While some tuning of UKESM1 was undertaken during spin-up, the slow turnover of the ocean component and conventional spin-up modes used here limited its scope, supporting the future tailoring of accelerated spin-up techniques to UKESM1 to reduce ocean biases, as well as achieve better equilibration

Acknowledgments

The authors are extremely grateful for the input and support provided by colleagues within the UKESM core team at the Met Office and associated NERC research centres. The development of UKESM1 has involved an extended period of close collaboration across this team over several years, and the work presented here would not have been possible without this support.

AY, JP, CGJ, LdM, EEP, SR, MS, SRJ, TK, DK and RE were supported by the National Environmental Research Council (NERC) National Capability Science Multi-Centre (NCSMC) funding for the UK Earth System Modelling project: CGJ, TK, MS, and SR through grant NE/N017978/1; AY, JP, LdM and EEP through grant NE/N018036/1; RE and DK through grant NE/N017951/1. AS, JM, AW, YT, RH, JW and SW were supported by the Met Office Hadley Centre Climate Programme funded by BEIS and Defra. ATB, AGN, ACC and JH were supported by the National Environmental Research Council (NERC). CGJ, TK, SR, AY, JP and EEP additionally acknowledge the EU Horizon 2020 CRESCENDO project, grant number 641816.

The authors are additionally grateful to S. Khatiwala (air-sea CO_2 flux time-series estimates), S. Lauvset (GLODAPv2) and R. Lumpkin (overturning streamfunction) for their assistance with data products.

6 Code and data availablity

All simulations used in this work were performed using version 10.9 of the UM, version 5.0 of JULES, NEMO version 3.6, CICE version 5.1.2 and OASIS3-MCT version 3.0. Model output from the NEMO ocean model was handled using the XML Input-Output Server (XIOS) library [Meurdesoif, 2013].

Identifiers for simulations in the ocean branch of spin-up are listed in Table **??**, with u-aw310 the final piControl simulation and the source of the majority of model output shown in this paper.

All simulation data used in this study are archived at the Met Office and are available for research purposes through the JASMIN platform (`www.jasmin.ac.uk`). For further details please contact `UM_collaboration@metoffice.gov.uk` referencing this paper.

References

Anderson, T.R., Spall, S.A., Yool, A., Cipollini, P., Challenor, P.G., and Fasham, M.J.R.: Global fields of sea surface dimethylsulphide predicted from chlorophyll, nutrients and light, J. Mar. Syst., 30, 1–20, 2001.

Aranami, K. and Tsunogai, S.: Seasonal and regional comparison of oceanic and atmospheric dimethylsulfide in the northern North Pacific: Dilution effects on its concentration during winter, J. Geophys. Res., 109, doi:10.1029/2003JD004288, 2004.

Archibald, A.T., O'Connor, F.M., Abraham, N.L., Archer-Nicholls, S., Chipperfield, M.P., Dalvi, M., Folberth, G.A., Dennison, F., Dhomse, S.S., Griffiths, P.T., Hardacre, C., Hewitt, A.J., Hill, R.S., Johnson, C.E., Keeble, J., Köhler, M.O., Morgenstern, O., Mulcahy, J.P., Ordóñez, C., Pope, R.J., Rumbold, S.T., Russo, M.R., Savage, N.H., Sellar, A., Stringer, M., Turnock, S.T., Wild, O., and Zeng, G.: Description and evaluation of the UKCA stratosphere-troposphere chemistry scheme (StratTrop vn 1.0) implemented in UKESM1, Geosci. Model Dev., 13, 1223-1266, doi:10.5194/gmd-13-1223-2020, 2020.

Armstrong, R.A., Lee, C., Hedges, J.I., Honjo, S., and Wakeham, S.G.: A new, mechanistic model for organic carbon fluxes in the ocean: based on the quantitative association of POC with ballast minerals, Deep-Sea Res. Pt. II, 49, 219–236, 2002.

Artoili, Y., Blackford, J. C., Butenschon, M., Holt, J. T., Wakelin, S. L., Thomas, H., Borges, A. V., and Allen, J. I.: The carbonate system of the North Sea: Sensitivity and model validation, J. Mar. Syst. 102, 1–13, 2012.

Behrenfeld, M. J. and Falkowski, P. G.: Photosynthetic rates derived from satellite-based chlorophyll concentration, Limnol. Oceanogr., 42, 1–20, 1997.

Best, M. J., Pryor, M., Clark, D.B., Rooney, G.G., Essery, R.L.H., Ménard, C.B., Edwards, J.M., Hendry, M.A., Porson, A., Gedney, N., Mercado, L.M., Sitch, S., Blyth, E., Boucher, O., Cox, P.M., Grimmond, C.S.B., and Harding, R.J.: The Joint UK Land Environment Simulator (JULES), model description – Part 1: Energy and water fluxes, Geosci. Model Dev., 4, 677-699, doi:10.5194/gmd-4-677-2011, 2011.

Blackford, J. C. and Gilbert, F. J.: pH variability and CO_2 induced acidification in the North Sea, J. Mar. Syst., 64, 229–241, doi:10.1016/j.jmarsys.2006.03.016, 2007.

Burton, C., Betts, R., Cardoso, M., Feldpausch, T.R., Harper, A., Jones, C.D., Kelley, D. I., Robertson, E., and Wiltshire, A.: Representation of fire, land-use change and vegetation dynamics in the Joint UK Land Environment Simulator vn4.9 (JULES), Geosci. Model Dev., 12, 179–193, doi:10.5194/gmd-12-179-2019, 2019

Carr, M.-E., Friedrichs, M. A. M., Schmeltz, M., Aita, M. N., Antoine, D., Arrigo, K. R., Asanuma, I., Aumont, O., Barber, R., Behrenfeld, M., Bidigare, R., Buitenhuis, E. T., Campbell, J., Ciotti, A., Dierssen, H., Dowell, M., Dunne, J., Esaias, W., Gentili, B., Gregg, W., Groom, S., Hoepffner, N., Ishizaka, J., Kameda, T., Le Quéré, C., Lohrenz, S., Marra, J., Mélin, F., Moore, K., Morel, A., Reddy, T. E., Ryan, J., Scardi, M., Smyth, T., Turpie, K., Tilstone, G., Waters, K., and Yamanaka, Y.: A comparison of global estimates of marine primary production from ocean color, Deep-Sea Res. Pt. II, 53, 741–770, 2006.

Carslaw, K. S., Boucher, O., Spracklen, D. V., Mann, G. W., Rae, J. G. L., Woodward, S., and Kulma la, M.: A review of natural aerosol interactions and feedbacks within the Earth system, Atmospheric Chemistry and Physics, 10, 1701-1737, doi:10.5194/acp-10-1701-2010, 2010.

Cheng L., Trenberth, K.E., Fasullo, J., Boyer, T., Abraham, J., and Zhu, J.: Improved estimates of ocean heat content from 1960 to 2015, Science Advances, 3, e1601545, doi:10.1126/sciadv.1601545, 2017.

Ciais, P., Sabine, C., Bala, G., Bopp, L., Brovkin, V., Canadell, J., Chhabra, A., DeFries, R., Galloway, J., Heimann, M., Jones, C., Le Quéré, C., Myneni, R.B., Piao, S., and Thornton, P.: Carbon and Other Biogeochemical Cycles, in: Climate Change 2013: The Physical Science Basis, Contribution of Working Group I to the Fifth Assessment Report of the Intergovernmental Panel on Climate Change, edited by: Stocker, T.F., Qin, D., Plattner, G.-K., Tignor, M., Allen, S.K., Boschung, J., Nauels, A., Xia, Y., Bex, V., and Midgley, P.M., Cambridge University Press, Cambridge, UK and New York, NY, USA, 465—570, doi:10.1017/CBO9781107415324.015, 2013.

Clark, D.B., Mercado, L.M., Sitch, S., Jones, C.D., Gedney, N., Best, M.J., Pryor, M., Rooney, G.G., Essery, R.L.H., Blyth, E., Boucher, O., Harding, R.J., Huntingford, C., and Cox, P.M.: The Joint UK Land Environment Simulator (JULES), model description – Part 2: Carbon fluxes and vegetation dynamics, Geosci. Model Dev., 4, 701–722, doi:10.5194/gmd-4-701-2011, 2011.

Collins, W. J., Bellouin, N., Doutriaux-Boucher, M., Gedney, N., Halloran, P., Hinton, T., Hughes, J., Jones, C. D., Joshi, M., Liddicoat, S., Martin, G., O'Connor, F., Rae, J., Senior, C., Sitch, S., Totterdell, I., Wiltshire, A., and Woodward, S.: Development and evaluation of an Earth-system model – HadGEM2, Geosci. Model Dev. Discuss., 4, 997–1062, doi:10.5194/gmdd-4-997-2011, 2011.

Couldrey, M.P., Oliver, K.I.C., Yool, A., Halloran, P.R., Achterberg, E.P.: On which timescales do gas transfer velocities control North Atlantic CO2 flux variability? Global Biogeochemical Cycles 30, 787–802. doi:10.1002/2015GB005267, 2016.

Cox, P.M.: Description of the "TRIFFID" Dynamic Global Vegetation Model, Hadley Centre Technical Note 24, Met Office, Bracknell, UK, 2001.

Craig A., Valcke S., Coquart L., 2017: Development and performance of a new version of the OASIS coupler, OASIS3-MCT_3.0, Geoscientific Model Development, 10, pp. 3297-3308, doi:10.5194/gmd-10-3297-2017.

Cui, Y., Kump, L.R., Ridgwell, A.J., Charles, A.J., Junium, C.K., Diefendorf, A.F., Freeman, K.H., Urban, N.M., and Harding, I.C.: Slow release of fossil carbon during the Palaeocene<96>Eocene Thermal Maximum, Nature Geoscience, 4, 481, doi:10.1038/ngeo1179, 2011.

Cunningham, S.A., Alderson, S.G., King, B.A., and Brandon, M.A.: Transport and variability of the Antarctic Circumpolar Current in Drake Passage, J. Geophys. Res., 108, 8084, doi:10.1029/2001JC001147, 2003.

de Lavergne, C., Palter, J.B., Galbraith, E.D., Bernardello, R., and Marinov, I.: Cessation of deep convection in the open Southern Ocean under anthropogenic climate change, Nat. Clim. Change, 4, 278–282, doi:10.1038/NCLIMATE2132, 2014.

de Mora, L., Yool, A., Palmieri, J., Sellar, A., Kuhlbrodt, T., Popova, E., Jones, C., and Allen, J. I.: BGC-val: a model- and grid-independent Python toolkit to evaluate marine biogeochemical models, Geosci. Model Dev., 11, 4215-4240, doi:10.5194/gmd-11-4215-2018, 2018.

Doney, S.C., Lindsay, K., Fung, I., and John, J.: Natural Variability in a Stable, 1000-Yr Global Coupled Climate–Carbon Cycle Simulation, J. Climate, 19, 3033-3054, doi:10.1175/JCLI3783.1, 2006.

Donohue, K.A., Tracey, K.L., Watts, D.R., Chidichimo, M.P., and Chereskin, T.K.: Mean Antarctic Circumpolar Current transport measured in Drake Passage, Geophys. Res. Lett., 43, 11,760-11,767, doi:10.1002/2016GL070319, 2016.

Döös, K., and Webb, D.J.: The Deacon Cell and the other Meridional Cells of the Southern Ocean, J. Phys. Oceanogr., 24, 429–442, doi:10.1175/1520-0485(1994)024<0429:TDCATO>2.0.CO;2, 1994.

DRAKKAR Group: Eddy–permitting Ocean Circulation Hindcasts of past decades, CLIVAR Exchanges No. 42, 12, 8-10, 2007.

Dunne, J. P., John, J. G., Shevliakova, E., Stouffer, R. J., Krasting, J. P., Malyshev, S. L., Milly, P. C. D., Sentman, L. T., Adcroft, A. J., Cooke, W., Dunne, K. A., Griffies, S. M., Hallberg, R. W., Harrison, M. J., Levy, H., Wittenberg, A. T., Phillips, P. J., and Zadeh, N.: GFDL's ESM2 Global Coupled Climate–Carbon Earth System Models. Part II: Carbon System Formulation and Baseline Simulation Characteristics, J. Climate, 26, 2247–2267, doi:10.1175/JCLI-D-12-00150.1, 2013.

Dutkiewicz, S., Follows, M. J., and Parekh, P.: Interactions of the iron and phosphorus cycles: a three-dimensional model study, Global Biogeochem. Cy., 19, GB1021, doi:10.1029/2004GB002342, 2005.

Edson, J.B., Jampana, V., Weller, R.A., Bigorre, S.P., Plueddemann, A.J., Fairall, C.W., Miller, S.D., Mahrt, L., Vickers, D., and Hersbach, H.: On the Exchange of Momentum over the Open Ocean. J. Phys. Oceanogr., 43, 1589–1610, doi:10.1175/JPO-D-12-0173.1, 2013.

Eyring, V., Bony, S., Meehl, G. A., Senior, C. A., Stevens, B., Stouffer, R. J., and Taylor, K. E.: Overview of the Coupled Model Intercomparison Project Phase 6 (CMIP6) experimental design and organization, Geosci. Model Dev., 9, 1937-1958, doi:10.5194/gmd-9-1937-2016, 2016.

Forget, G., Campin, J.-M., Heimbach, P., Hill, C. N., Ponte, R. M., and Wunsch, C.: ECCO version 4: an integrated framework for non-linear inverse modeling and global ocean state estimation, Geosci. Model Dev., 8, 3071–3104, doi:10.5194/gmd-8-3071-2015, 2015.

Fukumori, I., Wang, O., Fenty, I., Forget, G., Heimbach, P., and Ponte, R.M.: ECCO Version 4 Release 4, available at https://ecco.jpl.nasa.gov/drive/files/Version4/Release4/doc/v4r4_synopsis.pdf, 2019.

Garcia, H. E., Locarnini, R. A., Boyer, T. P., Antonov, J. I., Baranova, O. K., Zweng, M. M., and Johnson, D. R.: World ocean atlas 2009, volume 3: dissolved oxygen, apparent oxygen utilization, and oxygen saturation, in: NOAA Atlas NESDIS 70, edited by: Levitus, S., US Government Printing Office, Washington, DC, 344 pp., 2010a.

Garcia, H. E., Locarnini, R. A., Boyer, T. P., Antonov, J. I., Zweng, M. M., Baranova, O. K., and Johnson, D. R., World ocean atlas 2009, volume 4: nutrients (phosphate, nitrate, silicate),in: NOAA Atlas NESDIS 71, edited by: Levitus, S., US Government Printing Office, Washington, DC, 398 pp., 2010b.

Garcia, H.E., Locarnini, R.A., Boyer, T.P., Antonov, J.I., Baranova, O.K., Zweng, M.M., Reagan, J.R., and Johnson, D.R.: World Ocean Atlas 2013, Volume 3: Dissolved Oxygen, Apparent Oxygen Utilization, and Oxygen Saturation. S. Levitus, Ed., A. Mishonov Technical Ed.; NOAA Atlas NESDIS 75, 27 pp., 2014.

Garcia, H.E., Locarnini, R.A., Boyer, T.P., Antonov, J.I., Baranova, O.K., Zweng, M.M., Reagan, J.R., and Johnson, D.R.: World Ocean Atlas 2013, Volume 4: Dissolved Inorganic Nutrients (phosphate, nitrate, silicate). S. Levitus, Ed., A. Mishonov Technical Ed.; NOAA Atlas NESDIS 76, 25 pp., 2014.

Gebbie, G. and Huybers, P.: The Mean Age of Ocean Waters Inferred from Radiocarbon Observations: Sensitivity to Surface Sources and Accounting for Mixing Histories, J. Phys. Oceanogr., 42, 291–305, doi:10.1175/JPO-D-11-043.1, 2012.

Gent, P.R., and McWilliams, J.C.: Isopycnal mixing in ocean circulation models, J. Phys. Oceanogr., 20, 150-155, doi: 10.1175/1520-0485(1990)020<0150:IMIOCM>2.0.CO;2, 1990.

Gnanadesikan, A., Slater, R. D., Gruber, N., and Sarmiento, J. L.: Oceanic vertical exchange and new production: a comparison between models and observations, Deep-Sea Res. II, 49, 363–401, 2002.

Good, S.A., Martin, M.J., and Rayner, N.A.: EN4: quality controlled ocean temperature and salinity profiles and monthly objective analyses with uncertainty estimates, Journal of Geophysical Research: Oceans, 118, 6704–6716, doi:10.1002/2013JC009067, 2013.

Gregg, W. W. and Casey, N. W.: Modeling coccolithophores in the global oceans, Deep-Sea Res. Pt. II, 54, 447–477, doi:10.1016/j.dsr2.2006.12.007, 2013.

Gruber, N.: Anthropogenic CO_2 in the Atlantic Ocean, Global Biogeochem. Cy., 12, 165–191, 1998.

Halloran, P. R., Bell, T. G., and Totterdell, I. J.: Can we trust empirical marine DMS parameterisations within projections of future climate?, Biogeosciences, 7, 1645–1656, doi:10.5194/bg-7-1645-2010, 2010.

Halloran, P. R., Booth, B. B. B., Jones, C. D., Lambert, F. H., McNeall, D. J., Totterdell, I. J., and Völker, C.: The mechanisms of North Atlantic CO_2 uptake in a large Earth System Model ensemble, Biogeosciences, 12, 4497-4508, doi:10.5194/bg-12-4497-2015, 2015.

Hantson, S., Arneth, A., Harrison, S.P., Kelley, D.I., Prentice, I.C., Rabin, S. S., Archibald, S., Mouillot, F., Arnold, S.R., Artaxo, P., Bachelet, D., Ciais, P., Forrest, M., Friedlingstein, P., Hickler, T., Kaplan, J.O., Kloster, S., Knorr, W. ,Laslop, G., Li, F., Melton, J.R., Meyn, A., Sitch, S., Spessa, A., van der Werf, G.R., Voulgarakis, A., and Yue, C.: The status and challenge of global fire modelling, Biogeosciences, 13, 3359–3375, doi:10.5194/bg-13-3359-2016, 2016.

Harper, A.B., Cox, P.M., Friedlingstein, P., Wiltshire, A.J., Jones, C.D., Sitch, S., Mercado, L.M., Groenendijk, M., Reich, P.B., Soudzilovskaia, N.A., and van Bodegom, P.: Improved representation of plant functional types and physiology in the Joint UK Land Environment Simulator (JULES v4.2) using plant trait information, Geosci. Model Development, 9, 2415–2440, doi:10.5194/gmd-9-2415-2016, 2016.

Hartmann, D.L., Klein Tank, A.M.G., Rusticucci, M., Alexander, L.V., Brönnimann, S., Charabi, Y., Dentener, F.J., Dlugokencky, E.J., Easterling, D.R., Kaplan, A., Soden, B.J., Thorne, P.W., Wild M., and Zhai, P.M.: Observations: Atmosphere and Surface, In: Stocker, T.F., Qin, D., Plattner, G.-K., Tignor, M., Allen, S.K., Boschung, J., Nauels, A., Xia, Y., Bex V., and Midgley, P.M. (eds.), Climate Change 2013: The Physical Science Basis, Contribution of Working Group I to the Fifth Assessment Report of the Intergovernmental Panel on Climate Change, Cambridge University Press, Cambridge, United Kingdom, 2013.

Hewitt, H. T., Copsey, D., Culverwell, I. D., Harris, C. M., Hill, R. S. R., Keen, A. B., McLaren, A. J., and Hunke, E. C.: Design and implementation of the infrastructure of HadGEM3: the next-generation Met Office climate modelling system, Geosci. Model Dev., 4, 223-253, doi:10.5194/gmd-4-223-2011, 2011.

Hobbs, W., Palmer, M.D., and Monselesan, D.: An Energy Conservation Analysis of Ocean Drift in the CMIP5 Global Coupled Models, J. Climate, 29, 1639-1653, doi:10.1175/JCLI-D-15-0477.1, 2016.

Honjo, S., Manganini, S. J., Krishfield, R. A., and Francois, R.: Particulate organic carbon fluxes to the ocean interior and factors controlling the biological pump: A synthesis of global sediment trap programs since 1983, Prog. Oceanogr., 76, 217–285, doi:10.1016/j.pocean.2007.11.003, 2008.

Ilyina, T., Six, K. D., Segschneider, S., Maier-Reimer, E., Li, H., and Núñez-Riboni, I.: Global ocean biogeochemistry model HAMOCC: Model architecture and performance as component of the MPI-Earth system model in different CMIP5 experimental realizations, J. Adv. Model. Earth Syst., 5, 287–315, doi:10.1029/2012MS000178, 2013.

Jiang, Z.-P., Tyrrell, T., Hydes, D.J. Dai, M., and Hartman, S.E.: Variability of alkalinity and the alkalinity-salinity relationship in the tropical and subtropical surface ocean, Global Biogeochem. Cycles, 28, 729–742, doi:10.1002/2013GB004678, 2014.

Johns, T.C., Durman, C.F., Banks, H.T., Roberts, M.J., McLaren, A.J., Ridley, J.K., Senior, C.A., Williams, K.D., Jones, A., Rickard, G.J., Cusack, S., Ingram, W.J., Crucifix, M., Sexton, D.M., Joshi, M.M., Dong, B., Spencer, H., Hill, R.S., Gregory, J.M., Keen, A.B., Pardaens, A.K., Lowe, J.A., Bodas-Salcedo, A., Stark, S., and Searl, Y.: The New Hadley Centre Climate Model (HadGEM1): Evaluation of Coupled Simulations, J. Climate, 19, 1327–1353, doi:10.1175/JCLI3712.1, 2006.

Johnson, G.C., Lyman, J.M., and Loeb, N.G.: Improving estimates of Earth's energy imbalance. Nature Climate Change, 6, 639–640, doi:10.1038/nclimate3043, 2016.

Jones, C. D., Hughes, J. K., Bellouin, N., Hardiman, S. C., Jones, G. S., Knight, J., Liddicoat, S., O'Connor, F. M., Andres, R. J., Bell, C., Boo, K.-O., Bozzo, A., Butchart, N., Cadule, P., Corbin, K. D., Doutriaux-Boucher, M., Friedlingstein, P., Gornall, J., Gray, L., Halloran, P. R., Hurtt, G., Ingram, W. J., Lamarque, J.-F., Law, R. M., Meinshausen, M., Osprey, S., Palin, E. J., Parsons Chini, L., Raddatz, T., Sanderson, M. G., Sellar, A. A., Schurer, A., Valdes, P., Wood, N., Woodward, S., Yoshioka, M., and Zerroukat, M.: The HadGEM2-ES implementation of CMIP5 centennial simulations, Geosci. Model Dev., 4, 543–570, doi:10.5194/gmd-4-543-2011, 2011.

Jones, C. D., Arora, V., Friedlingstein, P., Bopp, L., Brovkin, V., Dunne, J., Graven, H., Hoffman, F., Ilyina, T., John, J. G., Jung, M., Kawamiya, M., Koven, C., Pongratz, J., Raddatz, T., Randerson, J. T., and Zaehle, S.: C4MIP – The Coupled Climate-Carbon Cycle Model Intercomparison Project: experimental protocol for CMIP6, Geosci. Model Dev., 9, 2853-2880, doi:10.5194/gmd-9-2853-2016, 2016.

Kattge, J., Díaz, S., Lavorel, S., Prentice, I. C., Leadley, P., Bönisch, G., Garnier, E., Westoby, M., Reich, P.B., Wright, I.J., Cornelissen, J.H., Violle, C. ,Harrison, S.P., Van Bodegom, P.M., Reichstein, M. , Enquist, B.J., Soudzilokvkaia, N.A., Ackerly, D.D., Anand, M., Atkin, O., Bahn, M., Baker, T.R., Baldocchi, D. , Bekker, R., Blanco, C.C., Blonder, B., Bond, W.J., Bradstock, R., Bunker, D.E., Casanoves, F., Cavender-Bares, J., Chambers, J.Q., Chapin III, F.S., Chave, J., Coomes, D., Cornwell, W.K., Craine, J.M., Dobrin, B.H., Duarte, L., Durka, W., Elser, J., Esser, G., Estiarte, M., Fagan, W.F., Fang, J., Fernández-Méndez, F., Fidelis, A., Finegan, B., Flores, O., Ford, H., Frank, D., Freschet, G.T., Fyllas, N.M., Gallagher, R.V., Green, W.A., Gutierrez, A.G., Hickler, T.

, Higgins, S.I., Hodgson, J.G., Jalili, A., Jansen, S., Joly, C.A., Kerkhoff, A.J., Kirkup, D., Kitajima, K., Kleyer, M., Klotz, S., Knops, J.M., Kramer, K., Kühn, I., Kurokawa, H., Laughlin, D., Lee, T.D., Leishman, M., Lens, F., Lenz, T., Lewis, S.L., Lloyd, J., Llusià, J., Louault, F., Ma, S., Mahecha, M.D., Manning, P., Massad, T., Medlyn, B.E., Messier, J., Moles, A.T., Müller, S.C., Nadrowski, K., Naeem, S., Niinemets, Ü. , Nöllert, S., Nüske, A., Ogaya, R., Oleksyn, J., Onipchenko, V.G., Onoda, Y., Ordoñez, J., Overbeck, G., Ozinga, W.A., Patiño, S., Paula, S., Pausas, J.G., Peñuelas, J., Phillips, O.L., Pillar, V., Poorter, H., Poorter, L., Poschlod, P., Prinzing, A., Proulx, R., Rammig, A., Reinsch, S., Reu, B., Sack, L., Salgado-Negret, B., Sardans, J., Shiodera, S., Shipley, B., Siefert, A., Sosinski, E., Soussana, J., Swaine, E., Swenson, N., Thompson, K., Thornton, P. , Waldram, M., Weiher, E., White, M. , White, S., Wright, S.J., Yguel, B., Zaehle, S., Zanne, A.E., and Wirth, C.: TRY – a global database of plant traits, Global Change Biology, 17, 2905-2935, doi:10.1111/j.1365-2486.2011.02451.x, 2011.

Kettle, A.J., Andreae, M.O., Amouroux, D., Andreae, T.W., Bates, T.S., Berresheim, H., Bingemer, H. and Boniforti, R., Curran, M.A.J., DiTullio, G.R., Helas, G., Jones, G.B., Keller, M.D., Kiene, R.P., Leck, C., Levasseur, M., Malin, G., Maspero, M., Matrai, P., McTaggart, A.R., Mihalopoulos, N., Nguyen, B.C., Novo, A., Putaud, J.P., Rapsomanikis, S., Roberts, G., Schebeske, G., Sharma, S., Simó, R., Staubes, R., Turner, S., Uher, G.: A global database of sea surface dimethylsulfide DMS. measurements and a procedure to predict sea surface DMS as a function of latitude, longitude, and month. Global Biogeochem. Cycles 13, 399–444, doi:10.1029/1999GB900004, 1999.

Key, R. M., Kozyr, A., Sabine, C. L., Lee, K., Wanninkhof, R., Bullister, J. L., Feely, R. A., Millero, F. J., Mordy, C., and Peng, T.–H.: A global ocean carbon climatology: results from Global Data Analysis Project (GLODAP), Global Biogeochem. Cy., 18, GB4031, doi:10.1029/2004GB002247, 2004.

Khatiwala, S., Visbeck, M., and Cane, M.A.: Accelerated simulation of passive tracers in ocean circulation models, Ocean Modelling, 9, 51–69, doi:10.1016/j.ocemod.2004.04.002, 2005.

Khatiwala, S.: A computational framework for simulation of biogeochemical tracers in the ocean, Global Biogeochem. Cycles, 21, GB3001, doi:10.1029/2007GB002923, 2007.

Khatiwala, S., Primeau, F., and Hall, T.: Reconstruction of the history of anthropogenic CO_2 concentrations in the ocean, Nature, 462, 346–349, doi:10.1038/nature08526, 2009.

Khatiwala, S., Primeau, F., Holzer, M.: Ventilation of the deep ocean constrained with tracer observations and implications for radiocarbon estimates of ideal mean age, Earth and Planetary Science Letters 325-326, 116–125, 2012.

Khatiwala, S., Tanhua, T., Mikaloff Fletcher, S., Gerber, M., Doney, S. C., Graven, H. D., Gruber, N., McKinley, G. A., Murata, A., Ríos, A. F., and Sabine, C. L.: Global ocean storage of anthropogenic carbon, Biogeosciences, 10, 2169-2191, doi:10.5194/bg-10-2169-2013, 2013.

Kok, J. F., Ward, D. S., Mahowald, N. M., and Evan, A. T.: Global and regional importance of the direct dust-climate feedback, Nature Communications, 9, 241, doi:10.1038/s41467-017-02620-y, 2018.

Kriest, I.: Calibration of a simple and a complex model of global marine biogeochemistry, Biogeosciences, 14, 4965-4984, doi:10.5194/bg-14-4965-2017, 2017.

Kuhlbrodt, T., Jones, C.G., Sellar, A., Storkey, D., Blockley, E., Stringer, M., Hill, R., Graham, T., Ridley, J., Blaker, A., Calvert, D., Copsey, D., Ellis, R., Hewitt, H., Hyder, P., Ineson, S., Mulcahy, J., Siahaan, A., and Walton, J.: The low-resolution version of HadGEM3 GC3.1: Development and evaluation for global climate. Journal of Advances in Modeling Earth Systems, 10, 2865-2888, doi:10.1029/2018MS001370, 2018.

Kwiatkowski, L., Yool, A., Allen, J. I., Anderson, T. R., Barciela, R., Buitenhuis, E. T., Butenschön, M., Enright, C., Halloran, P. R., Le Quéré, C., de Mora, L., Racault, M.-F., Sinha, B., Totterdell, I. J., and Cox, P. M.: iMarNet: an ocean biogeochemistry model inter-comparison project within a common physical ocean modelling framework, Biogeosciences Discuss., 11, 10537–10569, doi:10.5194/bgd-11-10537-2014, 2014.

Kwon, E.Y., Primeau, F., and Sarmiento, J.L.: The impact of remineralization depth on the air-sea carbon balance, Nat. Geosci., 2, 630–635, doi:10.1038/ngeo612, 2009.

Large, W.G. and Yeager, S.G.: The global climatology of an interannually varying air-sea flux data set. Climate Dynamics, 33, 341–364, doi:10.1007/s00382-008-0441-3, 2009.

Latif, M., Martin, T., and Park, W.: Southern ocean sector centennial climate variability: Dynamics and implications for recent decadal trends, J. Clim., 26, 7767–7782, doi:10.1175/JCLI-D-12-00281.1, 2013

Lauvset, S.K., Key, R.M., Olsen, A., van Heuven, S., Velo, A., Lin, X., Schirnick, C., Kozyr, A., Tanhua, T., Hoppema, M., Jutterström, S., Steinfeldt, R., Jeansson, E., Ishii, M., Pérez, F.F., Suzuki, T., and Watelet, S.: A new global interior ocean mapped climatology: the $1^\circ \times 1^\circ$ GLODAP version 2, Earth Syst. Sci. Data, 8, 325–340, doi:10.5194/essd-8-325-2016, 2016.

Lee, K., Tong, L.T., Millero, F.J., Sabine, C.L., Dickson, A.G., Goyet, C., Park, G.-H., Wanninkhof, R., Feely, R.A., Key, R.M.: Global relationships of total alkalinity with salinity and temperature in surface waters of the world's oceans, Geophys. Res. Lett., 33, L19605, doi:10.1029/2006GL027207, 2006.

Lengaigne, M., Menkes, C., Aumont, O., Gorgues, T., Bopp, L., André, J.-M., and Madec, G.: Influence of the oceanic biology on the tropical Pacific climate in a coupled general circulation model, Clim. Dynam., 28, 503–516, doi:10.1007/s00382-006-0200-2, 2007.

Lenssen N., Schmidt, G., Hansen, J., Menne, M., Persin, A., Ruedy, R., and Zyss, D.: Improvements in the GISTEMP uncertainty model, J. Geo. Res. Atmos., 124, 6307-6326, doi:10.1029/2018JD029522, 2019.

Le Quéré, C., Andrew, R.M., Friedlingstein, P., Sitch, S., Hauck, J., Pongratz, J., Pickers, P.A., Korsbakken, J.I., Peters, G.J., Canadell, J.G., Arneth, A., Arora, V.K., Barbero, L., Bastos, A., Bopp, L., Chevallier, F., Chini, L.P., Ciais, P., Doney, S.C., Gkritzalis, T., Goll, D.S., Harris, I., Haverd, V., Hoffman, F.M., Hoppema, M., Houghton, R.A., Hurtt, G., Ilyina, T., Jain, A.K., Johannessen, T., Jones, C.D., Kato, E., Keeling, R.F., Goldewijk, K.K., Landschützer, P., Lefévre, N., Lienert, S., Liu, Z., Lombardozzi, D., Metzl, N., Munro, D.R., Nabel, J.E.M.S., Nakaoka, S.-I., Neill, C., Olsen, A., Ono, T., Patra, P., Peregon, A., Peters, W., Peylin, P., Pfeil, B., Pierrot, D., Poulter, B., Rehder, G., Resplandy, L., Robertson, E., Rocher, M., Rödenbeck, C., Schuster, U., Schwinger, J., Séférian, R., Skjelvan, I., Steinhoff, T., Sutton, A., Tans, P.P., Tian, H., Tilbrook, B., Tubiello, F.N., van der Laan-Luijkx, I.T., van der Werf, G.R., Viovy, N., Walker, A.P., Wiltshire, A.J., Wright, R., Zaehle, S., and Zheng, B.: Global Carbon Budget 2018, Earth System Science Data, 10, 1–54, doi:10.5194/essd-10-2141-2018, 2018.

Lindsay, K., Bonan, G.B., Doney, S.C., Hoffman, F.M., Lawrence, D.M., Long, M.C., Mahowald, N.M., Moore, J.K., Randerson, J.T., and Thornton, P.E.: Preindustrial Control and 20th Century Carbon Cycle Experiments with the Earth System Model CESM1(BGC), J. Climate, 27, 8981–9005, doi:10.1175/JCLI-D- 12-00565.1, 2014.

Liss, P. S. and Merlivat, L.: The role of air-sea exchange in geochemical cycling, in: Air-sea gas exchange rates: Introduction and synthesis. 113–128, 1986.

Liu, W., Fedorov, A., and Sévellec, F.: The Mechanisms of the Atlantic Meridional Overturning Circulation Slowdown Induced by Arctic Sea Ice Decline, J. Climate, 32, 977–996, doi:10.1175/JCLI-D-18-0231.1, 2019.

Locarnini, R.A., Mishonov, A.V., Antonov, J.I., Boyer, T.P., Garcia, H.E., Baranova, O.K., Zweng, M.M., Paver, C.R., Reagan, J.R., Johnson, D.R., Hamilton, M., and Seidov, D.: World Ocean Atlas 2013, Volume 1: Temperature. S. Levitus, Ed., A. Mishonov Technical Ed.; NOAA Atlas NESDIS 73, 40 pp., 2013.

Loeb, N.G., Wielicki, B.A., Doelling, D.R., Smith, G.L., Keyes, D.F., Kato, S., Manalo-Smith, N., and Wong, T.: Toward Optimal Closure of the Earth's Top-of-Atmosphere Radiation Budget, J. Climate, 22, 748–766, doi:10.1175/2008JCLI2637.1, 2009.

Loveland, T.R., Reed, B.C., Brown, J.F., Ohlen, D.O., Zhu, Z., Yang, L., and Merchant, J.W.: Development of a global land cover characteristics database and IGBP DISCover from 1 km AVHRR data, Int. J. Remote Sensing, 21, 1303–1330, doi:10.1080/014311600210191, 2000.

Lumpkin, R. and Speer, K.: Global Ocean Meridional Overturning, J. Phys. Oceanogr., 37, 2550–2562, doi:10.1175/JPO3130.1, 2007.

Madec, G., Delecluse, P., Imbard, M., and Lévy, C.: OPA 8.1 ocean general circulation model reference manual, Note du Pole de modélisation, Institut Pierre Simon Laplace, France, Technical Report 11, 91 pp., 1998.

Madec, G.: NEMO reference manual, ocean dynamic component: NEMO–OPA, Note du Pole de modélisation, Institut Pierre Simon Laplace, Technical Report 27, Note du pÃ´le de modÃ©lisation, Institut Pierre Simmon Laplace, France, No. 27, ISSN No. 1288–1619, 2008.

Madec, G., and the NEMO Team: NEMO ocean engine, version 3.6 stable. Note du Pole de modelisation de l'Institut Pierre-Simon Laplace no. 27, IPSL, Paris, France, 2016.

Mahowald, N. M., Baker, A. R.,Bergametti, G., Brooks, N., Duce, R. A., Jickells, T. D., Kubilay, N., Prospero, J. M., and Tegen, I.: Atmospheric global dust cycle and iron inputs to the ocean, Global Biogeochem. Cy., 19, GB4025, doi:10.1029/2004GB002402, 2005.

Meier-Reimer, E., Kriest, I., Segschneider, J., and Wetzel, P.: The HAMburg Ocean Carbon Cycle Model HAMOCC 5.1 – Technical Description Release 1.1, Tech. Report 14, Reports on Earth System Science, Max Planck Institute for Meteorology, Hamburg, Germany, 2005.

Mayewski, P.A., Meredith, M.P., Summerhayes, C.P., Turner, J., Worby, A., Barrett, P.J. Casassa, G., Bertler, N.A.N., Bracegirdle, T., Naveira Garabato, A.C., Bromwich, D., Campbell, H., Hamilton, G.S., Lyons, W.B., Maasch, K.A., Aoki, S., Xiao, C., van Ommenet T., State of the Antarctic and Southern Ocean climate system, Rev. Geophys., 47, RG1003, doi:10.1029/2007RG000231, 2009.

Mann, G.W., Carslaw, K.S., Spracklen, D.V., Ridley, D.A., Manktelow, P.T., Chipperfield, M.P., Pickering, S.J., and Johnson, C.E.: Description and evaluation of GLOMAP-mode: a modal global aerosol microphysics model for the UKCA composition-climate model, Geosci. Model Dev., 3, 519-551, doi:10.5194/gmd-3-519-2010, 2010.

Marshall, J., Donohoe, A., Ferreira, D., and McGee, D.: The ocean's role in setting the mean position of the Inter-Tropical Convergence Zone, Clim. Dyn., 42, 1967–1979, doi:10.1007/s00382-013-1767-z, 2014.

Meredith, M.P., Woodworth, P.L., Chereskin, T.K., Marshall, D.P., Allison, L.C., Bigg, G.R., Donohue, K., Heywood, K.J., Hughes, C.W., Hibbert, A., Hogg, A.M., Johnson, H.L., Jullion, L., King, B.A., Leach, H., Lenn, Y.-D., Morales Maqueda, M.A., Munday, D.R., Naveira Garabato, A.C., Provost, C., Sallée, J.-B., and Sprintall, J.: Sustained monitoring of the Southern Ocean at Drake Passage: Past achievements and future priorities, Rev. Geophys., 49, RG4005, doi:10.1029/2010RG000348, 2011.

Meurdesoif Y. Xios: an efficient and highly configurable parallel output library for climate modelling, The Second Workshop on Coupling Technologies for Earth System Models, Boulder, Colorado, USA, 20–22 February 2013, CW2013, 2013.

Monterey, G. and Levitus, S.: Seasonal Variability of Mixed Layer Depth for the World Ocean, 96 pp. NOAA Atlas NESDIS 14, U.S. Gov. Printing Office, Washington, D.C., 1997.

Morgenstern, O., Braesicke, P., O'Connor, F.M., Bushell, A.C., Johnson, C.E., Osprey, S.M., and Pyle, J.A.: Evaluation of the new UKCA climate-composition model – Part 1: The stratosphere, Geosci. Model Dev., 2, 43-57, doi:10.5194/gmd-2-43-2009, 2009.

Morgenstern, O., Hegglin, M.I., Rozanov, E., O'Connor, F.M., Abraham, N.L., Akiyoshi, H., Archibald, A.T., Bekki, S., Butchart, N., Chipperfield, M.P., Deushi, M., Dhomse, S.S., Garcia, R.R., Hardiman, S.C., Horowitz, L.W., Jöckel, P., Josse, B., Kinnison, D., Lin, M., Mancini, E., Manyin, M.E., Marchand, M., Marécal, V., Michou, M., Oman, L.D., Pitari, G., Plummer, D.A., Revell, L.E., Saint-Martin, D., Schofield, R., Stenke, A., Stone, K., Sudo, K., Tanaka, T.Y., Tilmes, S., Yamashita, Y., Yoshida, K., and Zeng, G.: Review of the global models used within phase 1 of the Chemistry-Climate Model Initiative (CCMI), Geosci. Model Dev., 10, 639-671, doi:10.5194/gmd-10-639-2017, 2017.

Moriarty, R. and O'Brien, T. D.: Distribution of mesozooplankton biomass in the global ocean, Earth Syst. Sci. Data, 5, 45-55, doi:10.5194/essd-5-45-2013, 2013.

Morice C.P., Kennedy, J.J., Rayner, N.A., and Jones, P.D.: Quantifying uncertainties in global and regional temperature change using an ensemble of observational estimates: the HadCRUT4 dataset, J. Geophys. Res., 117, D08101, doi:10.1029/2011JD017187, 2012.

Mulcahy, J. P., Jones, C., Sellar, A., Johnson, B., Boutle, I. A., Jones, A., et al.: Improved aerosol processes and effective radiative forcing in HadGEM3 and UKESM1, Journal of Advances in Modeling Earth Systems, 10, 2786-2805, doi:10.1029/2018MS001464, 2018.

Myhre, G., Shindell, D., Bron, F.-M., Collins, W., Fuglestvedt, J., Huang, J., et al.: Anthropogenic and natural radiative forcing. In T. F. Stocker, et al. (Eds.), Climate Change 2013 – The Physical Science Basis. Contribution of Working Group I to the Fifth Assessment Report of the Intergovernmental Panel on Climate Change (pp. 571-658). Cambridge, UK: Cambridge University Press, 2013.

O'Connor, F.M., Johnson, C.E., Morgenstern, O., Abraham, N.L., Braesicke, P., Dalvi, M., Folberth, G.A., Sanderson, M.G., Telford, P.J., Voulgarakis, A., Young, P.J., Zeng, G., Collins, W.J., and Pyle, J.A.: Evaluation of the new UKCA climate-composition model – Part 2: The Troposphere, Geosci. Model Dev., 7, 41-91, doi:10.5194/gmd-7-41-2014, 2014.

O'Reilly, J. E., Maritorena, S., Mitchell, B. G., Siegal, D. A., Carder, K. L., Garver, S. A., Kahru, M., and McClain, C.: Ocean color chlorophyll algorithms for SeaWiFS, J. Geophys. Res., 103, 24937–24953, 1998.

Orr, J.C., Najjar, R., Sabine, C.L., and Joos, F.: AbioticHOWTO, Internal OCMIP Report, LSCE/CEA Saclay, Gifsur-Yvette, France, 25 pp., http://ocmip5.ipsl.jussieu.fr/OCMIP/phase2/simulations/Abiotic/HOWTO-Abiotic.html, 1999b.

Orr, J.C., Fabry, V.J., Aumont, O., Bopp, L., Doney, S.C., Feely, R.A., Gnanadesikan, A., Gruber, N., Ishida, A., Joos, F., Key, R.M., Lindsay, K., Maier–Reimer, E., Matear, R., Monfray, P., Mouchet, A., Najjar, R.G., Plattner, G.–K., Rodgers, K.B., Sabine, C.L., Sarmiento, J.L., Schlitzer, R., Slater, R.D., Totterdell, I.J., Weirig, M.–F., Yamanaka, Y., and Yool, A.: Anthropogenic ocean acidification over the twenty-first century and its impact on calcifying organisms, Nature, 437, 681–686, 2005.

Orr, J. C. and Epitalon, J.-M.: Improved routines to model the ocean carbonate system: mocsy 2.0, Geosci. Model Dev., 8, 485–499, doi:10.5194/gmd-8-485-2015, 2015.

Orr, J.C., Najjar, R.G., Aumont, O., Bopp, L., Bullister, J.L., Danabasoglu, G., Doney, S.C., Dunne, J.P., Dutay, J.-C., Graven, H., Griffies, S.M., John, J.G., Joos, F., Levin, I., Lindsay, K., Matear, R.J., McKinley, G. A., Mouchet, A., Oschlies, A., Romanou, A., Schlitzer, R., Tagliabue, A., Tanhua, T., and Yool, A.: Biogeochemical protocols and diagnostics for the CMIP6 Ocean Model Intercomparison Project (OMIP), Geosci. Model Dev., 10, 2169–2199, doi:10.5194/gmd-10-2169-2017, 2017.

Pacifico, F., Harrison, S. P., Jones, C. D., Arneth, A., Sitch, S., Weedon, G. P., Barkley, M. P., Palmer, P. I., Serça, D., Potosnak, M., Fu, T.-M., Goldstein, A., Bai, J., and Schurgers, G.: Evaluation of a photosynthesis-based biogenic isoprene emission scheme in JULES and simulation of isoprene emissions under present-day climate conditions, Atmos. Chem. Phys., 11, 4371-4389, doi:10.5194/acp-11-4371-2011, 2011.

Poulter, B., MacBean, N., Hartley, A., Khlystova, I., Arino, O., Betts, R., Bontemps, S., Boettcher, M., Brockmann, C., Defourny, P., Hagemann, S., Herold, M., Kirches, G., Lamarche, C., Lederer, D., Ottlé, C., Peters, M., and Peylin, P.: Plant functional type classification for earth system Initiative, Geosci. Model Dev., 8, 2315–2328, doi:10.5194/gmd-8-2315-2015, 2015. models: results from the European Space Agency's Land Cover Climate Change

Quinn, P., and Bates, T.S.: The case against climate regulation via oceanic phytoplankton sulphur emissions, Nature, 480, 51, doi:10.1038/nature10580, 2011.

Rae, J.G.L., Hewitt, H.T., Keen, A.B., Ridley, J.K., West, A.E., Harris, C.M., Hunke, E.C., and Walters, D.N.: Development of the Global Sea Ice 6.0 CICE configuration for the Met Office Global Coupled model, Geosci. Model Dev., 8, 2221-2230, doi:10.5194/gmd-8-2221-2015, 2015.

Raven, J.A. and Falkowski, P.G.: Oceanic sinks for atmospheric CO_2, Plant Cell Environ., 22, 741–755, 1999.

Rayner, N.A., Parker, D.E., Horton, E.B., Folland, C.K., Alexander, L.V., Rowell, D.P., Kent, E.C., and Kaplan, A.: Global analyses of sea surface temperature, sea ice, and night marine air temperature since the late nineteenth century, J. Geophys. Res., 108, 4407, doi:10.1029/2002JD002670, 2003.

Ridley, J. K., Blockley, E. W., Keen, A. B., Rae, J. G. L., West, A. E., and Schroeder, D.: The sea ice model component of HadGEM3-GC3.1, Geosci. Model Dev., 11, 713-723, doi:10.5194/gmd-11-713-2018, 2018.

Séférian, R., Bopp, L., Gehlen, M., Orr, J., Ethé, C., Cadule, P., Aumont, O., Salas y Mélia, D., Voldoire, A., and Madec, G.: Skill assessment of three earth system models with common marine biogeochemistry, Clim. Dynam., 40, 2549–2573, doi:10.1007/s00382-012-1362-8, 2013.

Séférian, R., Gehlen, M., Bopp, L., Resplandy, L., Orr, J.C., Marti, O., Dunne, J.P., Christian, J.R., Doney, S.C., Ilyina, T., Lindsay, K., Halloran, P.R., Heinze, C., Segschneider, J., Tjiputra, J., Aumont, O., and Romanou, A.: Inconsistent strategies to spin up models in CMIP5: implications for ocean biogeochemical model performance assessment, Geosci. Model Dev., 9, 1827-1851, doi:10.5194/gmd-9-1827-2016, 2016.

Sellar, A.A., Jones, C.G., Mulcahy, J., Tang, Y., Yool, A., Wiltshire, A. O'Connor, F.M., Stringer, M., Hill, R., Palmiéri, J., Woodward, S., de Mora, L., Kuhlbrodt, T., Rumbold, S., Kelley, D.I., Ellis, R., Johnson, C.E., Walton, J., Abraham, N.L., Andrews, M.B., Andrews, T., Archibald, A.T., Berthou, S., Burke, E., Blockley, E., Carslaw, K., Dalvi, M., Edwards, J., Folberth, G.A., Gedney, N., Griffiths, P.T., Harper, A.B., Hendry, M.A., Hewitt, A.J., Johnson, B., Jones, A., Jones, C.D., Keeble, J., Liddicoat, S., Morgenstern, O., Parker, R.J., Predoi, V., Robertson, E., Siahaan, A., Smith, R.S., Swaminathan, R., Woodhouse, M., Zeng, G., and Zerroukat, M.: UKESM1: Description and evaluation of the UK Earth System Model, Journal of Advances in Modeling Earth Systems, 11, 4513-4558, doi:10.1029/2019MS001739, 2019.

Shannon, S., Smith, R., Wiltshire, A., Payne, T., Huss, M., Betts, R., Caesar, J., Koutroulis, A., Jones, D., and Harrison, S.: Global glacier volume projections under high-end climate change scenarios, The Cryosphere, 13, 325–350, doi:10.5194/tc-13-325-2019, 2019.

Simo, R. and Dachs, J.: Global ocean emission of dimethylsulfide predicted from biogeophysical data, Global Biogeochem. Cy., 16, doi:10.1029/2001GB001829, 2002.

Smeed, D., McCarthy, G., Rayner, D., Moat, B.I., Johns, W.E., Baringer, M.O., and Meinen, C.S.: Atlantic meridional overturning circulation observed by the RAPID-MOCHA-WBTS (RAPID-Meridional Overturning Circulation and Heatflux Array-Western Boundary Time Series) array at 26°N from 2004 to 2017. British Oceanographic Data Centre, Natural Environment Research Council, UK.

doi:10.5285/5acfd143-1104-7b58-e053-6c86abc0d94b, 2017.

Smethie Jr, W.M., Fine, R.A., Putzka, A., and Jones, E.P.: Tracing the flow of North Atlantic Deep Water using chlorofluorocarbons, J. Geophys. Res., 105, 14297-14323, 2000.

Sonnewald, M.: Ocean model utility dependence on horizontal resolution (Doctoral dissertation), retrieved from ePrints Soton (https://eprints.soton.ac.uk/397412/), University of Southampton, Southampton, UK, 2016.

Stephens G.L, Li, J., Wild, M., Clayson, C.A., Loeb, N., Kato, S., L'Ecuyer, T., Stackhouse, P.W., Lebsock, M., and T. Andrews: An update on Earth's energy balance in light of the latest global observations, Nature Geosci., 5, 691–696, 2012.

Storkey, D., Blaker, A. T., Mathiot, P., Megann, A., Aksenov, Y., Blockley, E. W., Calvert, D., Graham, T., Hewitt, H. T., Hyder, P., Kuhlbrodt, T., Rae, J. G. L., and Sinha, B.: UK Global Ocean GO6 and GO7: a traceable hierarchy of model resolutions, Geosci. Model Dev., 11, 3187-3213, doi:10.5194/gmd-11-3187-2018, 2018.

Stouffer, R.J., Weaver, A.J., and Eby, M.: A method for obtaining pre-twentieth century initial conditions for use in climate change studies, Clim. Dyn., 23, doi:10.1007/s00382-004-0446-5, 2004.

Takahashi, T., Sutherland, S. C., Wanninkhof, R., Sweeney, C., Feely, R. A., Chipman, D. W., Hales, B., Friederich, G., Chavez, F., Sabine, C., Watson, A., Bakker, D. C. E., Schuster, U., Metzl, N., Yoshikawa–Inoue, H., Ishii, M. Midorikawa, T., Nojiri, Y., Kortzinger, A., Steinhoff, T., Hoppema, M., Olafsson, J., Arnarson, T. S., Tillbrook, B., Johannessen, T., Olsen, A., Bellerby, R., Wong, C. S., Delille, B., Bates, N. R., and de Baar, H. J. W.: Climatological mean and decade change in surface ocean $p\mathrm{CO_2}$, and net sea–air $\mathrm{CO_2}$ flux over the global oceans, Deep-Sea Res. Pt. II, 56, 554–577, doi:10.1016/j.dsr2.2008.12.009, 2009.

Trenberth, K.E., Fasullo, J.T., and Balmaseda, M.A.: Earth's Energy Imbalance, J. Climate, 27, 3129–3144, doi:10.1175/JCLI-D-13-00294.1, 2014.

Valcke, S.: The OASIS3 coupler: a European climate modelling community software, Geosci. Model Dev., 6, 373-388, doi:10.5194/gmd-6-373-2013, 2013.

van der Ent, R. J. and Tuinenburg, O. A.: The residence time of water in the atmosphere revisited, Hydrol. Earth Syst. Sci., 21, 779–790, doi:10.5194/hess-21-779-2017, 2017.

Walters, D., Baran, A., Boutle, I., Brooks, M., Earnshaw, P., Edwards, J., Furtado, K., Hill, P., Lock, A., Manners, J., Morcrette, C., Mulcahy, J., Sanchez, C., Smith, C., Stratton, R., Tennant, W., Tomassini, L., Van Weverberg, K., Vosper, S., Willett, M., Browse, J., Bushell, A., Dalvi, M., Essery, R., Gedney, N., Hardiman, S., Johnson, B., Johnson, C., Jones, A., Mann, G., Milton, S., Rumbold, H., Sellar, A., Ujiie, M., Whitall, M., Williams, K., and Zerroukat, M.: The Met Office Unified Model Global Atmosphere 7.0/7.1 and JULES Global Land 7.0 configurations, Geosci. Model Dev. Discuss., doi:10.5194/gmd-2017-291, in review, 2017.

Walters, D., Baran, A. J., Boutle, I., Brooks, M., Earnshaw, P., Edwards, J., Furtado, K., Hill, P., Lock, A., Manners, J., Morcrette, C., Mulcahy, J., Sanchez, C., Smith, C., Stratton, R., Tennant, W., Tomassini, L., Van Weverberg, K., Vosper, S., Willett, M., Browse, J., Bushell, A., Carslaw, K., Dalvi, M., Essery, R., Gedney, N., Hardiman, S., Johnson, B., Johnson, C., Jones, A., Jones, C., Mann, G., Milton, S., Rumbold, H., Sellar, A., Ujiie, M., Whitall, M., Williams, K., and Zerroukat, M.: The Met Office Unified Model Global Atmosphere 7.0/7.1 and JULES Global Land 7.0 configurations, Geosci. Model Dev., 12, 1909-1963, doi:10.5194/gmd-12-1909-2019, 2019.

Wanninkhof, R.: Relationship between wind speed and gas exchange over the ocean revisited, Limnol. Oceanogr. Methods, 12, doi:10.4319/lom.2014.12.351, 2014.

Watanabe, S., Hajima, T., Sudo, K., Nagashima, T., Takemura, T., Okajima, H., Nozawa, T., Kawase, H., Abe, M., Yokohata, T., Ise, T., Sato, H., Kato, E., Takata, K., Emori, S., and Kawamiya, M.: MIROC-ESM 2010: model description and basic results of CMIP5-20c3m experiments, Geosci. Model Dev., 4, 845–872, doi:10.5194/gmd-4-845-2011, 2011.

Waugh, D.W., Hall, T.M., McNeil, B.I., Key, R., and Matear, R.J.: Anthropogenic CO_2 in the oceans estimated using transit time distributions, Tellus 58B, 376-389, doi:10.1111/j.1600- 0889.2006.00222.x, 2006.

Westberry, T., Behrenfeld, M. J., Siegel, D. A., and Boss, E.: Carbon-based primary productivity modeling with vertically resolved photoacclimation, Global Biogeochem. Cy., 22, GB2024, doi:10.1029/2007GB003078, 2008.

Williams, K.D., Copsey, D., Blockley, E.W., Bodas-Salcedo, A., Calvert, D., Comer, R., Davis, P., Graham, T., Hewitt, H.T., Hill, R., Hyder, P., Ineson, S., Johns, T.C., Keen, A.B., Lee, R.W., Megann, A., Milton, S.F., Rae, J.G.L., Roberts, M.J., Scaife, A.A., Schiemann, R., Storkey, D., Thorpe, L., Watterson, I.G., Walters, D.N., West, A., Wood, R.A., Woollings, T., and Xavier, P. K.: The Met Office Global Coupled model 3.0 and 3.1 (GC3.0 and GC3.1) configurations. Journal of Advances in Modeling Earth Systems, 10, 357-380, doi:10.1002/2017, 2017.

Woodward, S.: Mineral dust in HadGEM2, Hadley Centre Technical Report 87, Met Office, Exeter, UK, 2011.

Wunsch, C., and Heimbach, P.: How long to oceanic tracer and proxy equilibrium?, Quat. Sci. Rev., 27, 637-651, doi:10.1016/j.quascirev.2008.01.006, 2008.

Yool, A., Oschlies, A., Nurser, A. J. G., and Gruber, N.: A model-based assessment of the TrOCA approach for estimating anthropogenic carbon in the ocean, Biogeosciences, 7, 723-751, doi:10.5194/bg-7-723-2010, 2010.

Yool, A., Popova, E. E., and Anderson, T. R.: Medusa–1.0: a new intermediate complexity plankton ecosystem model for the global domain, Geosci. Model Dev., 4, 381–417, doi:10.5194/gmd-4-381-2011, 2011.

Yool, A., Popova, E. E., and Anderson, T. R.: MEDUSA–2.0: an intermediate complexity biogeochemical model of the marine carbon cycle for climate change and ocean acidification studies, Geosci. Model Dev. Discuss., 6, 1259–1365, doi:10.5194/gmdd-6-1259-2013, 2013.

Yool, A., Popova, E.E., and Coward, A.C.: Future change in ocean productivity: Is the Arctic the new Atlantic?, J. Geophys. Res. Oceans, 120, doi:10.1002/2015JC011167, 2015.

Zweng, M.M., Reagan, J.R., Antonov, J.I., Locarnini, R.A., Mishonov, A.V., Boyer, T.P., Garcia, H.E., Baranova, O.K., Johnson, D.R., Seidov, D., and Biddle, M.M.: World Ocean Atlas 2013, Volume 2: Salinity. S. Levitus, Ed., A. Mishonov Technical Ed.; NOAA Atlas NESDIS 74, 39 pp., 2013.

Property	**Units**	**0 m**	**500 m**	**1000 m**	**2000 m**
Temperature	°C ky^{-1}	-0.004	-0.000	0.010	0.023
		0.464	0.390	0.243	-0.194
Salinity	PSU ky^{-1}	0.001	0.001	0.003	0.002
		0.110	0.130	0.037	-0.040
DIN	mmol N m^{-3} ky^{-1}	0.046	0.069	0.045	-0.007
		2.871	-2.024	-1.075	0.098
Silicic acid	mmol Si m^{-3} ky^{-1}	0.049	0.246	0.350	0.047
		0.813	-2.437	-4.965	-0.797
Iron	mmol Fe m^{-3} ky^{-1}	-0.001	-0.000	0.000	0.000
		-0.281	-0.109	-0.020	-0.004
DIC	mmol C m^{-3} ky^{-1}	0.215	-0.213	-1.818	-3.615
		4.993	-10.514	-5.758	-0.897
Alkalinity	meq m^{-3} ky^{-1}	0.328	0.406	0.446	-0.017
		11.609	6.884	-1.076	-2.720
Oxygen	mmol O_2 m^{-3} ky^{-1}	0.012	-0.221	-0.372	-0.245
		-1.902	12.298	9.173	9.379

Table 1. Global mean drift rates for key ocean properties at different reference depths for the final 500 year periods of the ocean-only (upper row) and coupled (lower row) phases. Drift rates calculated as the linear fit across the final 500 year periods, and shown as ky^{-1}.

Figure 1. Schematic diagram of the components of UKESM1 and the associated code structuring and coupling relationships. Circular arrows indicate couplings between closely associated component executables, while large arrows indicate coupling between separate component executables (principally the atmosphere-land and ocean).

Figure 2. Simplified schematic diagram of the main simulation branches involved in the spin-up of UKESM1 components, and their approximate durations. The uppermost branch centres on ocean spin-up, the middle branch on land spin-up, and the lower branch on atmospheric chemistry spin-up. Colours indicate distinct configurations. Branches effectively occurred in parallel, and the main lines of state sharing between branches are indicated in solid black arrows.

Figure 3. Time-series plots of the full spin-up period. Colours indicate different phases, with two ocean phases followed by a UKESM1-CN phase and then a full UKESM1 phase, prior to the start of the piControl. Solid lines indicate 30-year rolling averages of the properties, with the shaded areas denoting the corresponding 30-year range of annual averages. Row 1 shows the evolution of ocean-average volume and surface temperature. Row 2 shows the evolution of ice area in the northern and southern polar regions. Row 3 shows the evolution in circulation strength for the AMOC and Drake Passage. The time axis is indexed such that the end of spin-up (and the start of the piControl) is at zero, with total spin-up duration (per Table **??**) indicated by the negative extent of the time axis.

Figure 4. Time-series plots of the 200 y period after the ocean-only (blue) phase branches to start the coupled (red) phase. Panel ordering follows that of Figure 3. Row 1 shows the evolution of ocean-average volume and surface temperature. Row 2 shows the evolution of ice area in the northern and southern polar regions. Row 3 shows the evolution in circulation strength for the AMOC and Drake Passage. The time axis indicates the time (in years) since the branching occurs, with a preceding 50 year period with ocean-only phase only.

Figure 5. Following Figure 3, rows 1 and 2 show time-series plots of the full spin-up period, with colours indicating different spin-up phases. Solid lines indicate 30-year rolling averages of the properties, with the shaded areas denoting the corresponding 30-year range of annual averages. The panels show globally-integrated net primary production (Pg C y^{-1}) and globally-integrated net air-sea flux (Pg C y^{-1}). Following Figure 4, row 3 shows the corresponding time-series plots of the same properties for the final 100 y periods of the ocean-only (blue) and coupled (red) phases. The time axis shows both phases running in parallel whereas they ran in series.

Figure 6. Time-series of globally-integrated land component properties during the land branch of spin-up. The upper two panels show soil and vegetation carbon (in Pg C), while the lower three panels show the fractional cover of total land area associated with tree, grass and bare soil. Gaps in the time-series were caused by data archiving failures. The uppermost panels include a grey zone to indicate C4MIP's "drift cone" of 0.1 Pg C y^{-1} Jones et al. [2016]. The numbers indicated with "#" are referenced in the text and Table **??**. The period shown follows on from after the initial land-only spin-up phase, using UKESM1-CN (from -865 y; #1) and then UKESM1 (from -210 y) prior to starting the piControl at 0 y.

Figure 7. Time-series of soil carbon integrated across biomes for the final spinup and piControl. In order to illustrate the scale of drift, the panels include a grey zone that indicates the 250 year period of the first Historical ensemble member (1850–2100). Additional branch dates for subsequent Historical ensemble members are indicated by dashed lines. The period shown is from the final period of UKESM1 spin-up (-110 y to 0 y) prior to start of the piControl (0 y onwards).

Figure 8. Time-series covering the final 500 years of the UKESM1 coupled spin-up and the first 200 years of the coupled UKESM1 piControl. The figure plots: years -500 to -200 UKESM1-CN (run IDs; u-ar783 and u-au835) followed by, years -200 to 0 UKESM1 (run IDs; u-av472, u-av651 and u-aw310), followed by, years 1 to 200 UKESM1 piControl. Panel 1 shows global mean top of atmosphere (TOA) net downward short wave (SW) radiation. Panel 2 shows the corresponding global mean TOA outgoing long wave (LW) radiation. Panel 3 shows the resulting balance of global mean TOA net radiation. Panel 4 shows global mean 1.5 m air temperature. Finally, panel 5 shows Arctic (blue) and Antarctic (black) sea-ice extent. In each panel, thick lines are an 11-year running mean, and the thin lines are annual mean values. Radiation values are in W m^{-2}, with positive values indicating a downward-directed flux for net SW down and net radiation, and an upward-directed flux for outgoing LW. Temperature is in units of degrees Kelvin, and sea-ice extent expressed as 10^6 km^2.

Figure 9. Observational (HadISST) and simulated sea surface temperature for northern (top; JJA) and southern (medium; DJF) summer. Differences (simulated - observed) for both seasons shown in bottom row. Temperature (and difference in temperature) in °C. HadISST data from the period 1870-1879.

Figure 10. Observed (red; HadISST) and simulated (blue) seasonal cycles of sea-ice extent (> 15% cover) for the Arctic (left) and Antarctic (right). Sea-ice extent in 10^6 km^2. HadISST data from the period 1870-1879.

Figure 11. A "thermohaline circulation" section of biases in modelled potential temperature (top) and salinity (bottom). The section tracks southwards "down" the Atlantic basin from the Arctic to the Atlantic sector of the Southern Ocean, before tracking northwards "up" the Pacific basin from the Pacific sector of the Southern Ocean to the Bering Straits. The aim is to capture the stereotypical transport of deep water from its formation as a "young" water mass in the high North Atlantic through to end as an "old" water mass in the North Pacific. Dotted lines mark the "boundaries" of the Southern Ocean at 40°S in each basin. Biases in potential temperature are in °C, and in practical salinity units (PSU) for salinity. Observational data from the World Ocean Atlas climatology for the period 1995-2004.

Figure 12. Observationally-derived (top) and simulated (bottom) meridional overturning circulation (MOC) for the global ocean. The model circulation shown is based on the decadally-averaged streamfunction. MOC in Sv, with both plots including Gent-McWilliams components [Gent and McWilliams, 1990]. Observational data from the ECCO V4r4 ocean circulation reanalysis for the period 1992-2017.

Figure 13. Annual average observational (left) and simulated (right) fields of surface dissolved inorganic nitrogen (top; mmol N m^{-3}), total surface chlorophyll (middle; mg m^{-3}), and vertically-integrated net primary production (bottom; g C m^{-2} d^{-1}). Note that total surface chlorophyll is shown on a logarithmic scale. Observational data are from the World Ocean Atlas (DIN; climatology from 1981-2010), SeaWiFS (chlorophyll; climatology for the period 2000-2009) and the VGPM, Eppley-VGPM and CbPM products (NPP; climatology for the period 2000-2009).

Figure 14. Observational (left) and simulated (right) annual average surface dissolved inorganic carbon (top) and total alkalinity (bottom). DIC in mmol C m^{-3}, alkalinity in meq m^{-3}. Observational data are from the GLODAPv2 climatology, from the pre-industrial period for DIC, and normalised to year 2002 for alkalinity.

Figure 15. A "thermohaline circulation" section of observed (top) and modelled (bottom) zonal average dissolved inorganic carbon. Figure 11 explains the format of this section. Concentrations in mmol C m^{-3}. Observational data are from the GLODAPv2 climatology, for the pre-industrial period.

Figure 16. Observationally-derived geographical map of major land biomes (top), together with a comparison of the land cover type found in each biome for the model and two observational products, IGBP and CCI (bottom). Each biome appears as a separate triplet of bars, with the colour composition of the bar relating to the vegetation cover types indicated in the key. The observational IGBP product is derived from year 1992 data, while the CCI product is derived from year 2000.

Figure 17. Geographical maps of fractional cover associated with each land cover type for the model (left) and two observational products, IGBP and CCI (middle and right, respectively). In each case, increasing colour intensity denotes greater fractional cover. The observational IGBP product is derived from year 1992 data, while the CCI product is derived from year 2000.

Figure 1.

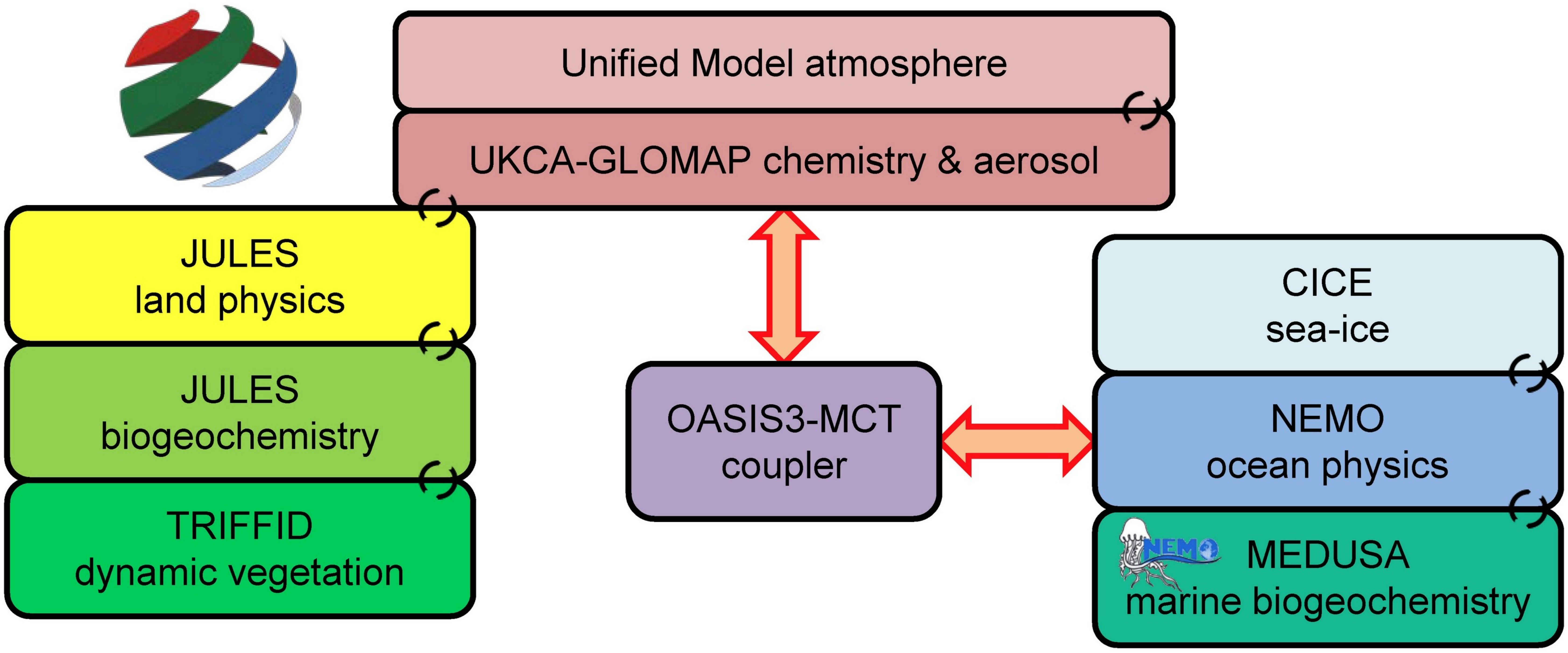
Unified Model atmosphere
UKCA-GLOMAP chemistry & aerosol
JULES
land physics
JULES
biogeochemistry
TRIFFID
dynamic vegetation
OASIS3-MCT
coupler
CICE
sea-ice
NEMO
ocean physics
NEMO
MEDUSA
marine biogeochemistry

Figure 2.

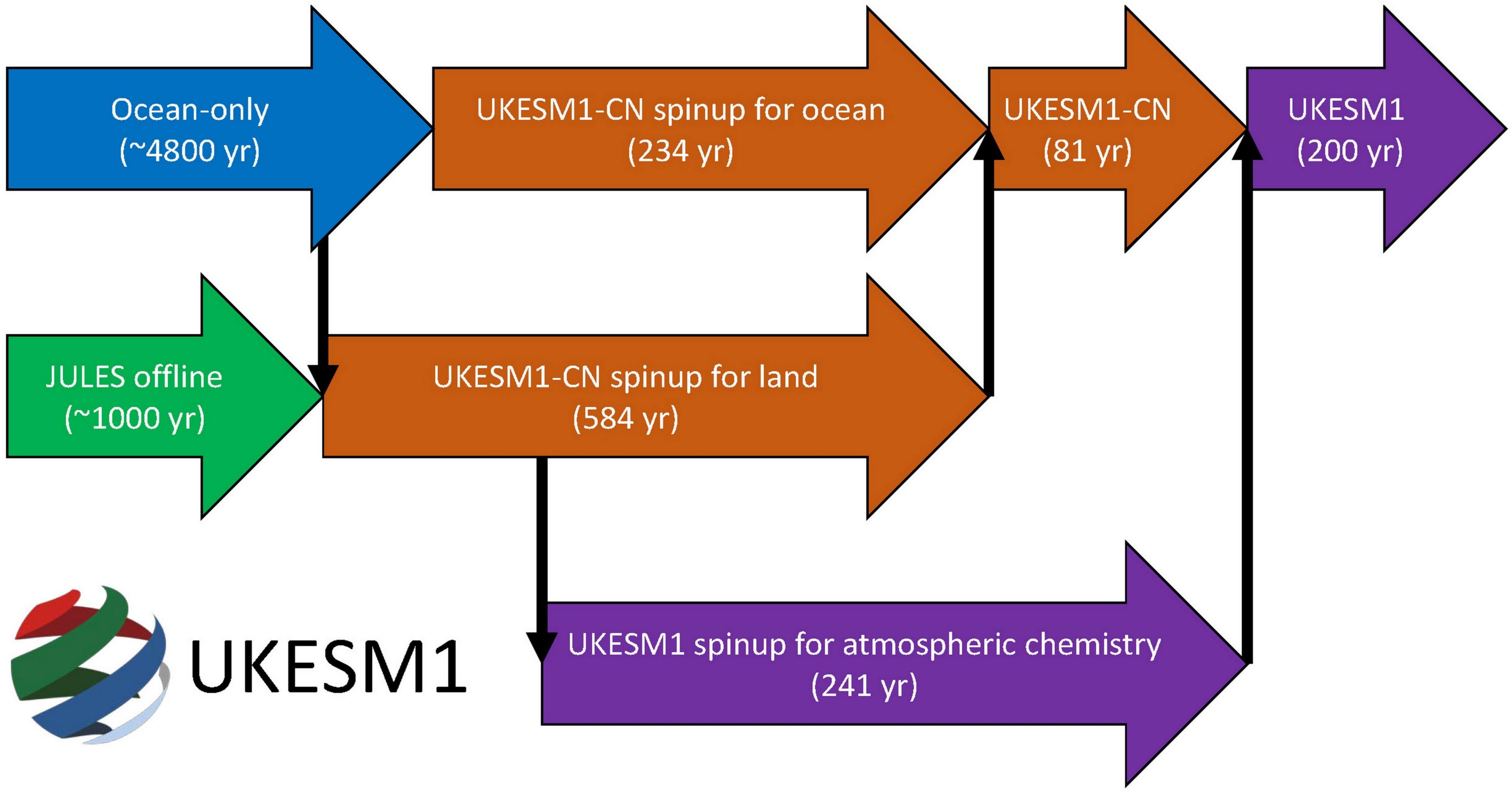
Ocean-only
(~4800 yr)
UKESM1-CN spinup for ocean
(234 yr)
UKESM1-CN
(81 yr)
UKESM1
(200 yr)
JULES offline
(~1000 yr)
UKESM1-CN spinup for land
(584 yr)
UKESM1
UKESM1 spinup for atmospheric chemistry
(241 yr)

Figure 3.

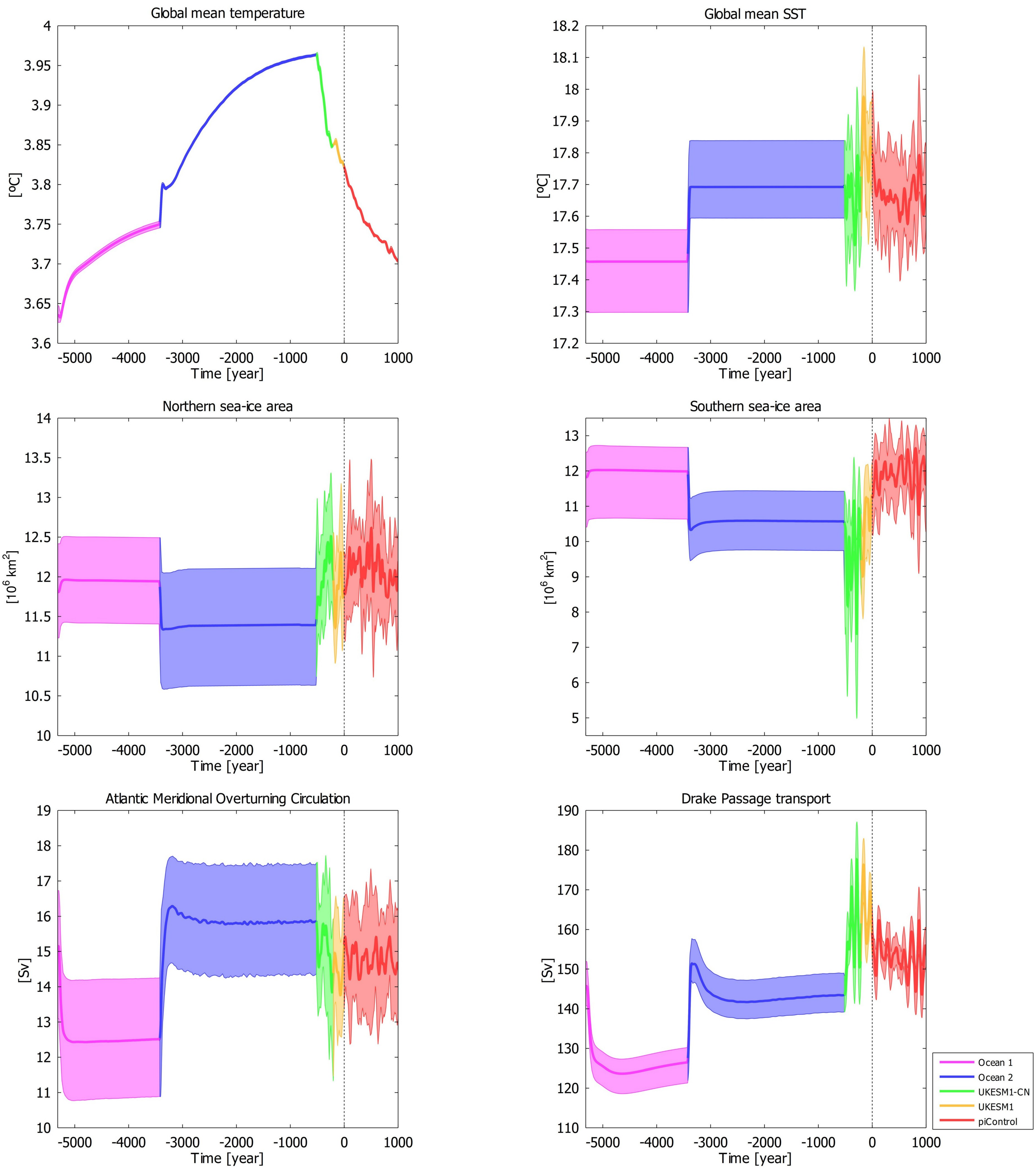
Global mean temperature
[°C]
Time [year]
Global mean SST
[°C]
Time [year]
Northern sea-ice area
[10^6 km^2]
Time [year]
Southern sea-ice area
[10^6 km^2]
Time [year]
Atlantic Meridional Overturning Circulation
[Sv]
Time [year]
Drake Passage transport
[Sv]
Time [year]
Ocean 1
Ocean 2
UKESM1-CN
UKESM1
piControl

Figure 4.

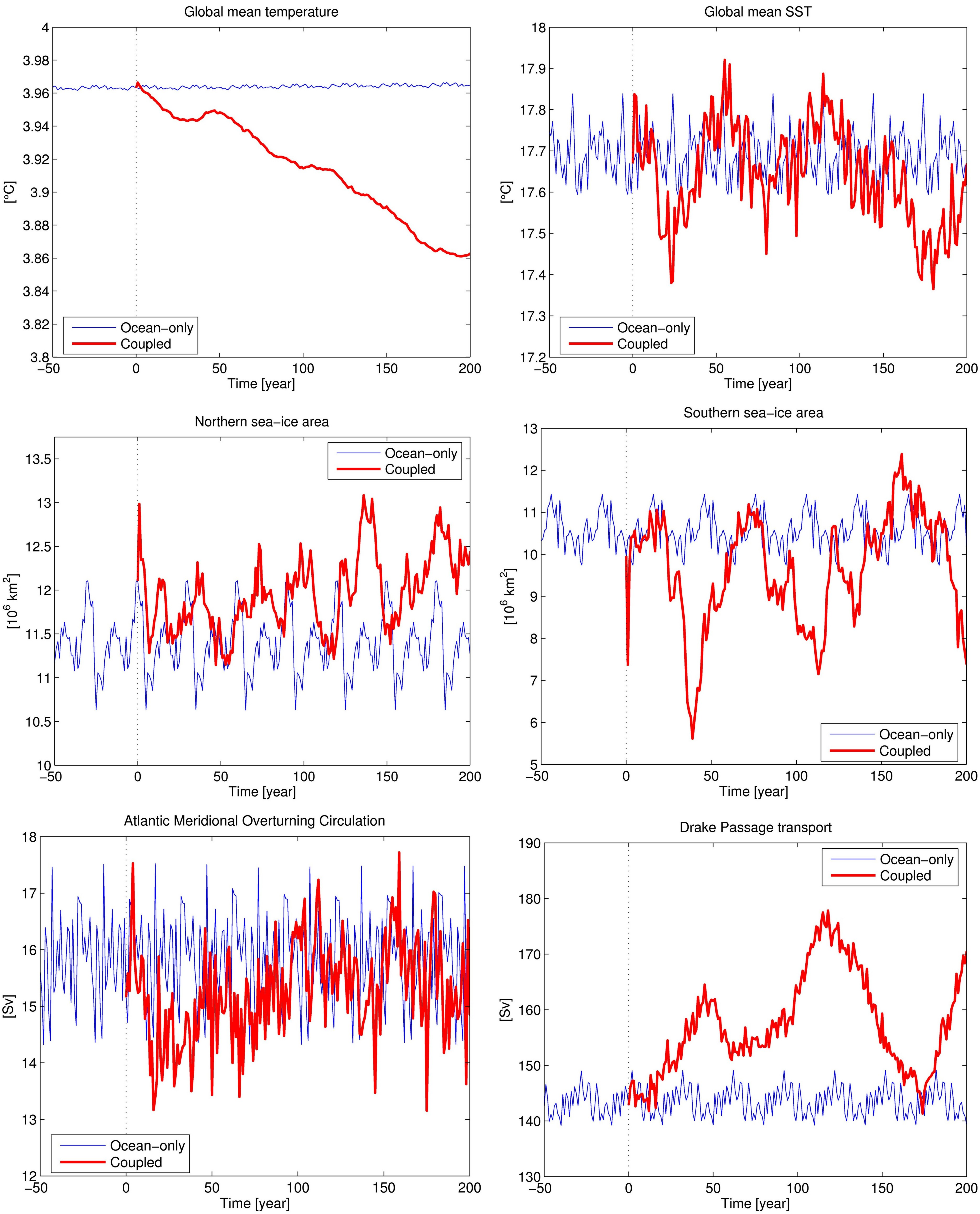
Global mean temperature
[°C]
Time [year]
Ocean−only
Coupled
Global mean SST
[°C]
Time [year]
Ocean−only
Coupled
Northern sea−ice area
[10^6 km^2]
Time [year]
Ocean−only
Coupled
Southern sea−ice area
[10^6 km^2]
Time [year]
Ocean−only
Coupled
Atlantic Meridional Overturning Circulation
[Sv]
Time [year]
Ocean−only
Coupled
Drake Passage transport
[Sv]
Time [year]
Ocean−only
Coupled

Figure 5.

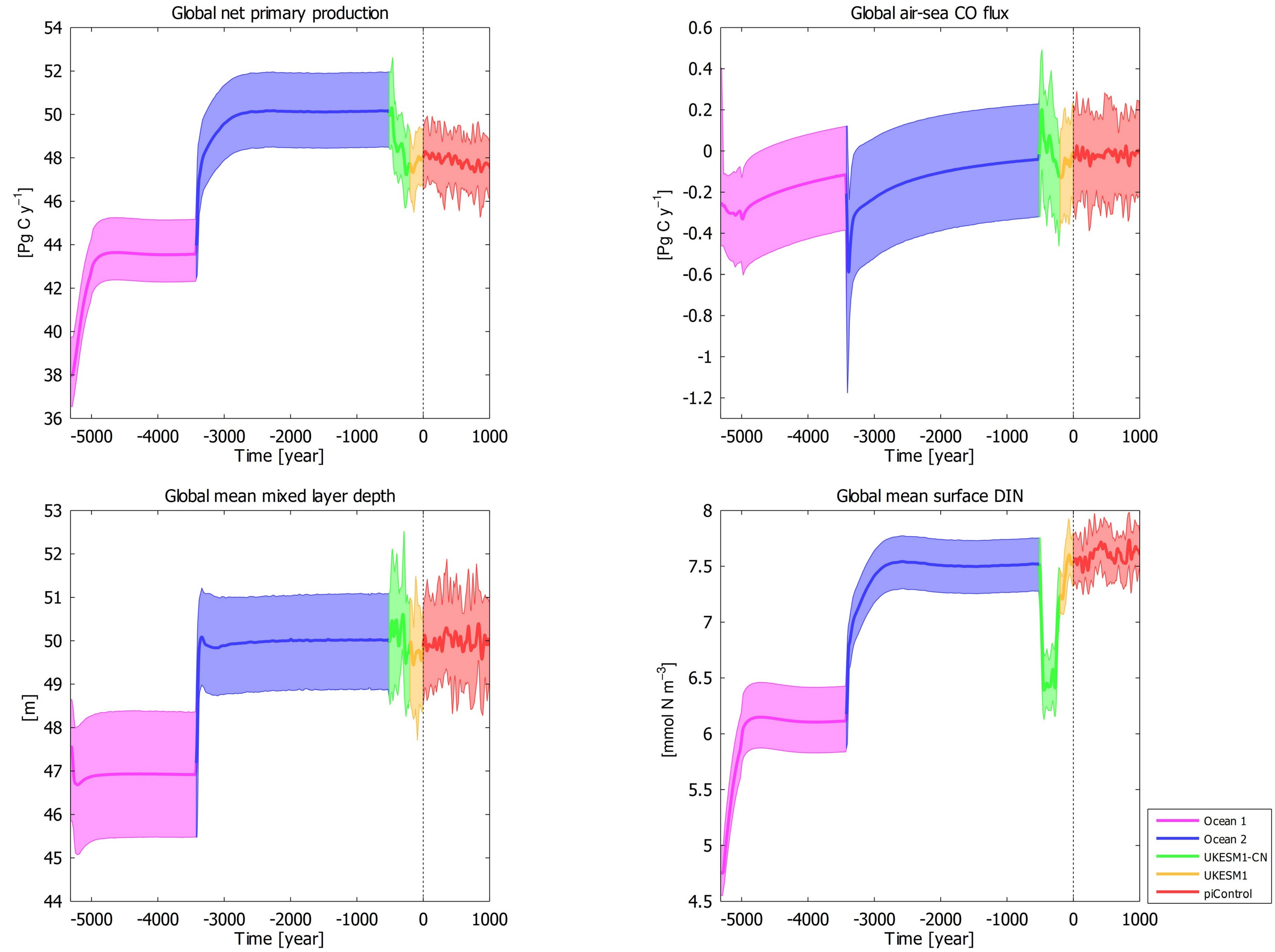
Global net primary production
[Pg C y^{-1}]
Time [year]
Global air-sea CO flux
[Pg C y^{-1}]
Time [year]
Global mean mixed layer depth
[m]
Time [year]
Global mean surface DIN
[mmol N m^{-3}]
Time [year]
Ocean 1
Ocean 2
UKESM1-CN
UKESM1
piControl

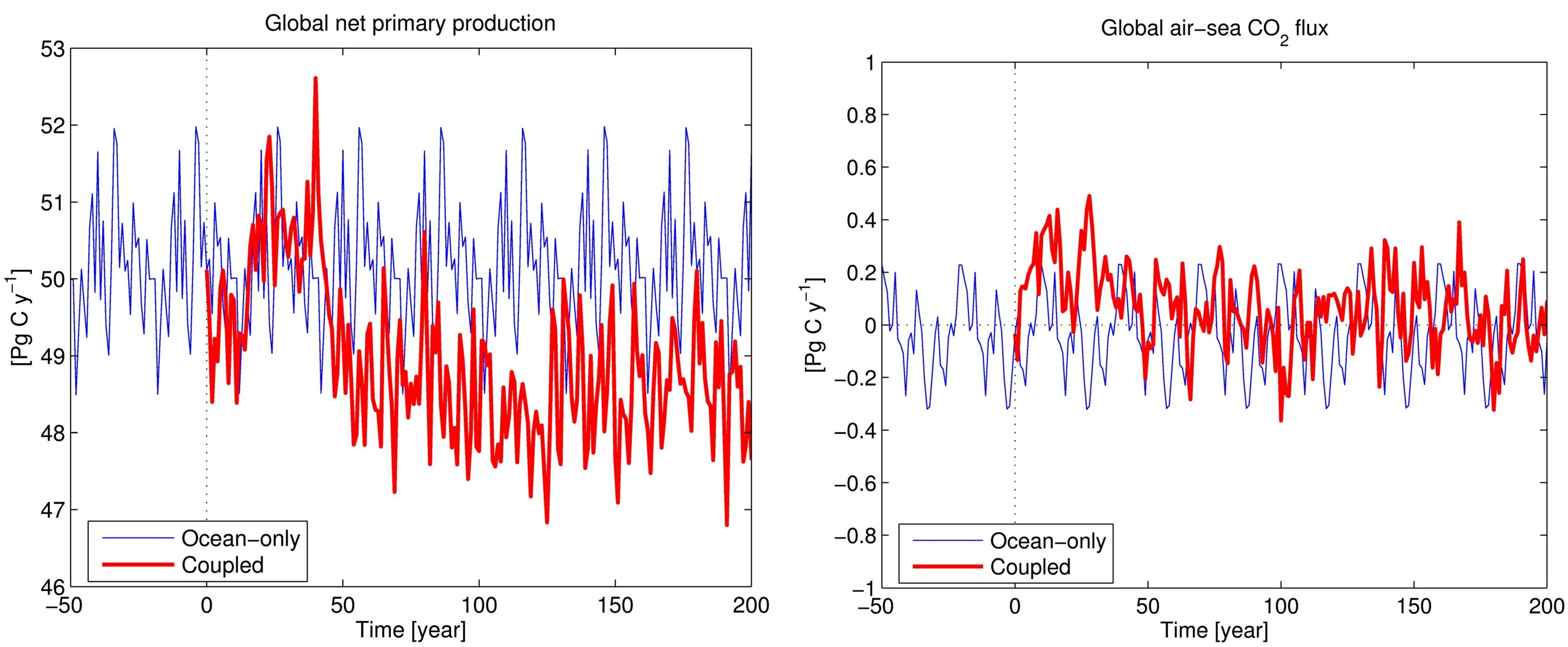
Global net primary production
[Pg C y^{-1}]
Time [year]
Ocean−only
Coupled
Global air−sea CO_2 flux
[Pg C y^{-1}]
Time [year]
Ocean−only
Coupled

Figure 6.

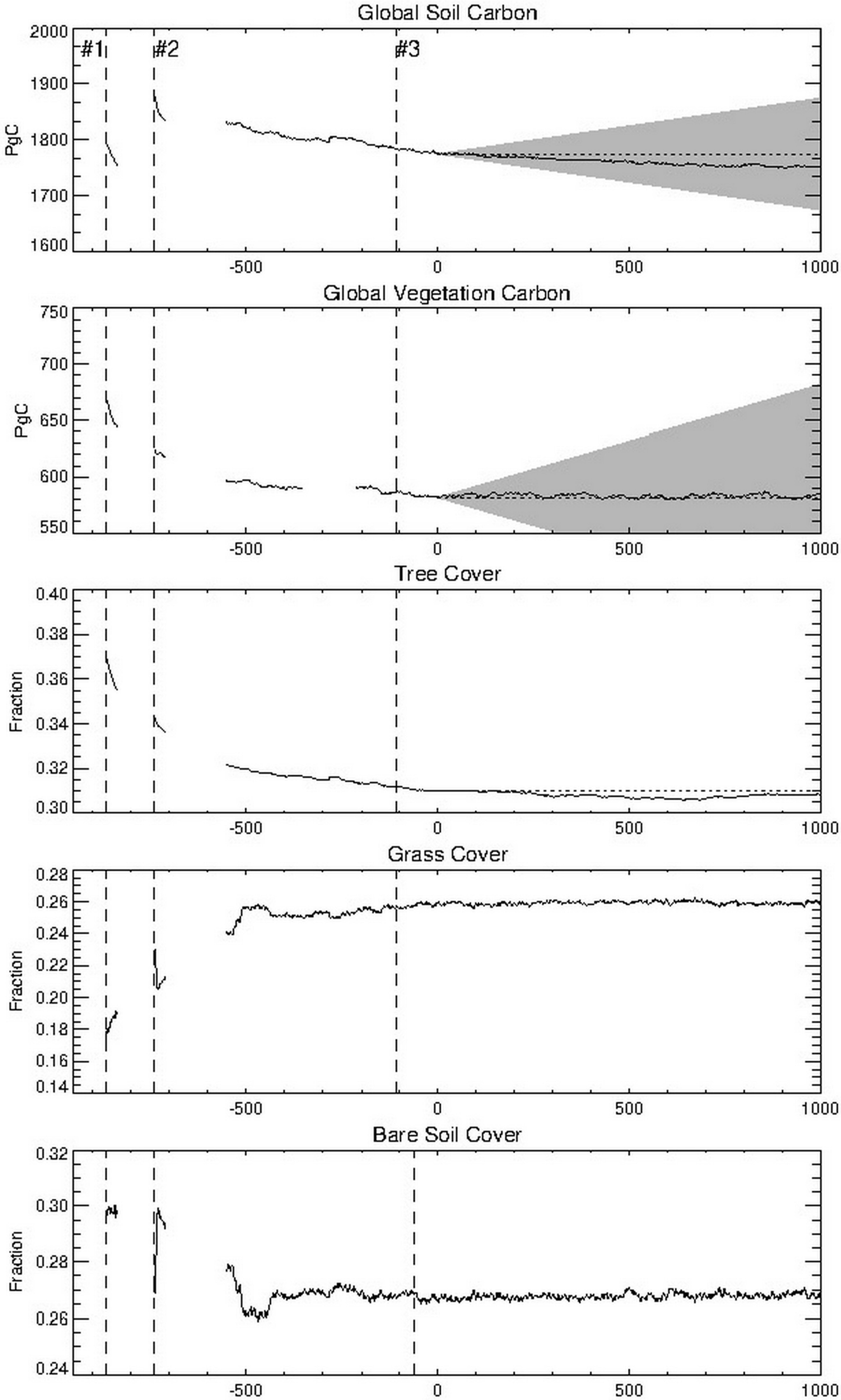
Global Soil Carbon
PgC
#1
#2
#3
2000
1900
1800
1700
1600
-500
0
500
1000
Global Vegetation Carbon
PgC
750
700
650
600
550
Tree Cover
Fraction
0.40
0.38
0.36
0.34
0.32
0.30
Grass Cover
Fraction
0.28
0.26
0.24
0.22
0.20
0.18
0.16
0.14
Bare Soil Cover
Fraction
0.32
0.30
0.28
0.26
0.24

Figure 7.

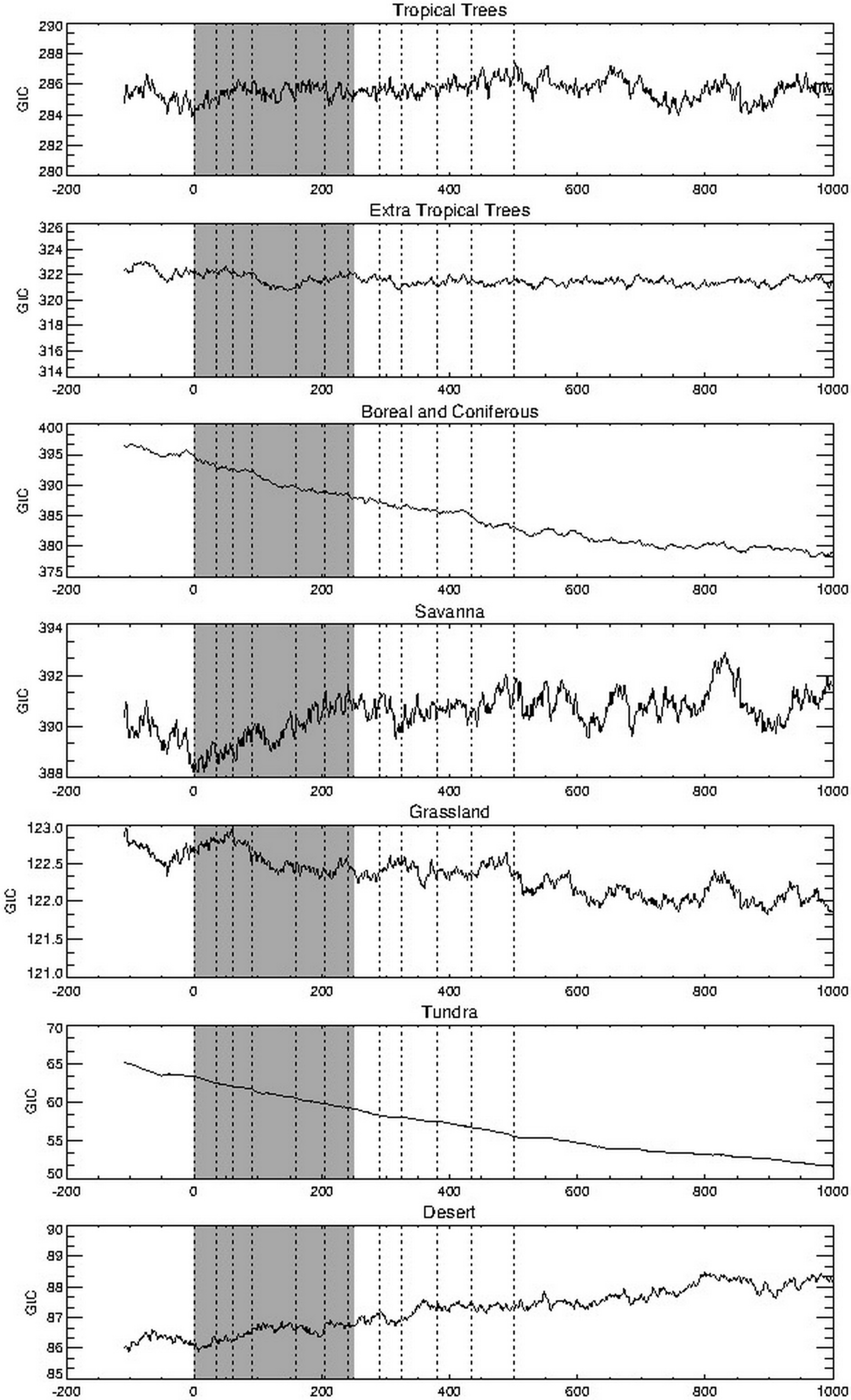
Tropical Trees
GIC
290
288
286
284
282
280
-200
0
200
400
600
800
1000
Extra Tropical Trees
GIC
326
324
322
320
318
316
314
Boreal and Coniferous
GIC
400
395
390
385
380
375
Savanna
GIC
394
392
390
388
Grassland
GIC
123.0
122.5
122.0
121.5
121.0
Tundra
GIC
70
65
60
55
50
Desert
GIC
90
89
88
87
86
85

Figure 8.

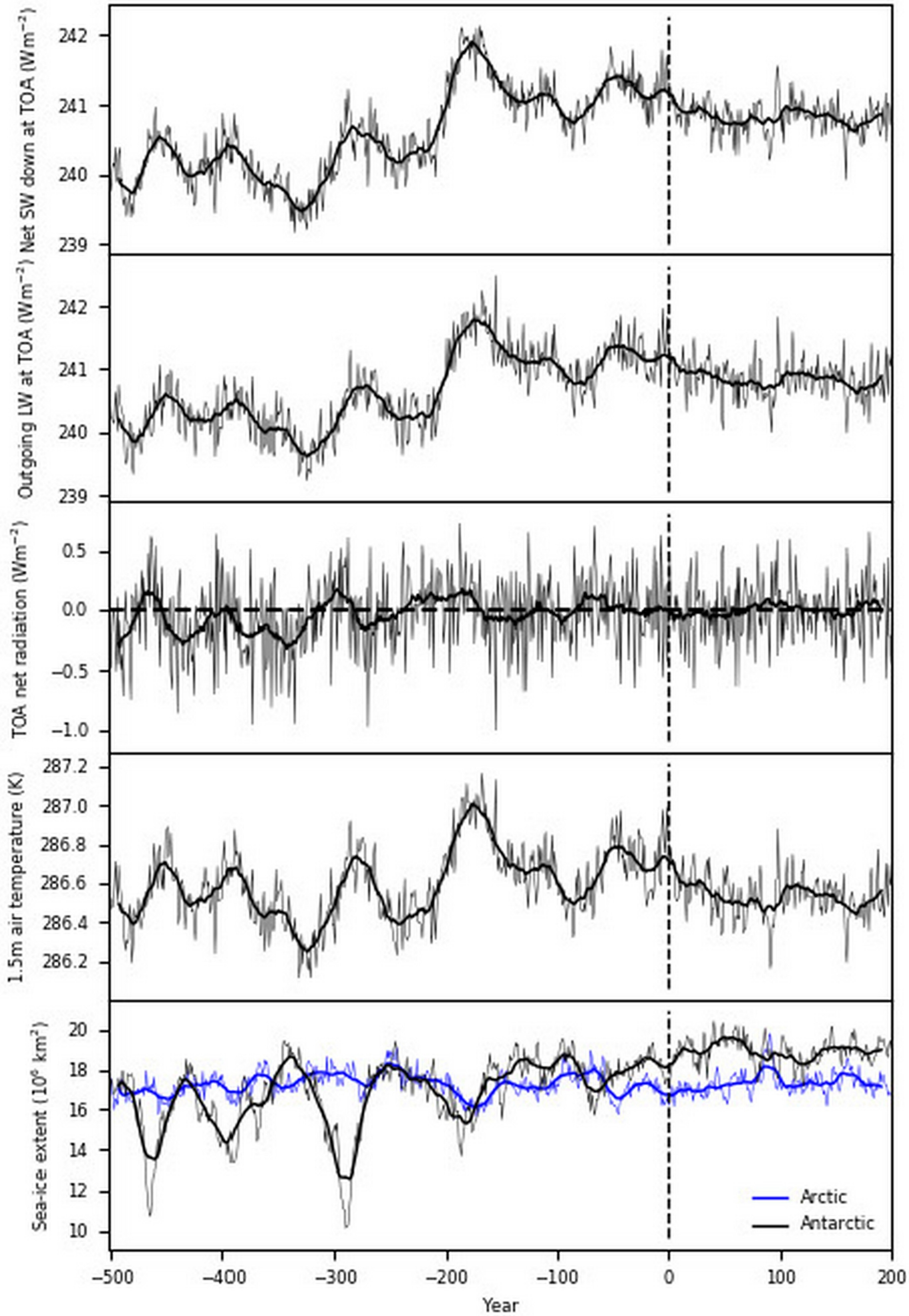
Net SW down at TOA (Wm^{-2})
Outgoing LW at TOA (Wm^{-2})
TOA net radiation (Wm^{-2})
1.5m air temperature (K)
Sea-ice extent (10^6 km^2)
Arctic
Antarctic
Year
−500
−400
−300
−200
−100
0
100
200

Figure 9.

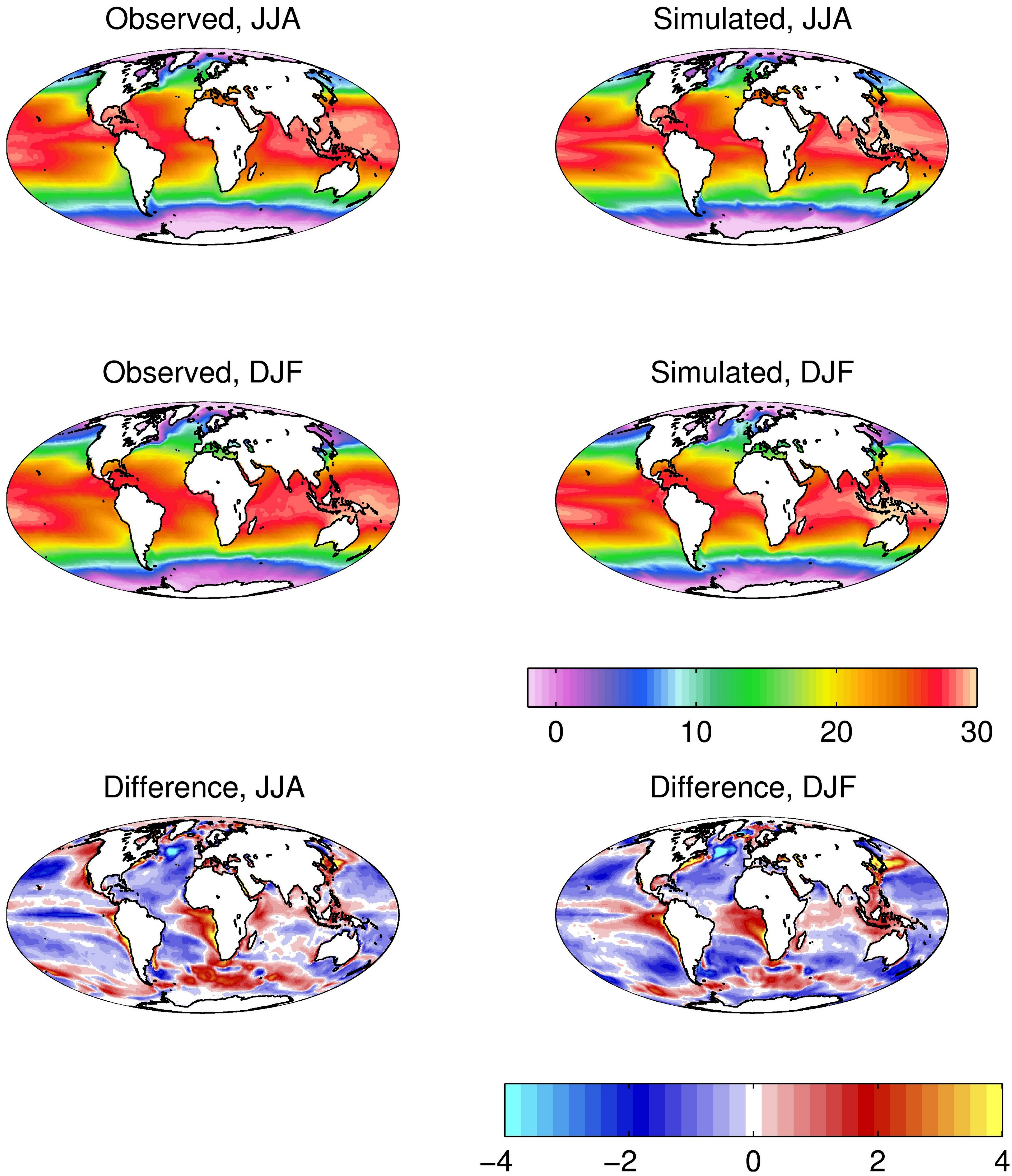
Observed, JJA
Simulated, JJA
Observed, DJF
Simulated, DJF
0
10
20
30
Difference, JJA
Difference, DJF
−4
−2
0
2
4

Figure 10.

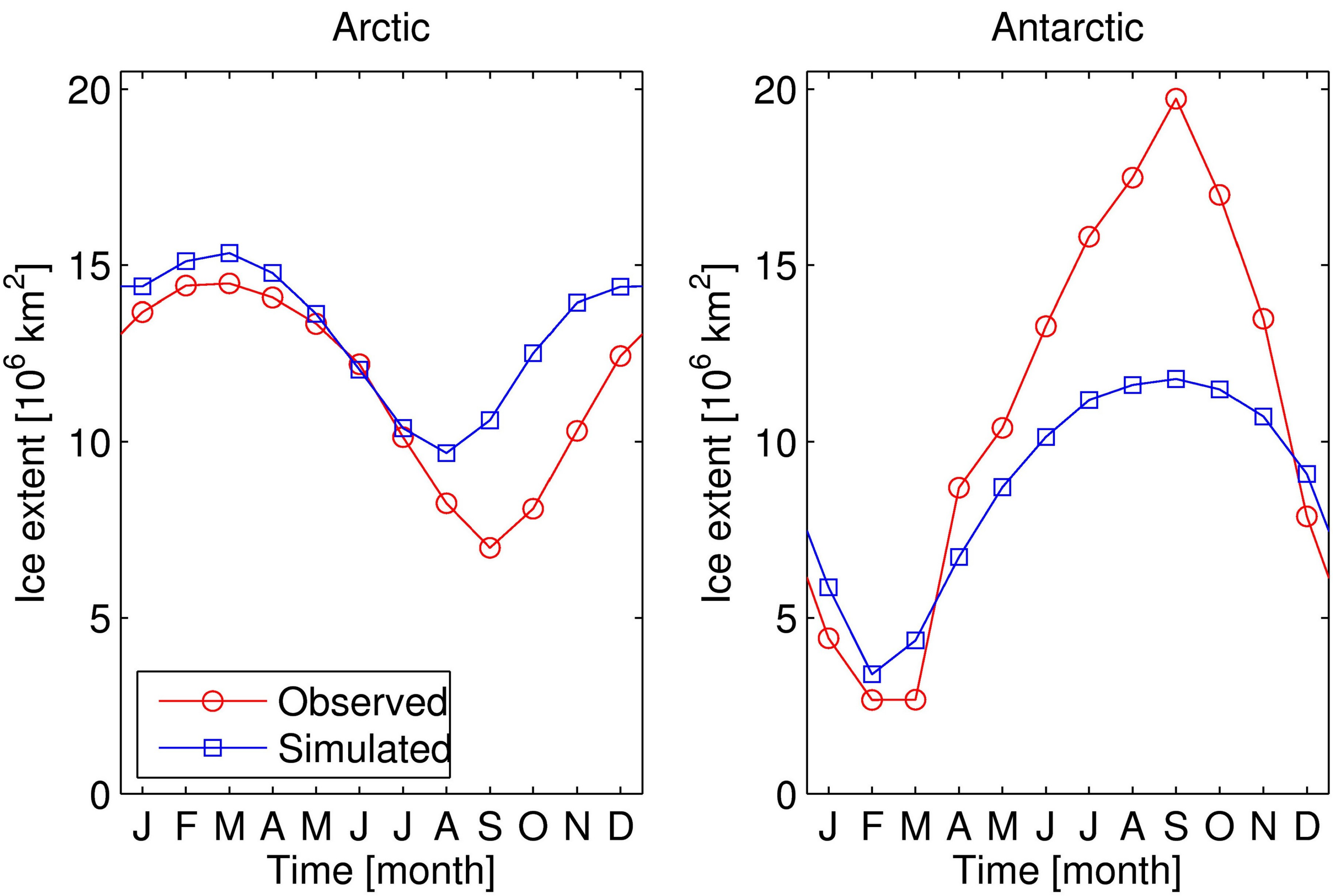
Arctic
Antarctic
Ice extent [10^6 km^2]
0
5
10
15
20
Observed
Simulated
J F M A M J J A S O N D
Time [month]

Figure 11.

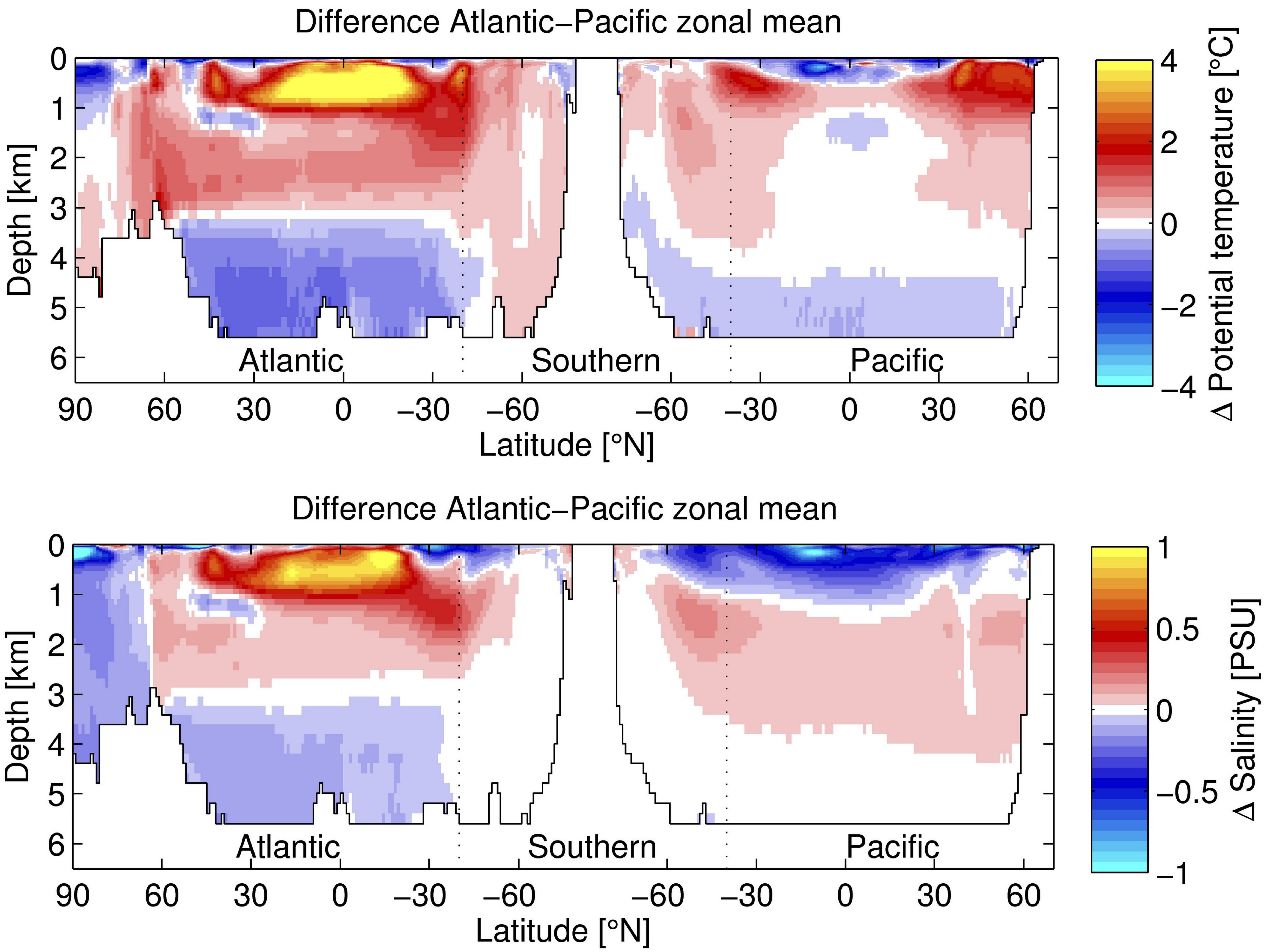
Difference Atlantic−Pacific zonal mean
Depth [km]
Atlantic
Southern
Pacific
Latitude [°N]
Δ Potential temperature [°C]
Difference Atlantic−Pacific zonal mean
Depth [km]
Atlantic
Southern
Pacific
Latitude [°N]
Δ Salinity [PSU]

Figure 12.

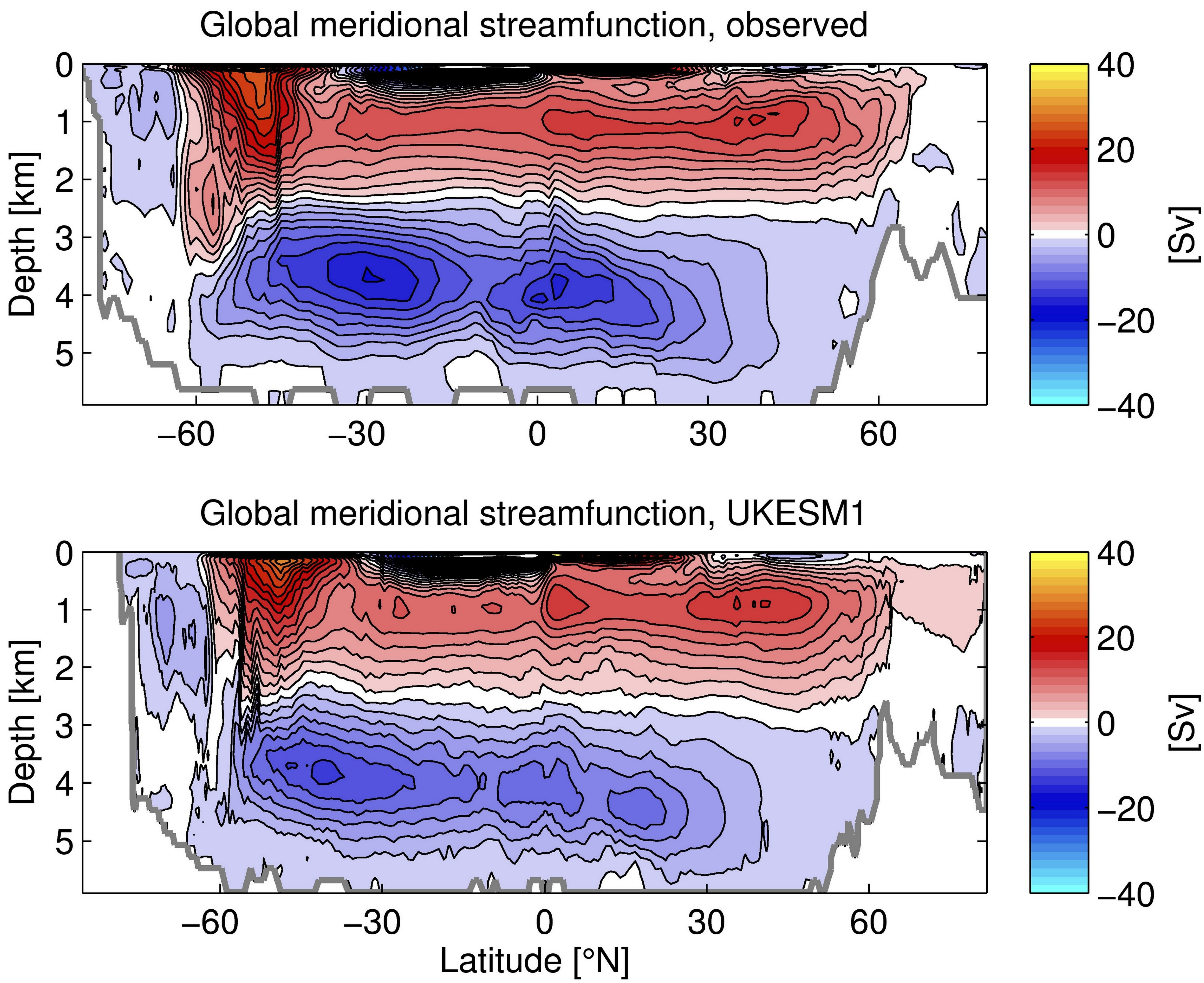
Global meridional streamfunction, observed
Depth [km]
0
1
2
3
4
5
–60
–30
0
30
60
40
20
0
–20
–40
[Sv]
Global meridional streamfunction, UKESM1
Depth [km]
0
1
2
3
4
5
–60
–30
0
30
60
Latitude [°N]
40
20
0
–20
–40
[Sv]

Figure 13.

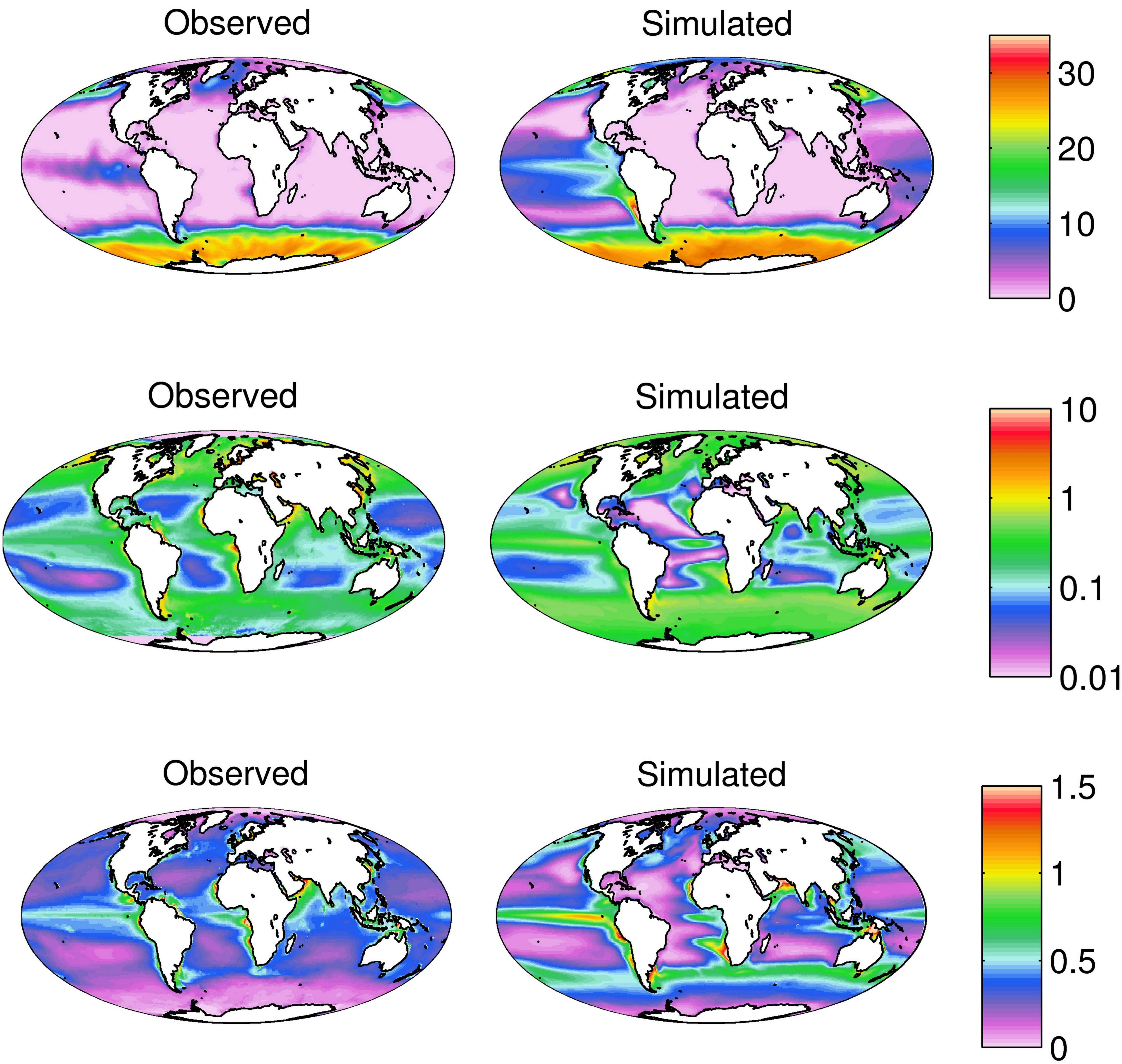
Observed
Simulated
30
20
10
0
Observed
Simulated
10
1
0.1
0.01
Observed
Simulated
1.5
1
0.5
0

Figure 14.

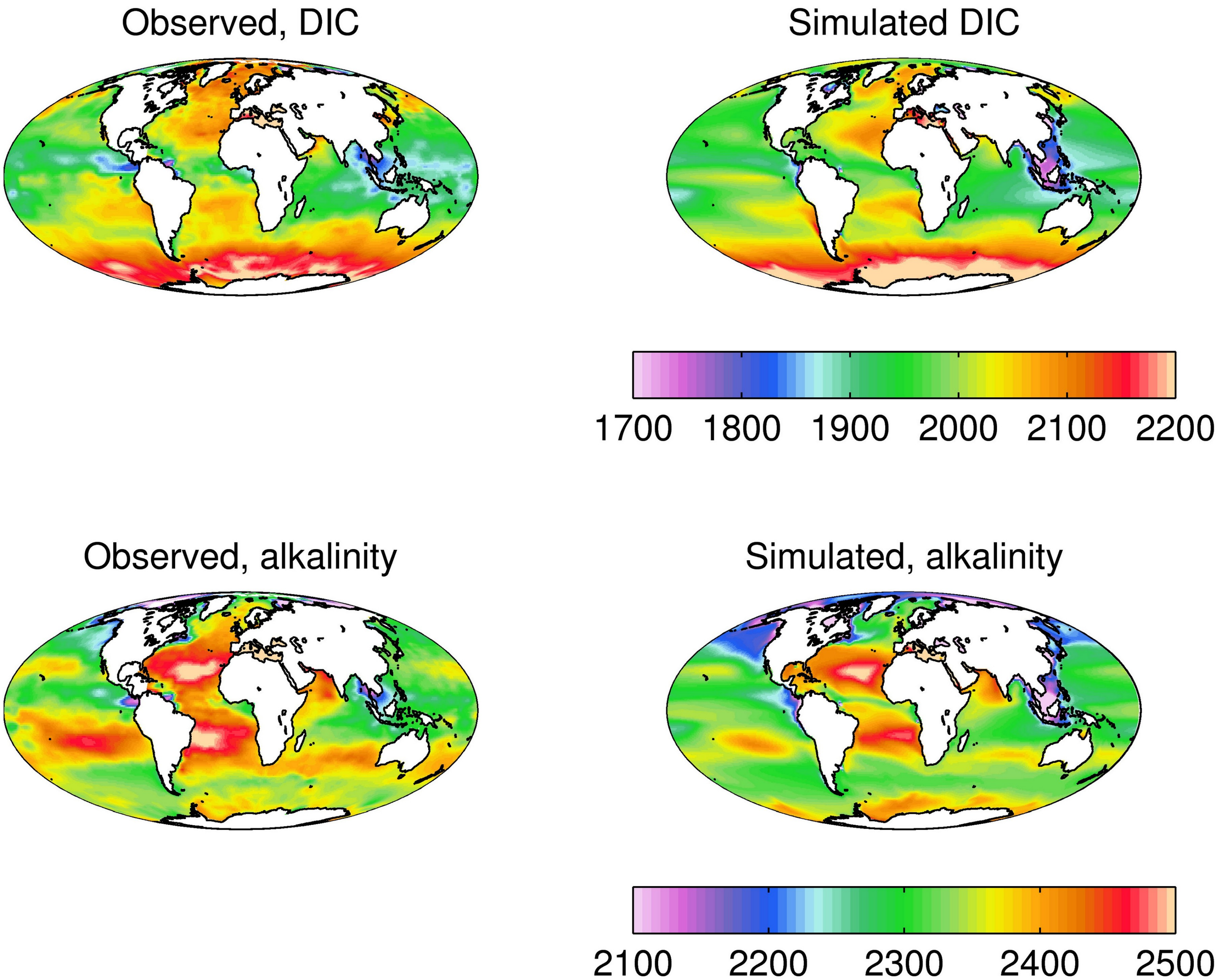
Observed, DIC
Simulated DIC
1700 1800 1900 2000 2100 2200
Observed, alkalinity
Simulated, alkalinity
2100 2200 2300 2400 2500

Figure 15.

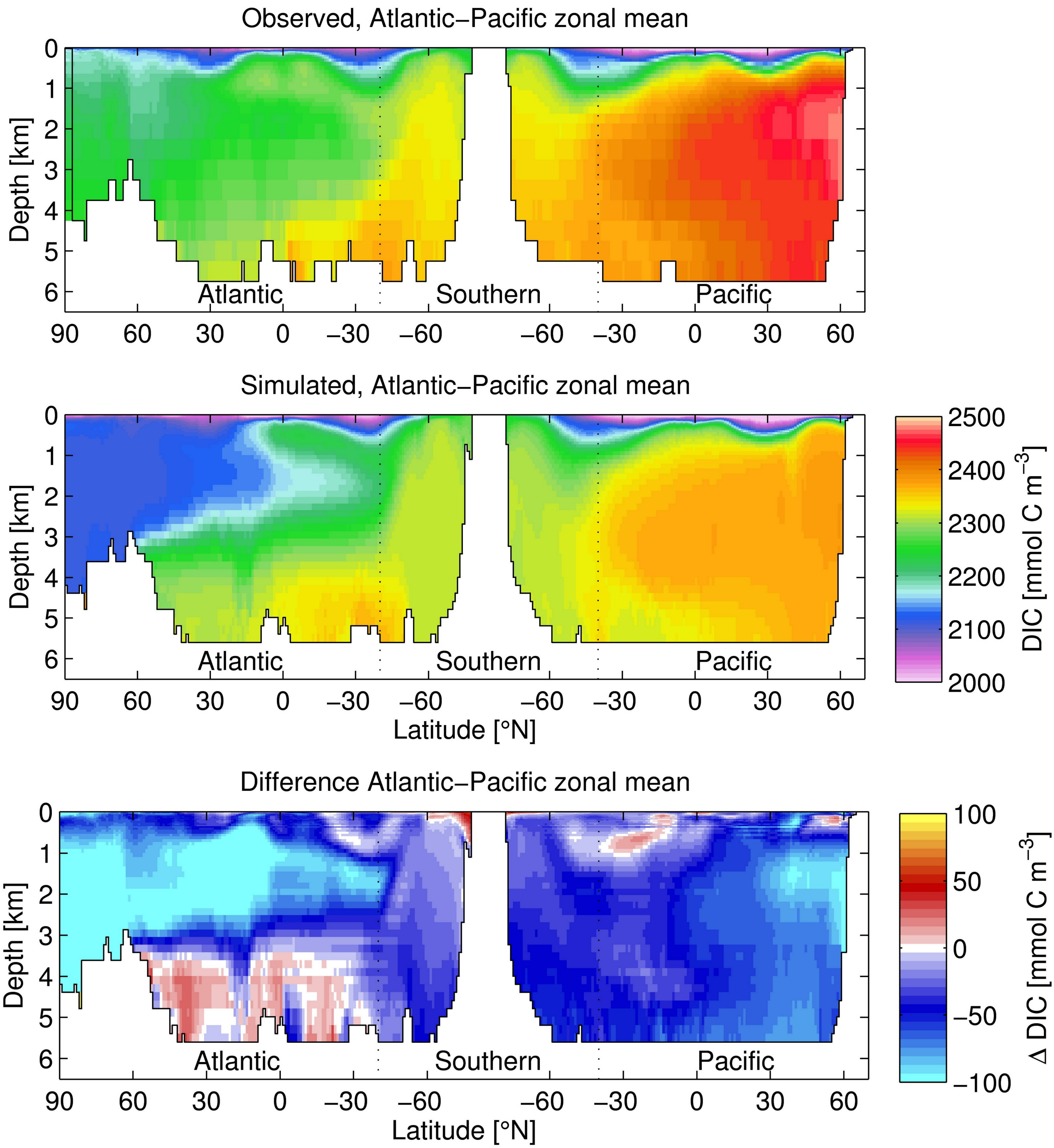
Observed, Atlantic−Pacific zonal mean
Depth [km]
Atlantic
Southern
Pacific
90 60 30 0 −30 −60 −60 −30 0 30 60
Simulated, Atlantic−Pacific zonal mean
Latitude [°N]
2500
2400
2300
2200
2100
2000
DIC [mmol C m−3]
Difference Atlantic−Pacific zonal mean
100
50
0
−50
−100
Δ DIC [mmol C m−3]

Figure 16.

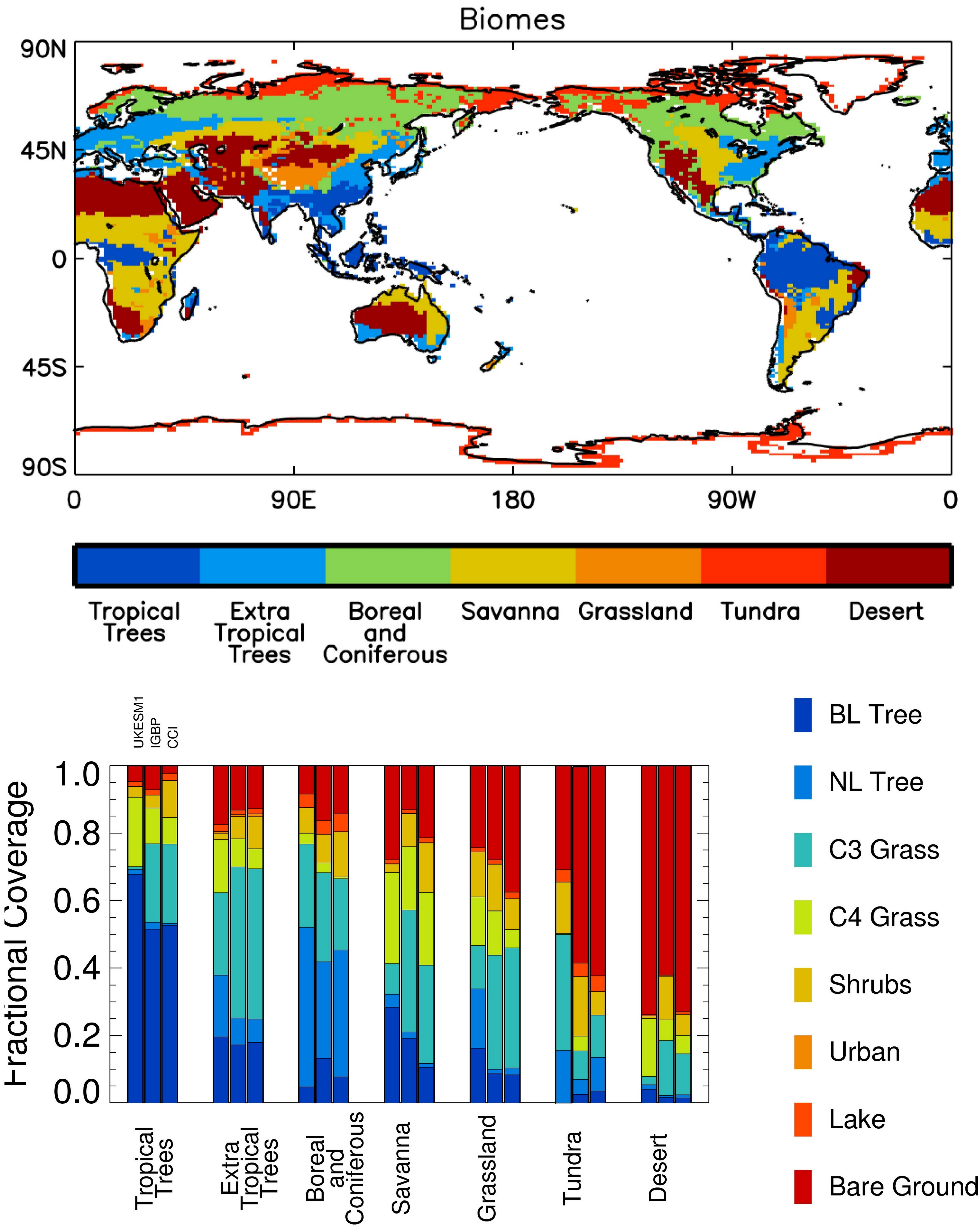

Biomes
90N
45N
0
45S
90S
0
90E
180
90W
0
Tropical Trees
Extra Tropical Trees
Boreal and Coniferous
Savanna
Grassland
Tundra
Desert
UKESM1
IGBP
CCI
Fractional Coverage
1.0
0.8
0.6
0.4
0.2
0.0
Tropical Trees
Extra Tropical Trees
Boreal and Coniferous
Savanna
Grassland
Tundra
Desert
BL Tree
NL Tree
C3 Grass
C4 Grass
Shrubs
Urban
Lake
Bare Ground

Figure 17.

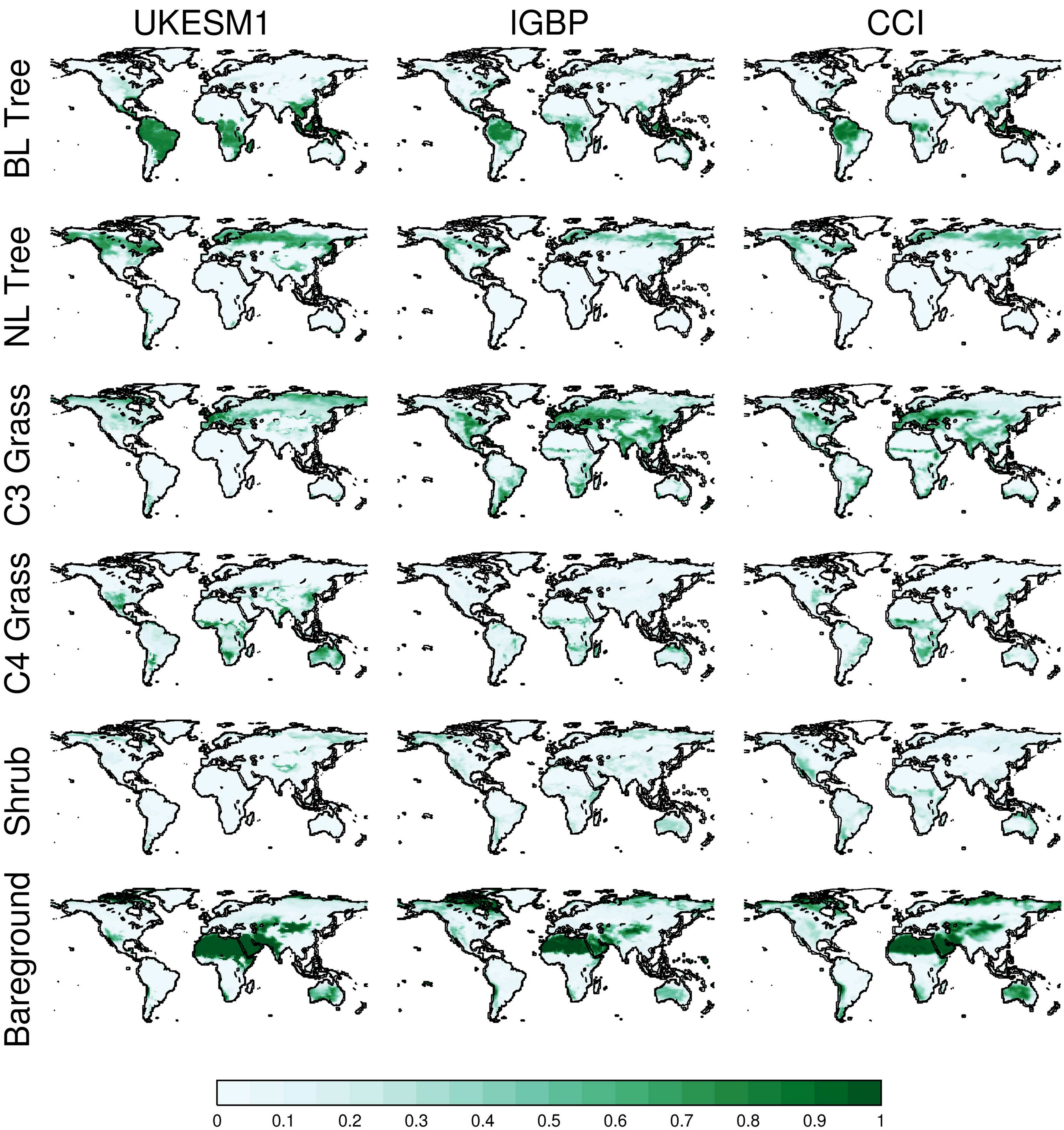
UKESM1
IGBP
CCI
BL Tree
NL Tree
C3 Grass
C4 Grass
Shrub
Bareground
0
0.1
0.2
0.3
0.4
0.5
0.6
0.7
0.8
0.9
1